

SECOND ANNUAL REPORT

DOE CONTRACT NO. DE-FG26-04NT15532

New Mexico Petroleum Recovery Research Center  
New Mexico Institute of Mining and Technology  
801 Leroy Place  
Socorro, NM 87801  
(505) 835-5142

Report Date:	June 25, 2007
Contract Date:	April 1, 2005
Completion Date (revised):	March 31, 2008
DOE Total Award (second period):	\$339,249.94
Program Manager:	Reid B. Grigg
Principal Investigator:	Reid B. Grigg
Other Major Contributors:	Robert K. Svec Zheng Wen Zeng Alexander Mikhailin Yi Liu Guoqiang Yin
Contracting Officer's Representative:	Dan Ferguson
Reporting Period:	April 1, 2006–March 31, 2007

## **DISCLAIMER**

This report was prepared as an account of work sponsored by an agency of the United States Government. Neither the United States Government nor any agency thereof, nor any of their employees, makes any warranty, express or implied, or assumes any legal liability or responsibility for the accuracy, completeness, or usefulness of any information, apparatus, product, or process disclosed, or represents that its use would not infringe privately owned rights. Reference herein to any specific commercial product, process, or service by trade name, trademark, manufacturer, or otherwise does not necessarily constitute or imply its endorsement, recommendation, or favoring by the United States Government or any agency thereof. The views and opinions of authors expressed herein do not necessarily state or reflect those of the United States Government or any agency thereof.

## **ABSTRACT**

This document presents the second year results from the project, “Improved Gas Flooding Efficiency,” Department of Energy Contract No. DE-FC26-04NT15532. This study focuses on laboratory studies with related analytical and numerical models, as well as work with operators for field tests to enhance our understanding of and capabilities for more efficient enhanced oil recovery (EOR).

Concern over increased greenhouse gas emissions is encouraging increased carbon dioxide (CO<sub>2</sub>) injection into geological formations, for EOR as well as for sequestration. The development of CO<sub>2</sub> plumes and their subsequent dissolution into formation brine are essential mechanisms in most sequestration scenarios and are apparent causes for long-term injectivity reduction in EOR WAG (water alternating with gas injection) projects. Chapter 1 reports laboratory tests on sandstone and carbonate core samples to understand end-point and transition saturations in CO<sub>2</sub>/brine systems. Gas injection into a brine saturation system to residual brine saturation with respect to gas and brine injection to a residual gas until all gas is produced were performed. The level of CO<sub>2</sub> saturation in the injected brine at reservoir pressure and temperature was varied from zero to over 90% saturation. Sandstone and carbonate rock samples were tested. In most tested cases, once CO<sub>2</sub> saturation was sufficient for a mobile gas, only limited increases in gas saturation occurred. Also, when switched to brine injection, gas saturation generally decreased only by dissolution into the brine; thus gas saturation (retention) and injectivity decreases persisted. This information is being used in CO<sub>2</sub>-EOR-WAG projects and for carbon sequestration into geological formations.

Anionic surfactants, good foaming agents, can be used in CO<sub>2</sub> foam flooding to improve high-pressure, high-density CO<sub>2</sub> reservoir sweep efficiency. In Chapter 2, kinetics and equilibrium adsorption were determined by examining adsorption behavior in a system of solid phase sandstone or limestone and of surfactant in 2 wt% brine. Parameters that effect kinetics and equilibrium on surfactant adsorption density for different solid to liquid ratios as well as surfactant concentration, rock type and state, and flow conditions are presented. Three systems were used: batch tests on crushed rock, circulation tests through core samples, and non-flow diffusion tests on brine-saturated cores. The density of an anionic surfactant adsorption on rock is best described as a function of surfactant available in the system (concentration plus volume), rather than by surfactant concentration as used by previous investigators. Experiments with solid

rock were carried out to determine surfactant capacity of the porous media through flow and non-flow rock samples and crushed rock samples. Adsorption end-points are compared for crushed sandstone, flow tests, and non-flow core samples. For limestone the crushed rock and non-flow systems were similar while the flow system was significantly lower. The time to reach equilibrium required less than one hour (generally minutes) for the crushed rock, hours to days for the flow-through tests, and weeks to over a month for the non-flow rock systems. The rate of adsorption dependent on availability (delivery) is generally much slower than the adsorption kinetics.

Results of eight series of adsorption and seven series of desorption experiments of CO<sub>2</sub> foaming surfactant CD1045 onto and from Berea sandstone, are used to develop a kinetic model for sorption in Chapter 3. Non-linear pseudo- first and second order kinetic models for adsorption and desorption processes were derived. A simplex optimization method was adapted for the calculation of kinetic parameters of these models. This method can be used for calculating not only the kinetic model parameters, but also the absolute errors between the model and the measurements, and thus the fitness of the model. Using this simplex method and the experimental results, the adsorption and desorption processes of surfactant onto and from Berea sandstone were found to follow the pseudo-second order adsorption model and pseudo-first order desorption model, respectively.

Chapter 4 report foam-coreflood tests under simulated reservoir conditions (1540 psig and 110°F). The general CO<sub>2</sub> foam flow behavior was studied using two sandstone cores 2.0 in. in diameter and 6.0 in. long, with which the optimum gas fractional flow ratio with the highest foam mobility reduction was determined. The results indicate that, for different cores, the  $f_g^*$  (critical gas fractional flow) is generally different. Even in the same core, due to the different flow rate and different foam flow mode,  $f_g^*$  may also be different. The higher the permeability and flow rate, the higher  $f_g^*$ . Three different foam flow regions were described in this study: the single phase region, the low gas fractional flow region and the high gas fractional flow region. In the single phase region, in the case of fixed CO<sub>2</sub> gas flow rate, gas mobility increases with increasing  $f_g$ . But the total mobility is independent of  $f_g$  in both fixed CO<sub>2</sub> gas flow rate and fixed CD aqueous flow rate. The gas mobility and total mobility decrease with increasing  $f_g$  in the low gas fractional flow region and increase with increasing  $f_g$  in the high gas fractional flow region.

## TABLE OF CONTENTS

DISCLAIMER .....	ii
ABSTRACT .....	iii
TABLE OF CONTENTS.....	v
LIST OF TABLES .....	vi
LIST OF FIGURES .....	viii
NOMENCLATURE .....	xii
INTRODUCTION .....	2
EXECUTIVE SUMMARY .....	5
EXPERIMENTAL RESULTS AND DISCUSSION .....	8
Chapter 1. CO <sub>2</sub> Retention and Injectivity Changes: Laboratory Tests: .....	8
Chapter 2. Effects of Flow Conditions and Surfactant Availability on Adsorption .....	28
Chapter 3. Development of Kinetic Models of a CO <sub>2</sub> -foaming Surfactant onto Berea Sandstone from Sorption Experiments .....	44
Chapter 4: Gas Mobility of CO <sub>2</sub> /Brine at Reservoir Conditions .....	63
CONCLUSIONS.....	102
ACKNOWLEDGMENTS .....	106
REFERENCES .....	107

## LIST OF TABLES

Table 1. Core Parameters .....	19
Table 2. Synthetic Brine Composition.....	19
Table 3. Flooding Parameters .....	20
Table 4. CD Adsorption by Diffusion into Brine Saturated Limestone Cubes .....	38
Table 5. CD Adsorption by Diffusion into Brine Saturated Sandstone Cubes.....	38
Table 6. CD Adsorption by Circulation of Surfactant Solution through Limestone Cores.....	39
Table 7. CD Adsorption by Circulation of Surfactant Solution through Sandstone Cores .....	39
Table 8. Adsorption Experiment Conditions .....	55
Table 9. Desorption Experiment Conditions .....	55
Table 10. Measurements of Ads. Test 1 .....	56
Table 11. Measurements of Des. Test 1.....	56
Table 12. Initials for Ads. Test 1 .....	56
Table 13. Simplex Operation Results of Ads Test 1.....	56
Table 14. Simplex Results of Ads. Tests1–8 .....	57
Table 15. Initials for Des. Test 1.....	57
Table 16. Simplex Operation Results of Des. Test 1 .....	57
Table 17. Simplex Results of Des Tests 1–7 .....	57
Table 18. The Properties of Berea Sandstone.....	83
Table 19. Experimental Methods Used in the CO <sub>2</sub> /Brine Coinjection Flooding Baseline Test ...	83
Table 20. Experimental Methods used in CO <sub>2</sub> Foam Flooding.....	83
Table 21. Summary of CO <sub>2</sub> /Brine Coinjection Baseline Experiments .....	84
Table 22. Experimental Strategy for $f_g^*$ Determination .....	85

Table 23. Comparison of Test Results with Earlier Results. <sup>125,126</sup> .....	86
Table 24. Coreflood Results used in Determining Optimum $f_g$ at Constant Total Flow Rate.....	86
Table 25. Experimental Results to Determine the Relationship between Total Motility and $f_g/(1-f_g)$ with CD Concentration of 0.05 wt% for Core SS-1. ....	87
Table 26. The Experimental Sequence for Adsorption and Desorption .....	87

## LIST OF FIGURES

Fig. 1. Coreflooding apparatus.....	20
Fig. 2. Comparison of brine production during CO <sub>2</sub> injection of two tests in Frio Core A.....	21
Fig. 3. Comparison of CO <sub>2</sub> production during brine injection for two tests in Frio Core A. ....	21
Fig. 4. Production rate of CO <sub>2</sub> during the injection of brine into Frio Core B for three different tests, each at different concentrations of CO <sub>2</sub> in the injected brine. ....	22
Fig. 5. Comparison of total CO <sub>2</sub> production rate at reservoir and ambient conditions at 37.8°C for Frio Core C.....	22
Fig. 6. Comparison of brine production during CO <sub>2</sub> injection of four tests in Indiana limestone.....	23
Fig. 7. Pressure drop versus flow rate for Indiana limestone on three different days. The indication was an decrease in permeability with time. ....	23
Fig. 8. Comparison of CO <sub>2</sub> production during brine injection for four tests in Indiana limestone.....	24
Fig. 9. Production rates for CO <sub>2</sub> at ambient conditions at a brine injection rate of 20 cc/hr in Indiana limestone.....	24
Fig. 10. Comparison of brine production versus time for both CO <sub>2</sub> injection Queen tests. One PV of injection is equal to about 38 minutes of injection. ....	25
Fig. 11. Comparison of pressure drop across the core during CO <sub>2</sub> injection versus time during brine injection for both Queen tests. One PV of injection is equal to about 38 minutes of injection.....	25
Fig. 12. Comparison of CO <sub>2</sub> cumulative production versus time during brine injection for both Queen tests. One PV of injection is equal to about 38 minutes of injection.....	26
Fig. 13. Comparison of CO <sub>2</sub> production rate versus time during brine injection for both Queen tests. One PV of injection is equal to about 38 minutes of injection.....	26
Fig. 14. Dolomite Flood 1 showing the injection and production of CO <sub>2</sub> , production of water, and differential pressure until CO <sub>2</sub> breakthrough.....	27
Fig. 15. Dolomite Flood 2 is similar to Flood 1 except production of CO <sub>2</sub> and water were recorded after CO <sub>2</sub> breakthrough. ....	27

Fig. 16. CO <sub>2</sub> saturation in several core types. For all systems, the original injection rate was about 20 cc/hr; for each Frio system it was then increased to 100 cc/hr (200 cc/hr for Frio B2h) with the indicated increase in saturation indicated by the “h”. Only for Queen was there mobile CO <sub>2</sub> .....	28
Fig. 17. Comparison of equilibrium time versus adsorption density for crushed rock, non-flow cubes, and flow-through core for limestone and sandstone systems.....	40
Fig. 18. CD adsorption density versus mass of CD available per gram of crushed limestone. ....	40
Fig. 19. CD adsorption density versus mass of CD available per gram of crushed sandstone. ....	41
Fig. 20. Comparison of CD adsorption density onto crushed limestone and solid limestone cubes, both non-flow tests. ....	41
Fig. 21. Comparison of CD adsorption density onto crushed sandstone and solid sandstone cubes, both non-flow.....	42
Fig. 22. Comparison of equilibrium time for several limestone and sandstone non-flow cube tests at 2000 ppm CD concentration. ....	42
Fig. 23. Comparison of CD adsorption density for crushed limestone and flow-through limestone core tests. ....	43
Fig. 24. Comparison of CD adsorption density for crushed sandstone and flow-through sandstone core tests.....	43
Fig. 25. Circulation experiment setup.....	58
Fig. 26 Flow-through experimental setup.....	58
Fig. 27 Simplex operations in a 2-variable case. ....	59
Fig. 28. Comparison of Ads. Test 1 and pseudo-second order modeled adsorption. ....	59
Fig. 29. Experimental results, $q_t$ , compared to pseudo-second order model calculated adsorption density, $q_c$ , in Ads Test 2-8: (a) Ads Test-2, -4, -5, and -6; (b) Ads. Test-3, -7, and -8.....	60
Fig. 30. Comparison of measured $q_t$ and modeled $q_c$ results of Des. Test 1.....	61
Fig. 31. Experimental results, $q_t$ , compared to pseudo-first order model calculated adsorption density, $q_c$ : (a) Des Test-2, 3 and 4; (b) Des. Test-5, 6 and 7. ....	62
Fig. 32. Sketches of capillary pressure and fractional-flow curves operating during a two-phase displacement. <sup>82</sup> .....	88

Fig. 33. Two foam-flow regime. <sup>121,122</sup> .....	88
Fig. 34. Schematic diagram of oil free core flooding setup.....	89
Fig. 35. Core SS-1 initial permeability with brine.....	89
Fig. 36. Core SS-2 initial brine permeability.....	90
Fig. 37. Gas mobility as a function of $fg/(1-fg)$ at constant total flow rate. ....	90
Fig. 38. Total mobility as a function of $fg/(1-fg)$ at constant total flow rate. ....	91
Fig. 39. Determination of $fg^*$ at constant gas flowrate with 110°F and 1540 psig in a fired Berea sandstone core. ....	91
Fig. 40. Determination of $fg^*$ for 0.25 wt% CD at constant N2 gas flow rate at 40°C and 1500 psig in an Indiana limestone. <sup>125</sup> .....	92
Fig. 41. Permeability effect on $fg^*$ for 0.25 wt% CD at 22 cc/hr constant N2 gas flow rate at 40°C and 1500 psig. <sup>125</sup> .....	92
Fig. 42. Plot total mobility as a function of $fg$ at a constant total flow rate. ....	93
Fig. 43. Schematic graph to determine the optimum $fg$ with the maximum MRF. ....	93
Fig. 44. Plot of total mobility as a function of $fg/(1-fg)$ at a constant CO <sub>2</sub> flow rate.....	94
Fig. 45. Plot of relationship between total mobility and ratio of gas to liquid fractional flow $fg$ , at a constant CD solution flow rate of 10 cc/hr.....	94
Fig. 46. Schematic representation of $fg^*$ reduction owing to a reduction in surfactant concentration at the constant CO <sub>2</sub> flow rate of 40cc/hr for Core SS-2.....	95
Fig. 47. Plot of CO <sub>2</sub> gas mobility as a function of $fg$ in CO <sub>2</sub> /brine co-injection baseline test at a total flow rate of 100 cc/hr in Core SS-2 with T=110° F and P =1540 psig.....	95
Fig. 48. Plot of N2 gas mobility as a function of $fg$ in N2/brine co-injection baseline test at a total flow rate of 100 cc/hr in a limestone with T=105° F and P =1500 psig.....	96
Fig. 49. Plot of gas mobility and total mobility as a function of total flow rate of CD/ CO <sub>2</sub> with fixed $fg$ for Core SS-2 at T=110° F and P =1540 psig. ....	96
Fig. 50. Gas mobility as a function of gas fraction flow for 0.25 wt% CD at 104°F and 1500 psig in limestone. <sup>126</sup> .....	97

Fig. 51. Total mobility as a function of gas fraction flow for 0.25 wt% CD at 40°C and 1500 psig in limestone. <sup>126</sup> .....	97
Fig. 52. CD adsorption profile for Core SS-1, concentration of 0.05% at 110°F and 1540 psig. ....	98
Fig. 53. CD adsorption profile for Core SS-2, concentration of 0.05 wt% & 0.25wt% at 110°F and 1540 psig. ....	98
Fig. 54. IFT test results for one foaming sample and one non-foaming sample.....	99
Fig. 55. Core SS-2 retention density of CD surfactant during the co-injection of CO <sub>2</sub> and CD solution of 0.25 wt% concentration at 110°F and 1540 psig.....	99
Fig. 56. CD adsorption profiles for Core SS-2. ....	100
Fig. 57. CD desorption profile for Core SS-2.....	100
Fig. 58. Equivalent CD retention density decreased from Core SS-2 with CD surfactant recovery during the desorption phase. ....	101

## NOMENCLATURE

BR = Brine

BPR = Back Pressure Regulator

CD = Chaser CD 1045<sup>TM</sup>

CLS = calcium lignosulfonate

CMC = Critical Micelle Concentration

CO<sub>2</sub> = carbon dioxide

CSG = co-injection of water and gas

Cc = cubic centimeter

CW = distilled water

ID = inside diameter

IFT = interfacial tension [mN/m]

OD = outside diameter

SAG = surfactant solution alternating with gas

WAG = water alternating with gas

A = cross-sectional area of the core [cm<sup>2</sup>]

C/C<sub>i</sub> = normalized concentration, fraction

dp = pressure drop [psi]

dp/ds = pressure gradient [psi/cm]

f<sub>g</sub> = gas fractional flow, fraction

f<sub>g</sub><sup>\*</sup> = critical gas fractional flow, fraction

K = permeability [md]

LS = limestone

MMP = minimum miscibility pressure

N<sub>2</sub> = nitrogen

P<sub>c</sub> = capillary pressure

P<sub>c</sub><sup>\*</sup> = limiting capillary pressure

P<sub>in</sub> = core inlet pressure [psig]

P<sub>out</sub> = core outlet pressure [psig]

PV = pore volume, fraction

$q_g$  = gas flow rate [cc/hr]  
 $q_t$  = total flow rate [cc/hr]  
 $q_l$  = liquid flow rate [cc/hr]  
SS = sandstone  
 $S_w$  = liquid saturation  
 $u_g$  = gas darcy velocity [cm/sec]  
 $u_w$  = aqueous darcy velocity [cm/sec]  
 $\rho$  = fluid densities [g/cm<sup>3</sup>]  
 $A_{ds}$  = CD adsorption density, mg surfactant/g rock  
 $C_i$  and  $C_r$  = initial and residual CD concentration in solution, ppm  
 $M_s$  = mass of the solution, g  
 $M_c$  = mass of the core sample, g  
 $A_{ds_i}$  = adsorption density after i-number of measurements, mg/g  
 $M_t$  = total initial mass of surfactant in the system, mg  
 $M_s$  = total initial mass of surfactant solution, g  
 $\Sigma \{m_{s_i}\}$  = sum of surfactant mass removed during sampling, mg  
 $\Sigma \{m_{l_i}\}$  = sum of surfactant solution mass removed during sampling, g  
 $C_{r_i}$  = residual concentration after i measurements, ppm  
 $M_c$  = mass of the core sample, g.  
 $A_i$  = surfactant in the rock and tubing at the  $i^{th}$  step, mg  
 $C_0$  = initial surfactant concentration of desorption, mg/l  
 $C_i$  = surfactant concentration at the  $i^{th}$  step, mg/l  
 $f$  = simplex function, mg/g  
 $i$  = index  
 $j$  = index  
 $k_{a1}$  = pseudo 1<sup>st</sup> order adsorption kinetic coefficient, h<sup>-1</sup>  
 $k_{a2}$  = pseudo 2<sup>nd</sup> order adsorption kinetic coefficient, g/(mg •h)  
 $k_{d1}$  = pseudo-first order desorption kinetic coefficient, h<sup>-1</sup>  
 $k_{d2}$  = pseudo-second order desorption kinetic coefficient, g/(mg •h)  
 $M$  = total number of measurements  
 $M_i$  = surfactant left in pore and tubing at the  $i^{th}$  step, mg

$n$  = number of simplex variables

$N$  = total steps of measurements at present

$PV$  = volume of the pore space and tubing, l

$q$  = surfactant adsorption density, mg/g

$q_0$  = initial adsorption density in desorption process, mg/g

$q_{cj}$  = calculated adsorption density from models, mg/g

$q_e$  = adsorption density at equilibrium, mg/g

$q_i$  = surfactant adsorption density at the  $i^{th}$  step, mg/g

$q_r$  = residual adsorption density in desorption process, mg/g

$q_{ij}$  = measured adsorption density in experiments, mg/g

$t$  = time, h

$Ve_i$  = effluent volume at the  $i^{th}$  step, l

$V_i$  = total surfactant solution volume at the  $i^{th}$  step, l

$W$  = mass of the rock specimen, g

$x, X$  = simplex variable

$\lambda$  = simplex contracting coefficient,  $0.0 < \lambda < 1.0$

$\mu$  = simplex expanding coefficient,  $1.2 < \mu < 2$

## INTRODUCTION

The objectives of this study are to acquire the information required to develop adsorption/desorption models for reservoir rock at reservoir conditions, to determine economic sweep efficiency/injectivity criteria for reservoir scale systems, to expand foam gas flooding to shallow reservoirs, and to develop models and modules for simulating CO<sub>2</sub> flooding mechanisms. This work devotes considerable energy to laboratory measurements to determine practical information for designing gas foam systems for a wide range of reservoir types; thus, through cost-effective and environmentally attractive means, adding to recoverable oil reserves in the US.

**Expected Improvements over Existing Technologies:** Despite favorable features of CO<sub>2</sub> flooding for EOR,<sup>1</sup> CO<sub>2</sub> flooding frequently suffers from poor sweep efficiency, high CO<sub>2</sub> utilization rate, the high cost of handling and recycling produced CO<sub>2</sub>, low oil productivity due to lower-than-expected injectivity, and limited application in reservoirs that cannot be operated at pressures at or above the MMP.<sup>2</sup>

Poor sweep efficiency and high CO<sub>2</sub> utilization rate result from a high mobility ratio caused by the low viscosity of CO<sub>2</sub> compared to that of water or oil. The effectiveness of WAG for mobility control during CO<sub>2</sub> flooding is adversely influenced by gravity segregation between water and CO<sub>2</sub>, and amplified by permeability contrasts. Foaming agents injected in the aqueous phase help control mobility. However, increased costs due to the adsorption of expensive chemicals onto reservoir rocks has limited the application of this technique. Foam quality, temperature, pressure, CO<sub>2</sub> injection rate and total injected volume each affects the ultimate oil recovery.<sup>3-5</sup> It is, therefore, advantageous to develop systems with lower concentrations of good foaming agents that will reduce the cost of using these agents. These systems are derived using a sacrificial agent; that is, a co-surfactant that reduce adsorption loss and/or concentration of the good foaming agent without reducing the effectiveness of the foam. In core tests the system of CD1045 with lignosulfonate reduces the pressure drop (increases the injectivity) while maintaining equally good sweep efficiency.<sup>3,6,7</sup> The combination of these two agents in small core tests appears to indicate that they could be tailored to vary injectivity, sweep efficiency, and sensitivity to oil saturation.<sup>3,6</sup>

To aid in predicting utilization of surfactant adsorption on pure minerals (silica, calcite, dolomite, kaolinite, and bentonite) that are common reservoir rock components, studies were performed to determine surfactant adsorption and desorption quantities, rates, mechanisms, and effects of physical parameters such as temperature, pressure, brine and surfactant composition and concentration, and pH on various rock components.<sup>7-11</sup> Work in this area will continue, particularly in determining adsorption values versus specific surface areas of the mineral to determine sweep efficiency in a homogeneous system. These results are required to develop models to be used in numerical simulation to predict usage in a reservoir.

WAG often reduces injectivity more than expected and the addition of mobility control agents inherently increases the severity of this problem. Any resistance increases the pressure drop, and therefore decreases injectivity.<sup>3,13</sup> Improved mobility control will reduce injectivity; thus, for this purpose, it is critical that the two be optimized. Causes of injectivity reduction that have been identified in ascending order of severity and amenability to remediation are: contamination, gas saturation, dissolution, and precipitation.<sup>6,7</sup>

**Scientific and Technical Basis and Merit:** Previous laboratory and field tests have confirmed the effectiveness of CO<sub>2</sub>-foam for mobility control and fluid diversion. Areas of progress in the past include:

- Identification of foam strength in high pressure CO<sub>2</sub> systems,<sup>7,14</sup>
- Identification of properties that affect foaming agent adsorption in a porous medium: rock type,<sup>16</sup> surfactant type,<sup>14</sup> surfactant concentration,<sup>14</sup> and co-surfactants,<sup>7,15</sup>
- Identification of co-surfactants and sacrificial agents,<sup>3,7,16</sup>
- Effects of heterogeneity with and without capillary contact,<sup>17</sup>
- Identification of a number of systems with varying degrees of selective mobility reduction,<sup>17</sup>
- Development of models to predict reservoir response to the identified foam systems, and
- Several successful field tests.<sup>3,7,17-27</sup>

**Benefits:** Project results will significantly benefit the future of gas injection EOR. Parameters will be determined that will result in improved sweep efficiency with better understanding of injectivity changes, assessing low pressure reservoir gas injection EOR potential, and some

applicable simulation modules for incorporation into existing simulators. Anticipated benefits include:

- Surfactant cost reduction: optimizing sacrificial agent and high quality foaming surfactant mixtures, and decreasing primary foaming agent adsorption and required concentration,
- Extending the life of the petroleum reservoir, maintaining or increasing employment, and increasing oil recovery,
- Expanding CO<sub>2</sub> flooding to low pressure reservoirs,
- Delayed production of CO<sub>2</sub> and increased retention of CO<sub>2</sub> in the reservoir (carbon management),
- Improved injectivity of CO<sub>2</sub> and water,
- Enhanced CO<sub>2</sub> flooding predictions, and
- Decrease of CO<sub>2</sub> mobility during the alternating injection of brine and CO<sub>2</sub>.

Carbon dioxide flooding potential has been effectively demonstrated in the US, particularly in the Permian Basin of west Texas and southeast New Mexico. Much of the research on CO<sub>2</sub> flooding can be applied to other gas flooding processes. Today almost 350,000 BOPD are being produced by gas injection in the US; ~70% of this oil or nearly 240,000 BOPD is from CO<sub>2</sub> injection projects.<sup>28</sup> With recent oil prices above \$60 per barrel, this oil production signifies over \$7 billion less in imports each year, and provides a significant number of domestic jobs as well. Out of the 350 billion barrels remaining in US oil reserves, the amount of oil presently produced by CO<sub>2</sub> flooding barely scratches the surface of this resource. The potential recovery is at least an order of magnitude greater.

Moderately successful future research will maintain current production rates, whereas good to excellent success in research, expanding market availability of CO<sub>2</sub> and/or sequestration incentives have the potential of increasing CO<sub>2</sub> use in EOR by severalfold. The potential is easily several billion dollars each year in reduced foreign imports and maximization of US resources.

## **EXECUTIVE SUMMARY**

This is the Second Annual Report on the project, “Improved Gas Flooding Efficiency,” Department of Energy (DOE) Contract No. DE-FC26-04NT15532. This project focuses on laboratory studies with related analytical and numerical models to enhance our understanding and capabilities for more efficient enhanced oil recovery (EOR). To date there have been 15 publications in referred journals and/or international meeting proceedings related to this work during the time of this contract that have been wholly or partially funded by this project.<sup>29-43</sup>

There is increasing pressure to inject gases into geological formation for greenhouse gas sequestration and to maximize hydrocarbon reserves using advanced techniques such as CO<sub>2</sub> injection. Thus a need exists to understand the formation and propagation of injected CO<sub>2</sub> plumes. The development of CO<sub>2</sub> plumes and subsequent dissolution into formation brine are essential mechanisms in most scenarios and are the subject of Chapter 1.

Relatively short cores (5.71 to 8.17 cm long and about 3.8 cm in diameter) were used in these tests and therefore care must be taken when extrapolating results to reservoir scale. Two sandstones were considered, Frio and Queen, and two carbonates, limestone and dolomite samples. Only in the Queen core was free CO<sub>2</sub> produced from the core during displacement of CO<sub>2</sub> by brine injection with end-point brine saturation. These findings of end-point saturation are significant parameters in determining flow patterns, retention rates, and injectivity changes and their longevity that will enable improved predictions of CO<sub>2</sub> behavior in reservoirs for EOR and/or sequestration considerations.

It was found that 0.2 to 0.3 PV fraction of free-phase CO<sub>2</sub> saturation was required to establish a CO<sub>2</sub> flow path, after which there was little brine production except through evaporation, which is a slow process. The CO<sub>2</sub> saturation can be increased by increasing flow rate, reducing pressure, and water evaporation. At the end of CO<sub>2</sub> injection there is relatively low CO<sub>2</sub> saturation and high brine saturation in the core; thus no reduction in CO<sub>2</sub> saturation was required to return to brine flow. Only in the Queen sand was free CO<sub>2</sub> produced during brine injection. Brine is equilibrated with CO<sub>2</sub> in a short time frame over a relatively short distance. Only when a channel was formed was brine produced that was not saturated with CO<sub>2</sub> while a significant residual CO<sub>2</sub> remained in the core. The injection of brine into a 100% CO<sub>2</sub> phase required 0.2 to 0.3 PV fraction saturation to establish a brine flow path. Finally, the sandstone and carbonate systems initially performed similarly. This was changed when through dissolution of the rock

matrix a solution channel was formed in the limestone, creating a dominant flow path that significantly altered the flow behavior of the core.

Chapter 2 relates the performance of tests to determine sorption kinetics. Values of CD adsorption density on crushed and non-flow solid limestone cubes were found to be the same and best described as a function of surfactant availability (mass of surfactant available per mass of solid) in the system. The shape of the adsorption isotherms on crushed sandstone, comparing surfactant availability with adsorption density, suggests that the slopes and possibly the density plateau depend on surfactant concentration and availability. The adsorption time dynamic depends on the state of solid and flow conditions. Time to reach equilibrium in non-flow core volumes was an order of magnitude greater compared to the circulation experiment, and 3 orders of magnitude greater compared to the crushed rock. Thus the rate of adsorption is dependent on the availability of surfactant, with the kinetics and equilibrium being comparably very rapid. When comparing flow versus non-flow systems in cube or core samples, the adsorption density on limestone underwent a significant decrease due to the flow in porous media while adsorption density on sandstone remained the same. This might be an indication of different adsorption mechanisms and/or energy levels that occur on limestone and sandstone surfaces. Tests such as heats of adsorption that are planned for the future should shed some light on the cause of these differences. These results should be considered when determining reservoir adsorption requirements.

Chapter 3 summarizes the modeling work to date on the sorption of surfactants in core. The pseudo- first and second order kinetic models for adsorption and desorption were derived in a mathematically complete format. These models are nonlinear. The adsorption models have two unknown parameters, and the desorption models have three unknown parameters. A simplex nonlinear optimization method was adapted for the determination of the unknown parameters for these kinetics models. This algorithm can be applied to determine not only the parameters of these nonlinear models, but also the absolute error between the model and the measured results. The adsorption and desorption processes of surfactant onto and from Berea sandstone were found to obey pseudo-second order adsorption model and the pseudo-first order desorption models, respectively. More experimental work under different conditions will be carried out to better understand the influences of different factors on the sorption processes.

In the final chapter (Chapter 4), gas mobility of CO<sub>2</sub>/brine was determined at reservoir conditions, using the gas fractional flow ( $f_g$ ) concept. The total mobility of CO<sub>2</sub>/brine increases with increasing  $f_g$  ranging from 0.6 to 0.9; but decreases with increasing  $f_g$  when  $f_g$  is less than 0.6. Total mobility (and or gas mobility) as a function of  $f_g$  is characterized by three intersected straight lines with two crossed points of  $f_g^0$  and  $f_g^*$ . Three foam flow regions are described in this study: a single phase region, a low gas fractional flow region and a high gas fractional region. In the single phase region, in the case of a fixed CO<sub>2</sub> gas flow rate, the gas mobility increases with increasing  $f_g$ . But total mobility is independent of  $f_g$  whether with a fixed CO<sub>2</sub> gas flow rate or a fixed surfactant solution aqueous flow rate. In the low gas fractional flow region, the gas mobility and total mobility decreases with increasing  $f_g$ . In the high gas fractional flow region, the gas mobility and total mobility increases with increasing  $f_g$ . For different cores, the  $f_g^*$  is generally different. Even in the same core, due to different flow rates and different foam flow mode,  $f_g^*$  may also vary. The higher the permeability and flow rate, the higher the  $f_g^*$ . The mobility reduction factor for Berea core reaches maximum at  $f_g=0.6$  and  $f_g =0.8$ , respectively. Gas mobility and foam mobility increases with increasing of total flow rate if the foam flow is shear thinning. During CO<sub>2</sub> foam flooding, with surfactant solution of 0.05 wt% concentration, it was difficult to establish adsorption equilibrium. Exploration of the reason for this would be an important task for future work. The adsorption/desorption of the surfactant are characterized as a rapid short period of adsorption/desorption to/from the rock surface followed by a long period of slow adsorption/desorption. The adsorption of surfactant onto rock increases with the occurrence of foam. Surfactant solution with a higher concentration will reach adsorption equilibrium in the core faster than it will with a lower concentration.

Each of these concepts is used to improve EOR by gas injection into oil reservoirs. Our understanding of the mobility and injectivity of CO<sub>2</sub> has room for improvement; these concepts can and should be used to improve the efficiency and ultimately economical recovery of hydrocarbons.

## EXPERIMENTAL RESULTS AND DISCUSSION

### Chapter 1: CO<sub>2</sub> Retention and Injectivity Changes

#### Introduction

The apparent consequences of increased greenhouse gas emissions will encourage increased carbon dioxide (CO<sub>2</sub>) injection into oil reservoirs for enhanced oil recovery (EOR) and encourage injection into other geological formations for sequestration.<sup>13</sup> The development of CO<sub>2</sub> plumes and their subsequent dissolution into formation brine are essential mechanisms in most sequestration scenarios and could aid in understanding long-term injectivity reduction in EOR WAG (water alternating with gas injection) projects. This paper describes laboratory tests on sandstone and carbonate core samples. Two types of displacement tests were performed; gas injection to a residual brine saturation with respect to gas, followed by brine injection to a residual gas with respect to brine. The level of CO<sub>2</sub> saturation in the injected brine at reservoir pressure and temperature was varied from zero to over 90% saturation. Sandstone and carbonate rock samples were tested. This variation in CO<sub>2</sub> saturation in the injected brine determined the effect on the CO<sub>2</sub> saturation or plume size in the core. This information can be used in CO<sub>2</sub>-EOR-WAG projects and for carbon sequestration into geological formations.

Injecting CO<sub>2</sub> into brine-saturated sandstone and carbonate core resulted in brine saturation reduction of 62 to 82% in the various tests. In each test, over 90% of the reduction occurred with less than 0.5 PV of CO<sub>2</sub> injected, with very little additional brine production after 0.5 PV of CO<sub>2</sub> injected. During brine injection, CO<sub>2</sub> production was equivalent to the rate expected from brine saturated with CO<sub>2</sub> at reservoir conditions, except for the first ~0.1 PV of the Queen Sandstone CO<sub>2</sub> production. This indicates that in each core at high end-point brine saturation at the tested flow rate (~2 m/day) the CO<sub>2</sub> plume was reduced through dissolution, not displacement. With increasing CO<sub>2</sub> saturation in the injected brine, the brine volume required to remove (dissolve) the CO<sub>2</sub> plume increased proportionally. Results from these experiments will be used to aid in predicting injectivity in CO<sub>2</sub>-EOR-WAG operations and CO<sub>2</sub> plume migration and CO<sub>2</sub> dissolution in EOR and sequestration.

Residual CO<sub>2</sub> saturation is suspected to be a significant factor for reducing injectivity during many water alternating with gas (WAG) processes for CO<sub>2</sub> EOR projects.<sup>13</sup> Also, there is

increasing interest in minimizing CO<sub>2</sub> (greenhouse gas) emissions by sequestering CO<sub>2</sub> in depleted oil and gas reservoirs or in saline aquifers.<sup>44</sup> The interest in increasing CO<sub>2</sub> injection into geological formations has aroused the awareness of the need for a better understanding of the mechanisms and extent of CO<sub>2</sub> plume development and its subsequent dissolution into formation brine. This paper describes laboratory tests on Frio and Queen Sandstones, Indiana limestone, and Lockport dolomite. Several types of displacement tests were performed; gas injection into a core until no additional free brine was produced (thus to a pseudo-residual brine saturation with respect to gas injection), followed by brine injection into a core partially saturated with gas. The level of CO<sub>2</sub> saturation in the injected brine at reservoir pressure and temperature was varied from zero to over 90%. The CO<sub>2</sub> saturation in the injected brine was varied to determine the effect on the CO<sub>2</sub> saturation or plume size in the core.

Determination of CO<sub>2</sub> saturation in a core was sought after injection of CO<sub>2</sub> into a core that was originally saturated with brine. This was then followed by the injection of brine into the core while differentiating brine displaced by free-phase CO<sub>2</sub> versus producing CO<sub>2</sub> dissolved in brine. Currently in the field, CO<sub>2</sub> is being injected into reservoirs nearing their waterflood economic limit and into aquifers; thus CO<sub>2</sub> is being injected into geological formations containing high brine saturation. To aid in conformance control and reduce the amount of CO<sub>2</sub> required for injection, CO<sub>2</sub> and water are alternately injected into oil reservoirs. Also, geologic carbon sequestration is being proposed that calls for the injection of large quantities of CO<sub>2</sub> into innumerable aquifers. Thus tests are required for both the understanding of how brine and CO<sub>2</sub> streams flow through porous media and how their mutual solubilities change their saturations with time.

## **Experimental**

### **Material**

Frio cores used in these tests were obtained from depths of 2493, 2496.6, and 2497.8 m in the Felix Jackson # 62 Well, located south of the S. Liberty DOE CO<sub>2</sub> pilot site in Chambers County, Texas. These cores were selected because they were consolidated sandstone (see Frio core parameters listed in Table 1). The DOE carbon sequestration test site south of Houston is at a shallower depth and the test horizon is in poorly consolidated rock. These tests were performed

in the consolidated core to simplify the development of test procedures. Table 2 lists the composition of the synthetic brine used in these tests, which is intended to represent the Frio reservoir brine. Indiana limestone is from a quarry near Victor, Indiana. The parameters for this core are also listed in Table 1. More details of the Frio sandstone and Indiana limestone are found in an earlier publication.<sup>32</sup> The Queen sandstone core used in these tests was obtained from the West Pearl Queen Field in southeast New Mexico, Stevison Federal well #1 at 1375.0 m. The permeability was measured at 21.61 md by mini-permeameter estimation (+/- 5.86). The whole core permeability was then determined by brine injection to be 15 md before the first test and 17 before the second test. Both compare well with mini-permeameter tests performed using air; one on the whole core and the other at the end of the core and the other on the whole core. Other parameters are found in Table 1 with the brine used listed in Table 2. The dolomite core is Lockport dolomite. The core parameters and brine are listed in Table 2.

### **Core Flooding Apparatus**

The core flooding apparatus is located in a temperature-controlled air bath, with a syringe pump and separator system outside the air bath (see Fig. 1). The dead volume of this system (non-flow path volume) and non-core volume (determined to be 4.3 cc) was minimized by reducing the number of pressure control devices, pressure transducers, and valves in the system. All the cores were prepared by wrapping them longitudinally in a lead (Pb) foil, which functioned as a diffusion barrier between the core and the overburden sleeve. In this way the diffusion of CO<sub>2</sub> from the core into the overburden fluid is minimized and the mass balance is optimized. During the analysis, care was taken to capture all the water using an ambient condition separator (liquid trap) to catch the brine/water and a salt breaker (vapor trap) to capture water vapor. For a volume check the liquid and vapor traps were weighed before and after each test and in a couple of cases at an intermediate point. The wet-test meter was used to determine gas production at ambient conditions. Included in the gas calculations were corrections for gas displaced by brine/water in the separator.

### **Test Procedures**

Frio sandstone tests were performed at the reservoir conditions of about 62.8°C (145°F) and 15.3 MPa (2200 psig), except for two comparison tests at 37.8°C (100°F) that will be described later.

The overburden pressure was maintained at 27.7 MPa (4000 psig). The brine was prepared with the composition indicated in Table 2. In some cases the brine had CO<sub>2</sub> dissolved in it to represent brine that had been in contact with CO<sub>2</sub>. The brine was indicated as dead brine (no dissolved CO<sub>2</sub>), 50% CO<sub>2</sub>-brine (brine saturated to about 50% CO<sub>2</sub>), and 90% CO<sub>2</sub>-brine (brine saturated to about 90% CO<sub>2</sub>). Brine saturated to 100% CO<sub>2</sub> was not used, to ensure no new free CO<sub>2</sub> occurred from CO<sub>2</sub> evolving from the brine. Pressure drop across the core and/or dissolved solid changes in the brine due to dissolution of core material or water vaporizing into the CO<sub>2</sub> phase could perturb brine 100% saturated with CO<sub>2</sub> and result in small but undesirable amounts of free CO<sub>2</sub> forming from the injected fully saturated brine.

In all but one case the coreflood was initiated in core 100% saturated with dead brine. Dehydrated CO<sub>2</sub> was then injected into the core until no free brine was produced for several PV. The CO<sub>2</sub> was stored outside the air bath at ambient temperature and injected at rates from 10 to 200 cc/hr (20 cc/hr was used unless otherwise indicated) at ambient temperature and about 15.3 MPa. The CO<sub>2</sub> injection volume at 63°C was about 65% higher than at ambient temperature; both at 15.3 MPa. The temperature of the air bath, core, and injection pump were recorded. The head plus end volume of the core system is 4.3 cc; thus in Figs. 2, 3, 5, 6, and 8 the volumes are shown starting at -4.3 cc.

All Indiana limestone tests were performed at about 37.8°C (100°F) and pore pressure of about 15.2 MPa (2200 psig). In the first four tests the core was initially saturated with dead brine and displaced with CO<sub>2</sub> until no free water was being produced, usually requiring 2–3 PV after the last production of free water was detected. In all but the third tests, the CO<sub>2</sub> injection rate was 20 cc/hr at room temperature or about 21.7 cc/hr at core conditions. In series three the injection rate was initially 21.7 cc/hr and then was increased incrementally to 43.4, 86.8, and 130.2 cc/hr.

All Queen tests were performed at reservoir conditions of about 35°C (95°F) and 14.5 MPa (2100 psig). The overburden pressure was maintained at 21.5 MPa (3100 psig). The brine was prepared with 220,000 ppm NaCl with no dissolved CO<sub>2</sub> before injection into the core. In each test the core was initially 100% saturated with dead brine. Dehydrated CO<sub>2</sub> was then injected into the core until no free brine was produced for several pore volumes (PV). The CO<sub>2</sub> was stored outside the air bath at ambient temperature and injected at 20 cc/hr at ambient temperature and about 14.5 MPa. The CO<sub>2</sub> unit volume at 35°C was about 8% higher than at ambient

temperature or a lower density; both at 14.5 MPa. There is a slight reduction in permeability indicated from 17 to 15 md before and after the first test series.

The Lockport dolomite tests were performed at room temperature, which varied from 18° to 23°C (65° to 73°F) and elevated pressures from 24.2 to 28.7 MPa (3500 to 4142 psia), see Table 2. The overburden pressure was maintained at about 34.6 MPa (5000 psig). The core was initially 100% saturated with dead water (degassed, distilled water). CO<sub>2</sub> was injected at 20 cc/hr into the core until free brine production had essentially stopped. Though water production does continue as water vapor in the produced CO<sub>2</sub>, it is at a slow rate.

## **Discussion of Results**

### **Results – Frio Sandstone**

Figure 2 compares two tests of CO<sub>2</sub> displacing brine in Frio Core A. In both about 7 cc of brine was produced before CO<sub>2</sub> breakthrough. After CO<sub>2</sub> breakthrough there was a small quantity of brine produced and then brine production stopped except for water dissolved in the CO<sub>2</sub>. Usually over 95% of the brine production occurred before 1 PV of CO<sub>2</sub> had been injected. Any continued production after less than 1 PV of CO<sub>2</sub> had been injected was from vaporized water. The salt vapor trap (Fig. 1) was weighed only at the end of the test and this value was added evenly over the duration of the test scaled to the injection rate in the brine/water production plots. The time when the vapor was actually produced is not known. In Fig. 2 the first system had an injection rate increase from 20 to 100 cc/hr after 200 cc of CO<sub>2</sub> had been injected. Additional free brine was produced following the injection rate increase. During the second test, injection was continued overnight at a reduced injection rate of 10 cc/hr and then increased to 100 cc/hr for a short time at the end of the test.

In each case the saturations reached what might be considered stable pseudo-end point saturation. However this stable saturation changed by increasing the flow rate, decreasing pressure, and by evaporating water. What is the definition of an end point or residual water saturation? For this report it will be referred to as a pseudo-end point. After completion of CO<sub>2</sub> injection, brine was injected into the core to displace the CO<sub>2</sub>. Figure 3 compares the first two brine injection tests, which used dead brine in Frio Core A after CO<sub>2</sub> injection in each test (see Fig. 2). In each about 4.3 cc of reservoir condition CO<sub>2</sub> was produced (the same as the end plate

dead volume); the CO<sub>2</sub> production rate then decreased significantly. After this change in production rate, approximately 4 to 5 cc of additional CO<sub>2</sub> at reservoir condition were produced at a fairly constant rate. Using values from Wiebe and Gaddy<sup>45</sup> adjusted for dissolved solids,<sup>46</sup> these rates are what would be expected from CO<sub>2</sub> dissolved in Frio brine fully saturated with CO<sub>2</sub> at the test conditions. The CO<sub>2</sub> produced after the dead volume was produced was not a free phase. The final value of produced CO<sub>2</sub> from the system, including blowdown to ambient pressure, was equal to the brine produced during CO<sub>2</sub> injection; thus a good material balance was obtained throughout the experiments.

The second set of experiments was performed on Frio Core B. In this set the tests used the same procedure as for Frio Core A, except that CO<sub>2</sub> dissolved in the injected brine varied from 0 to 90% of CO<sub>2</sub> saturation. In each case the production rate of CO<sub>2</sub> in cc/cc of brine produced was around 24. This was what would be expected from saturated brine. Figure 4 compares the production rate of CO<sub>2</sub> during the injection of brine into Frio Core B during three different tests. Excluded in Fig. 4 was the first PV of brine injection where the production of free CO<sub>2</sub> was occurring, which exceeded 150 cc/min during free-phase CO<sub>2</sub> production. Each of the three tests shown in Fig. 4 followed the injection of CO<sub>2</sub> into the core saturated with dead brine. The three tests differ in the concentration of CO<sub>2</sub> in the injected brine. During the early time period the production rates are essentially equal for all three scenarios. The brine produced from this 6.1 cm core was saturated with CO<sub>2</sub> and did not depend on the CO<sub>2</sub> concentration of the injected brine. Thus the brine was saturated with CO<sub>2</sub> over a relatively short flow path.

The injection test using 90% CO<sub>2</sub>-brine was not continued until free CO<sub>2</sub> was depleted in the core as in the other two cases. Injection and production continued long enough to verify the production rate of CO<sub>2</sub> during the first part of the injection. As shown in Fig. 4, CO<sub>2</sub> depletion in the core during the dead brine injection shows a rapid decline in the CO<sub>2</sub> production rate after most of the CO<sub>2</sub> had been produced. In the 50% CO<sub>2</sub>-brine the drop is slower and as might be expected the system stabilizes at a rate of about 3 cc/min, which is the same as the content of the brine being injected. When the pressure was released on the 50% CO<sub>2</sub>-brine system the produced CO<sub>2</sub> was equal to about that which would be evolved from 1 PV of brine saturated to 50% CO<sub>2</sub>, indicating that all the free-phase CO<sub>2</sub> had been removed.

The production of CO<sub>2</sub> during the injection of 50% CO<sub>2</sub>-brine at 37.8 and 62.8°C were similar, but the lower temperature appeared to be about 10–15% higher. This compares well with

the higher solubility of CO<sub>2</sub> in brine at lower temperatures. The final set of Frio tests was in core C. Figure 5 has an expanded production rate scale to demonstrate the rate comparison during free-phase CO<sub>2</sub> production and production evolving from CO<sub>2</sub> dissolved in brine at reservoir conditions. In these tests the first step was started with a dry core. This was then saturated with 100% dehydrated CO<sub>2</sub>; then dead brine was injected into the core. In this test about 9 cc of CO<sub>2</sub> at reservoir conditions were produced before production stabilized. This rate was equal to that of CO<sub>2</sub> evolved from brine saturated with CO<sub>2</sub> at 37.8°C and 15.2 MPa and 20 cc/hr flow rate. Then an additional 11 cc (reservoir conditions) of CO<sub>2</sub> were produced at a rate of about 8 cc/min at ambient conditions. This totals 20 cc of produced CO<sub>2</sub>. Subtracting the 4.3 cc dead volume yields 16 cc or almost 90% of the 18.1 cc core PV. Another 2 cc were produced during the remaining injection period and subsequent blowdown. This test required about 4 cc of brine or 0.22 PV to establish a brine flow path. Shortly after brine breakthrough, it appears that only CO<sub>2</sub> dissolved in the brine was produced.

### **Results – Limestone**

Several tests on Indiana limestone were conducted using the same procedure used for the Frio sandstone. All tests were performed at about 37.8°C and pore pressure of about 15.2 MPa. In the first four tests the core was initially saturated with dead brine and displaced with CO<sub>2</sub> until no free-phase water was being produced; usually requiring 2–3 PV after the last production of free-phase water was detected. In all but the third tests, the CO<sub>2</sub> injection rate was 20 cc/hr at room temperature and core pressure, or about 21.7 cc/hr at core conditions. In the third series the injection rate was initially 21.7 cc/hr and then increased incrementally to 43.4, 86.8, and 130.2 cc/hr while the incremental produced water was 7.8, 0.3, 0.1, and 0.1 cc, respectively. Again, the first 4.3 cc produced was from the line volume resulting in brine production from the core of about 4.0 cc and vapor production caught in the salt trap of 1.4 for a total of about 5.4 cc of brine from the core. The brine/water production in the third test is compared to the other three tests in Fig. 6. There is a contrast of the production at similar injection rates between the first two and last two tests of almost 1 cc (Fig. 6). This is believed to be due to the formation of a solution channel in the limestone core.

In Fig. 7, a comparison of flow tests at three different times during these tests indicates a permeability change (increase). As the number of tests and PV of fluid injected into the core

increased, the pressure drop versus flow rate increased. This is an indication that the core permeability was decreasing with time or PV of fluid injected. Tests performed after the last test indicated almost no pressure drop at all tested flow rates (20–200 cc/hr), indicating a very high permeability. In earlier tests with limestone, total core permeability increased over time until a solution channel through the core had been formed, and then the permeability drastically increased.<sup>47,48</sup> In each case there had been plugging or deposits advancing ahead of the solution channel.

Figure 8 compares the reservoir volumes of CO<sub>2</sub> produced for each test during the injection of brine. For Tests 1 and 2 dead brine was injected and for both there was a good material balance. For Tests 3 and 4, a 50% CO<sub>2</sub> saturated brine was injected. Again in both cases there was a good material balance, but a decrease in CO<sub>2</sub> production. This is also shown in Fig. 9 where the production rate in the later tests dropped before the free CO<sub>2</sub> was dissolved and produced. Indicating the brine was not being saturated when a channel formed. In Tests 1 and 2 the core had very little CO<sub>2</sub> remaining at blowdown. For Tests 3 and 4 the production dropped much more quickly to the baseline for the 50% CO<sub>2</sub>-brine and at blowdown both had significant amount of CO<sub>2</sub> remaining. Test 4 had almost 3 cc compared to about 1 cc remaining in Test 3 (Fig. 8). It is believed that the difference is due to the formation of the solution channel, where most of the flow bypassed the bulk of the core.

### **Results - Queen**

Figure 10 compares two tests of CO<sub>2</sub> displacing brine in the West Pearl Queen Core. In both just over 9 cc of brine was produced before CO<sub>2</sub> breakthrough (9.02 and 9.15 cc, respectively). Subtracting the 4.3 cc dead space leaves 4.72 and 4.85 cc or 0.373 and 0.383 PV, respectively (PV = 12.65 cc). After CO<sub>2</sub> breakthrough there was a small quantity of brine produced and then brine production stopped except for water dissolved in the CO<sub>2</sub>. About 90% of the brine production occurred before one PV of CO<sub>2</sub> had been injected. Much of the production after one PV of CO<sub>2</sub> was injected was from vaporized water. The salt vapor trap was weighed only at the end of the test and this value was added evenly over the duration of the test scaled by injection rate to the brine/water production plots. There were 0.6 and 0.2 grams of water captured in the vapor trap during the two tests, respectively. The time when the vapor was actually produced is

not known. The flow rate was not changed in any of the tests as was done in some of the earlier tests. Figure 11 compares the pressure drop across the core during the injection of CO<sub>2</sub>.

After completion of CO<sub>2</sub> injection, brine was injected into the core to displace the CO<sub>2</sub>. Figure 12 compares the two brine injection tests, which both used dead brine after the CO<sub>2</sub> injection in each test (see Fig. 10). In each, about 4.3 cc of reservoir condition CO<sub>2</sub> was produced (the same as the end plate dead volume), then another 0.94 to 1.14 cc of the free-phase CO<sub>2</sub> was produced before the rate decreased; this seemed to indicate a residual CO<sub>2</sub>. After this break, additional CO<sub>2</sub> was produced at a fairly constant rate. Using the values of Wiebe and Gaddy<sup>4</sup> adjusted for dissolved solids,<sup>46</sup> these rates are as expected from CO<sub>2</sub> dissolved in the brine fully saturated with CO<sub>2</sub> at test conditions. The final reservoir volume of produced CO<sub>2</sub> from the system, including blowdown to ambient pressure, was within 5% of the brine produced during CO<sub>2</sub> injection; thus a fair material balance.

Figure 13 compares the production of CO<sub>2</sub> during the injection of brine for the two tests. The production rates are essentially identical until the blowdown in the first test. The rate of about 170 cc/min at ambient is equivalent to the production of CO<sub>2</sub> at ambient conditions from a core at 14.5 MPa and 35°C. Then as the free CO<sub>2</sub> production ends the rate settles at about 8cc/min, which is about the solubility of CO<sub>2</sub> in brine.<sup>45</sup> At 58 minutes into Queen Test #1, blowdown started. During Queen Test #2 injection was stopped at 62 minutes and restarted at 73 minutes and continued until stopping injection at 140 minutes. Blowdown started at 153 minutes. For both tests the total CO<sub>2</sub> produced was equivalent and about equal to the reservoir volume of brine displaced. The 0.94 and 1.14 cc of free-phase CO<sub>2</sub> produced represent 0.074 and 0.090 PV in Queen Tests #1 and #2, respectively. This is compared to no free-phase CO<sub>2</sub> from the core seen in the Frio sandstone and Indiana limestone tests. This leaves a CO<sub>2</sub> residual saturation of 0.309 and 0.283 PV respectively, where any additional CO<sub>2</sub> production was from CO<sub>2</sub> dissolved in the brine.

The laboratory finding from the corefloods is what was found in the West Pearl Queen Reservoir Huff-n-Puff pilot. In this scenario, after injection of CO<sub>2</sub> the subsequent production would be relatively rapid for the first 20 to 25% of the injected CO<sub>2</sub> and much slower thereafter. A prolonged, slow, consistent production is derived from CO<sub>2</sub> dissolved in the brine and/or oil with a short production burst early in the Puff cycle after the soak period in the Huff-n-Puff schedule.<sup>49,50</sup> In the reservoir this would be a production rate of about 24 m<sup>3</sup> of CO<sub>2</sub> per m<sup>3</sup> of

produced brine (135 scf of CO<sub>2</sub> per barrel of produced brine). The potential for produced CO<sub>2</sub> that is dissolved in the oil can be at least an order of magnitude greater. This compares to about 500 m<sup>3</sup> of produced CO<sub>2</sub> at ambient condition from 1.0 m<sup>3</sup> of CO<sub>2</sub> at reservoir conditions (35°C and 14.5 MPa). Thus, CO<sub>2</sub> production from the reservoir comes from free CO<sub>2</sub>, CO<sub>2</sub> that was dissolved in brine, and CO<sub>2</sub> that was dissolved in produced oil. The production rate for the CO<sub>2</sub> will depend on the production rate of each. After CO<sub>2</sub> in the reservoir is reduced to residual CO<sub>2</sub> the later production rates of CO<sub>2</sub> will be from CO<sub>2</sub> dissolved in the produced brine and oil. Since there are a number of zones, and between and within zones a range of permeabilities and porosities, production from free and dissolved CO<sub>2</sub> may be occurring simultaneously.

### **Results - Dolomite**

As with the other rock types, the core was first saturated with water and water permeability was determined. During CO<sub>2</sub> flooding of carbonate rock, dissolution and subsequent precipitation can occur. Both fines movement and precipitation results in permeability decreasing while dissolution increases permeability. From experience we have found that decreased permeability early in the testing is dominant over dissolution increases in permeability. Whereas later in a coreflood dissolution dominates resulting in permeability increases.<sup>6,7</sup> In these tests the permeability decreased during the series of test.

Figure 14 shows a plot of data from Flood 1. In this test the core saturated with water had CO<sub>2</sub> injected at 20 cc/hr at the indicated conditions (Table 3). Plotted versus time are the differential pressures (left y-axis) and produced water, produced CO<sub>2</sub> at reservoir conditions, and injected CO<sub>2</sub> at reservoir conditions (right y-axis). The fluid production volumes were only recorded until gas breakthrough. At this point the separator top blew off several times and lost fluid, thus the results were not considered accurate from that point. Figure 14 shows that this is a pressure increase as CO<sub>2</sub> displaces water and two-phase flow occurs. After CO<sub>2</sub> breakthrough the average pressure drop is similar to the starting differential pressure across the core, except less stable. The initial condition is single-phase brine flow at 100% brine saturation; post-breakthrough, it is single-phase gas flow, but with two-phase saturation. Thus, under these conditions the relative permeability of the core to the less viscous CO<sub>2</sub> after breakthrough is similar to the permeability of the more viscous single-phase water before gas injection.

Dolomite Flood 2 is shown in Fig. 15. The pressure differential, cumulative CO<sub>2</sub> injection, cumulative water production, and cumulative CO<sub>2</sub> production plots all look similar to Flood 1 (Fig. 14), except some post-gas breakthrough data was obtained. No difference can be distinguished between the two.

### **Summary and Conclusions**

These were relatively short cores (5.71 to 8.17 cm), about 3.8 cm in diameter, and therefore care must be taken when extrapolating results to reservoir scale. Figure 16 compares the end-point saturation of each core with the comparison of end-point versus flow rate for Frio, 20 cc/hr (1.6 m/D) with 100 cc/hr “h” (8 m/D) and Frio B2h at 200 cc/hr (16 m/D). As stated earlier, only in the Queen core was there free CO<sub>2</sub> produced from the core during displacement of CO<sub>2</sub> by brine injection with end-point brine saturation. These findings of end-point saturation are significant parameters in determining flow patterns, retention rates, and injectivity changes and their longevity that will enable improved predictions of CO<sub>2</sub> behavior in reservoirs for EOR and/or sequestration considerations.

Conclusions of the work include:

1. From 0.2 to 0.3 PV fraction of free-phase CO<sub>2</sub> saturation was required to establish a CO<sub>2</sub> flow path, after which there was little brine production except through evaporation, which is a slow process. The CO<sub>2</sub> saturation can be increased by increasing flow rate, reducing pressure, and water evaporation.
2. At the end of CO<sub>2</sub> injection there is a relatively low CO<sub>2</sub> saturation and high brine saturation in the core, thus no reduction in CO<sub>2</sub> saturation was required to return to brine flow. Only in the Queen sand was free CO<sub>2</sub> produced during brine injection.
3. Brine is equilibrated with CO<sub>2</sub> in a short time frame over a relatively short distance. Only when a channel was formed was brine produced that was not saturated with CO<sub>2</sub> while a significant residual CO<sub>2</sub> remained in the core.
4. The injection of brine into a 100% CO<sub>2</sub> phase required 0.2 to 0.3 PV fraction saturation to establish a brine flow path.
5. The sandstone and carbonate systems initially performed similarly. This was changed when through dissolution of the rock matrix a solution channel was formed in the limestone, creating a dominant flow path that significantly altered the flow behavior of the core.

<b>Table 1. Core Parameters</b>						
	Frio Sandstone			Queen	Indiana	Lockport
	Frio A	Frio B	Frio C	Sandstone	Limestone	Dolomite
Depth [m]	2493.0	2496.6	2497.8	1375.0	Quarried	Quarried
Diam [cm]	3.73	3.66	3.73	3.81	3.84	3.78
Length [cm]	6.08	6.10	5.71	7.21	7.95	8.17
Bulk vol [cc]	66.44	64.18	62.39	82.20	92.07	91.68
Pore vol [cc]	18.51	18.01	18.29	12.65	16.28	15.72
Por [%]	27.9	28.1	29.3	15.4	17.7	17.1

**Table 2. Synthetic Brine Composition**

Component (mg/L)	Frio and Limestone	Queen	Dolomite
NaCl	82,753	220,000	-
CaCl <sub>2</sub>	8,584	-	-
MgCl <sub>2</sub>	2,152	-	-
KCl	362	-	-
NaHCO <sub>3</sub>	186	-	-
			-
Total Dissolved Solids	94,037	220,000	0

Table 3. Flooding Parameters				
	Frio Sandstone	Queen Sandstone	Indiana Limestone	Lockport Dolomite
Pressures (MPa)	15.17	14.45	15.17	24.14 – 28.62
Temperatures (°C)	37.8 & 62.8	35.0	37.8	18.3 – 22.5
Flow Rates (cc/hr)	10 - 200	20	20 – 120	20
Brine (% CO <sub>2</sub> saturated)	0, 50, & 90	0	0 & 50	0
System Dead Vol. (cc)	4.3	4.3	4.3	4.3

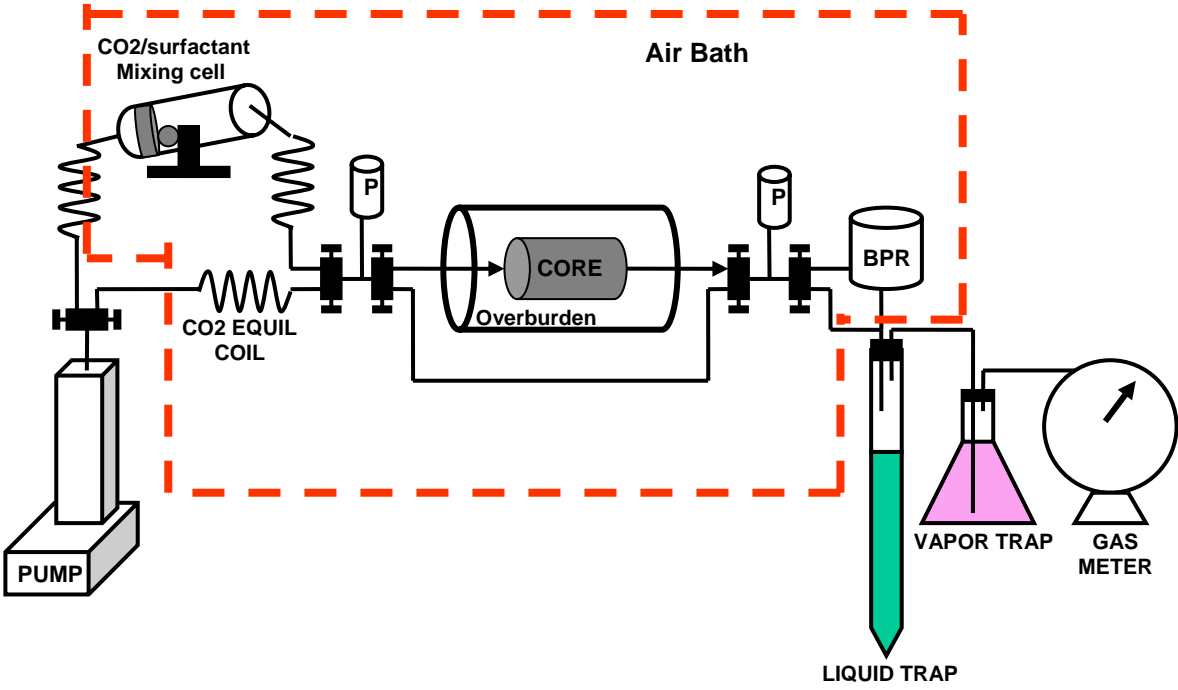


Fig. 1. Coreflooding apparatus.

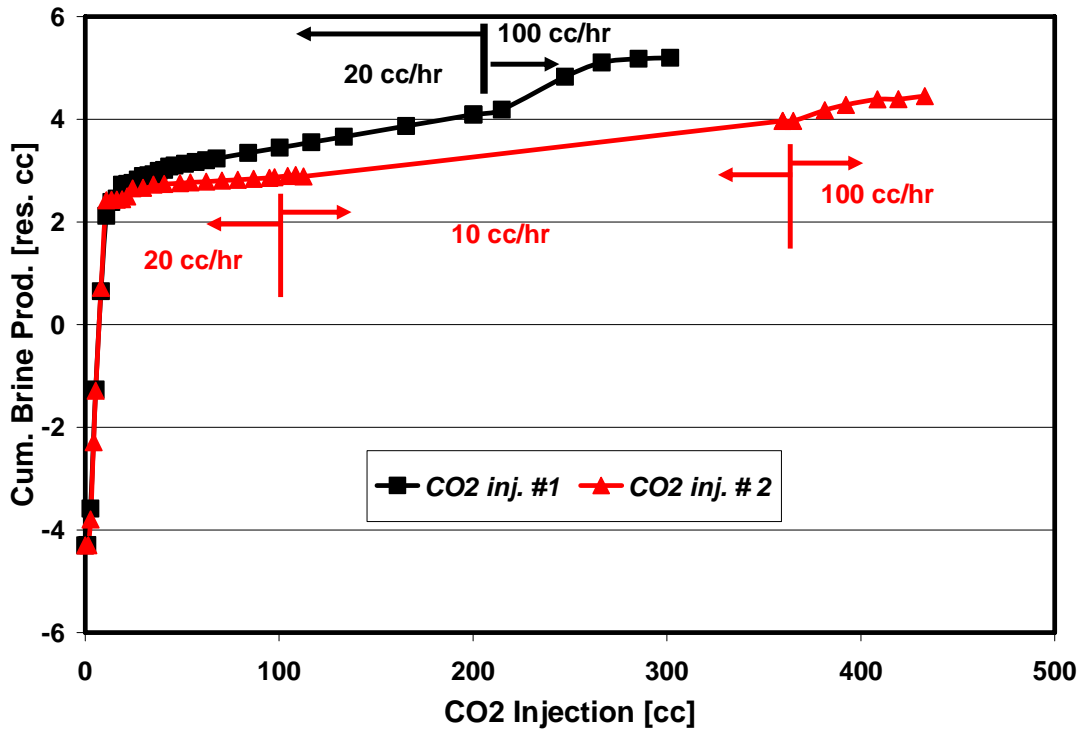


Fig. 2. Comparison of brine production during CO<sub>2</sub> injection of two tests in Frio Core A.

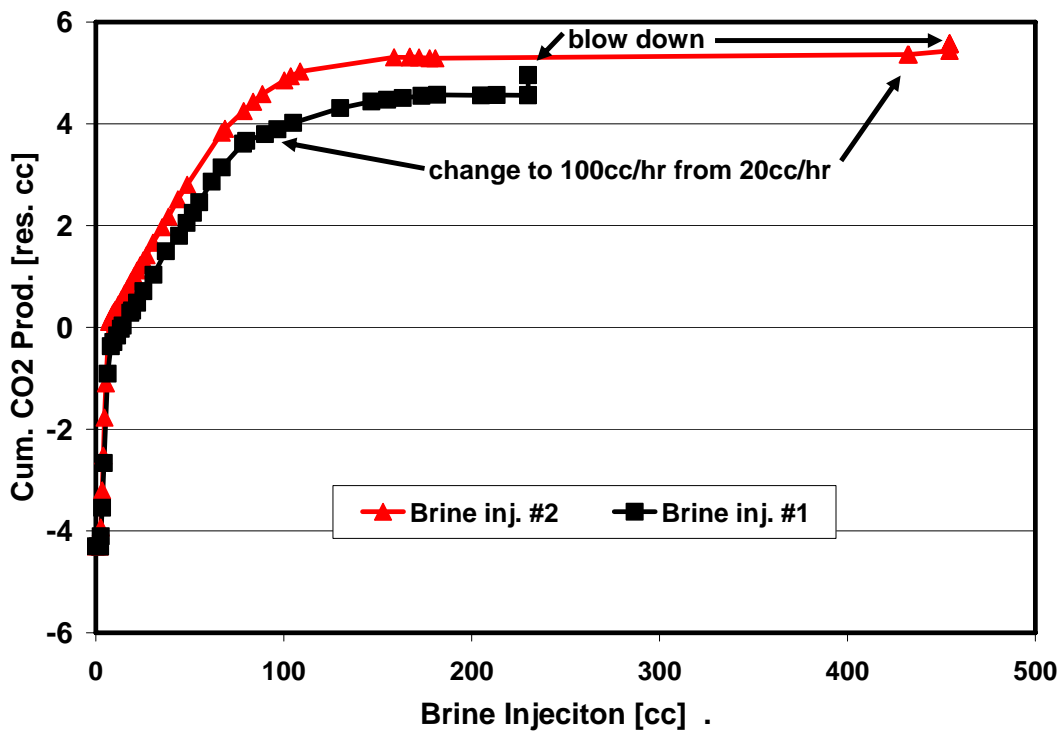


Fig. 3. Comparison of CO<sub>2</sub> production during brine injection for two tests in Frio Core A.

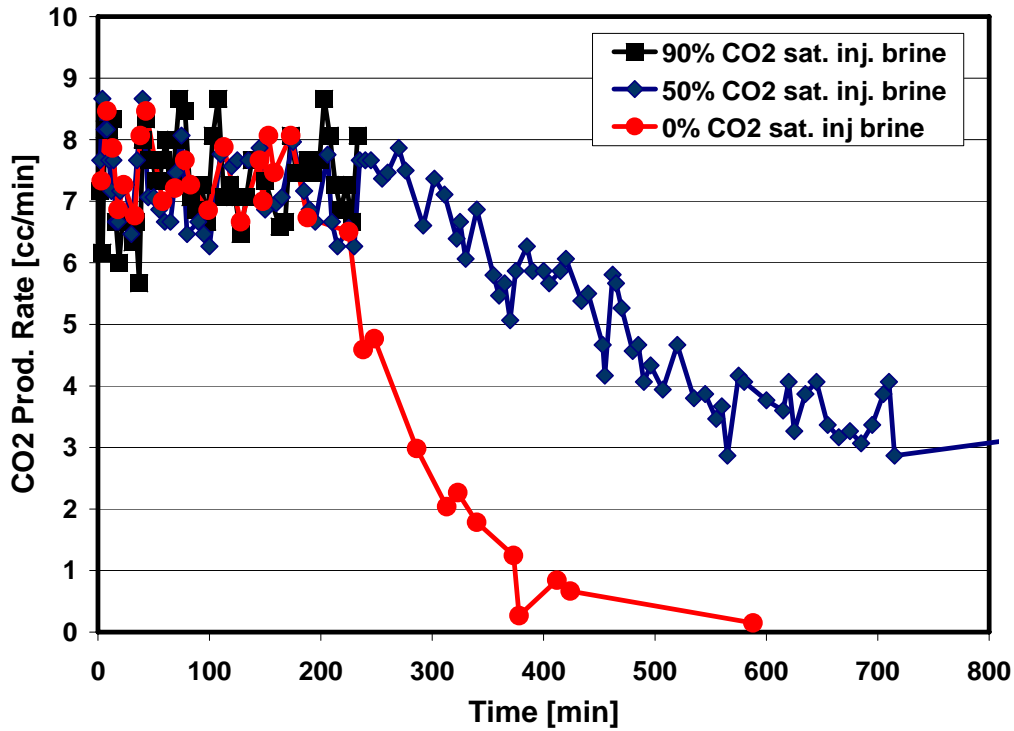


Fig. 4. Production rate of CO<sub>2</sub> during the injection of brine into Frio Core B for three different tests, each at different concentrations of CO<sub>2</sub> in the injected brine.

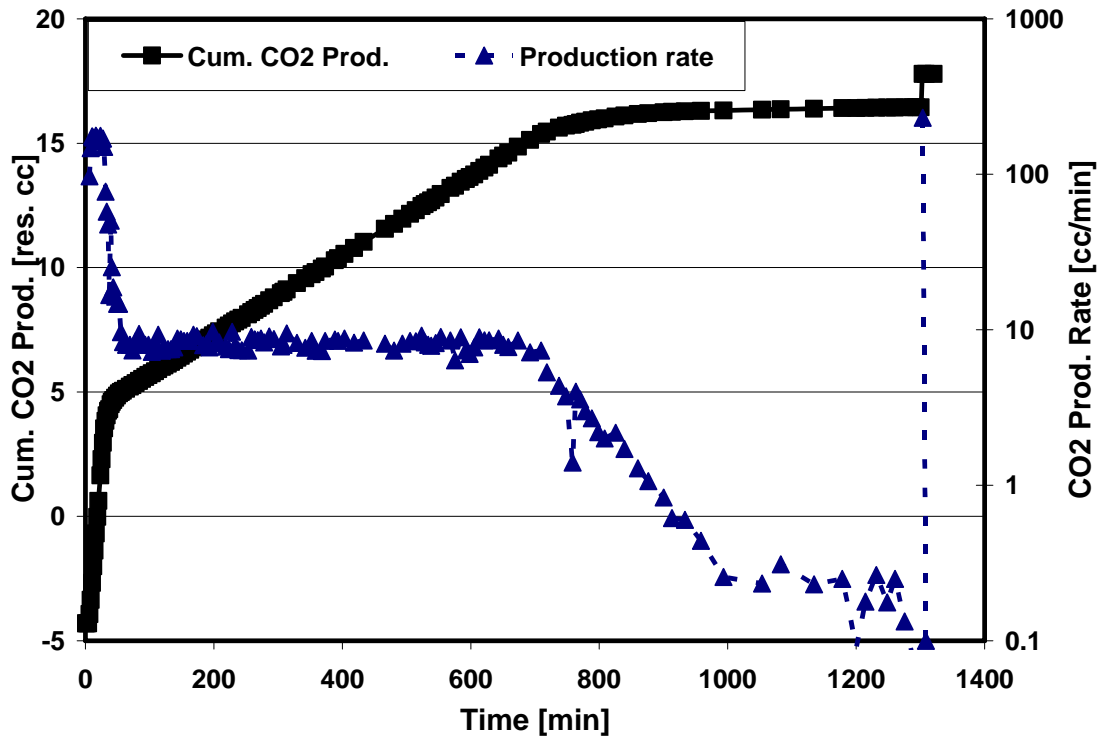


Fig. 5. Comparison of total CO<sub>2</sub> production rate at reservoir and ambient conditions at 37.8°C for Frio Core C.

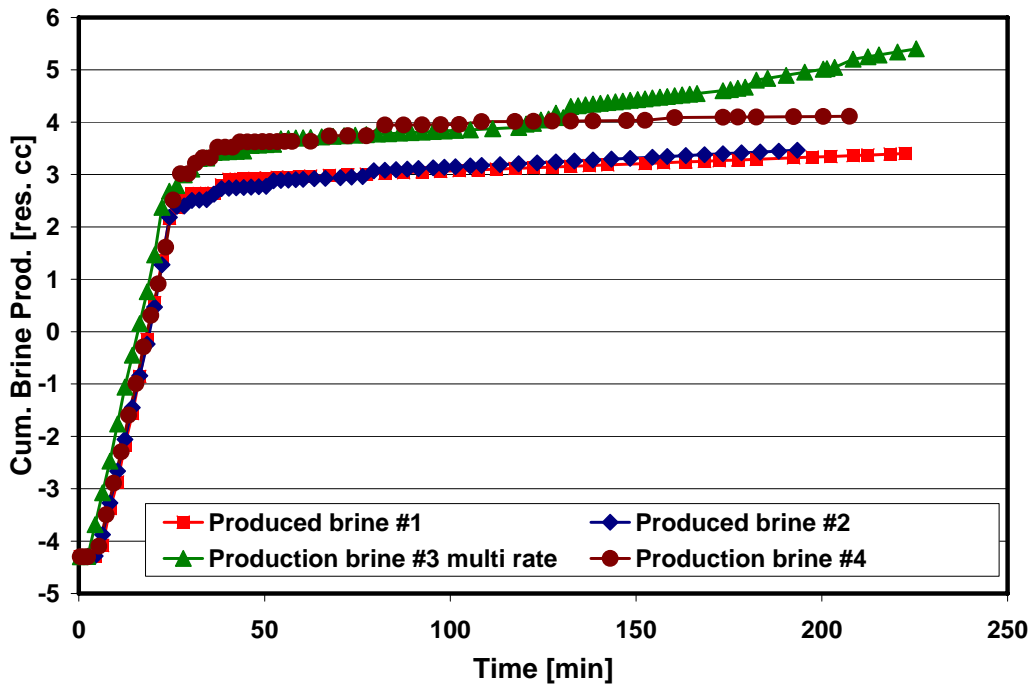


Fig. 6. Comparison of brine production during CO<sub>2</sub> injection of four tests in Indiana limestone.

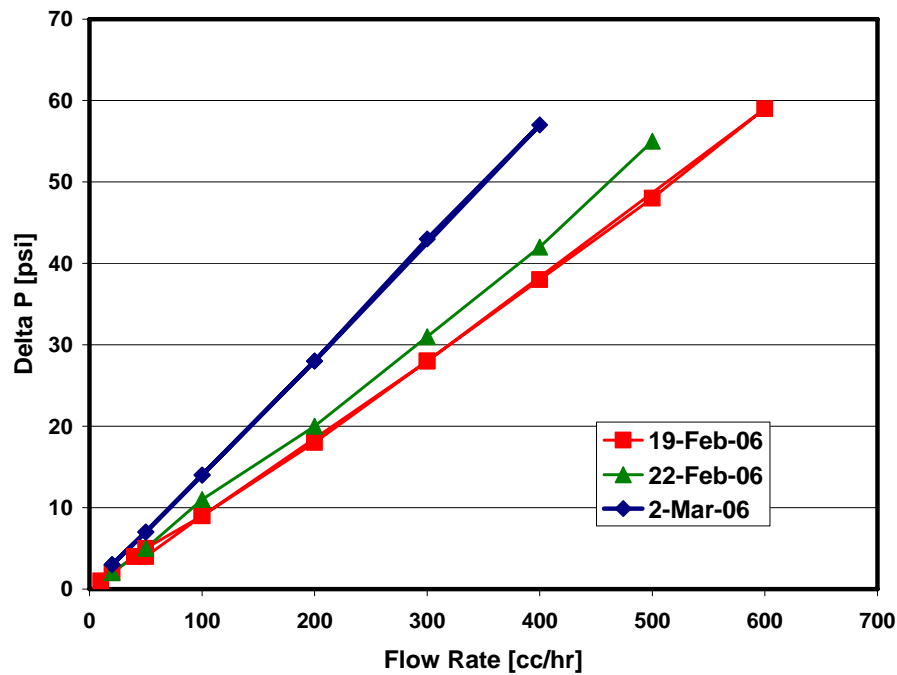


Fig. 7. Pressure drop versus flow rate for Indiana limestone on three different days. The indication was an decrease in permeability with time.

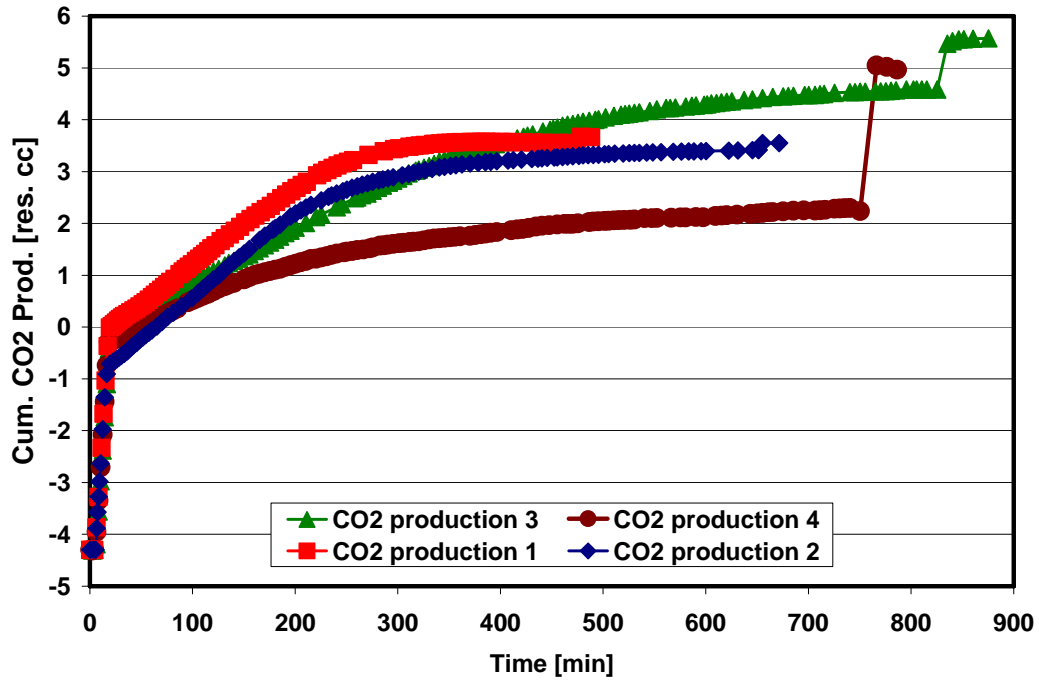


Fig. 8. Comparison of CO<sub>2</sub> production during brine injection for four tests in Indiana limestone.

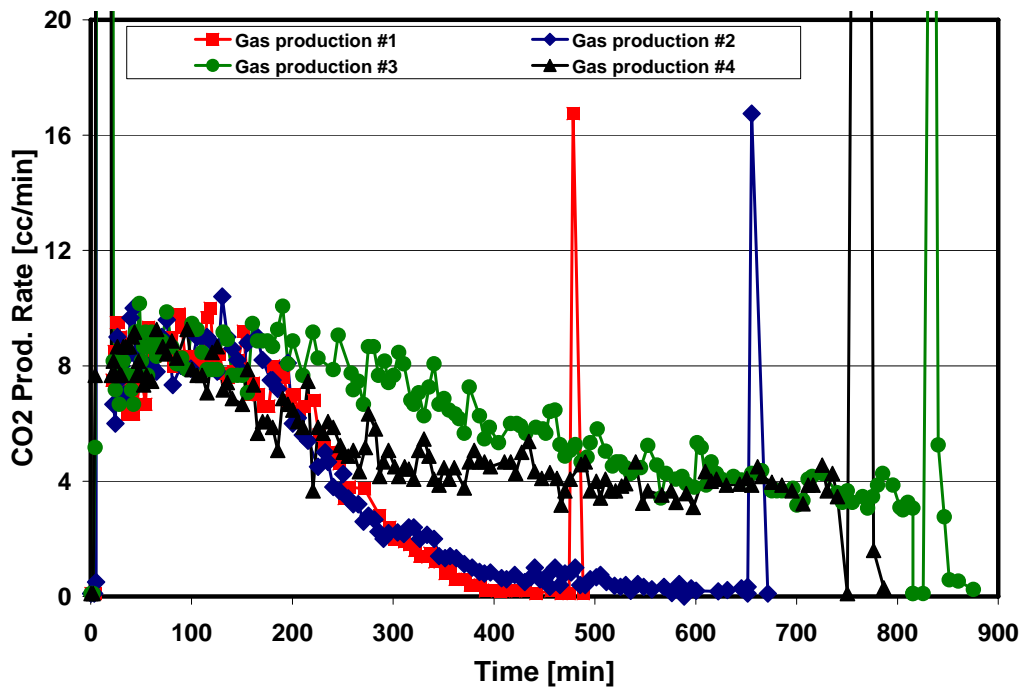


Fig. 9. Production rates for CO<sub>2</sub> at ambient conditions at a brine injection rate of 20 cc/hr in Indiana limestone.

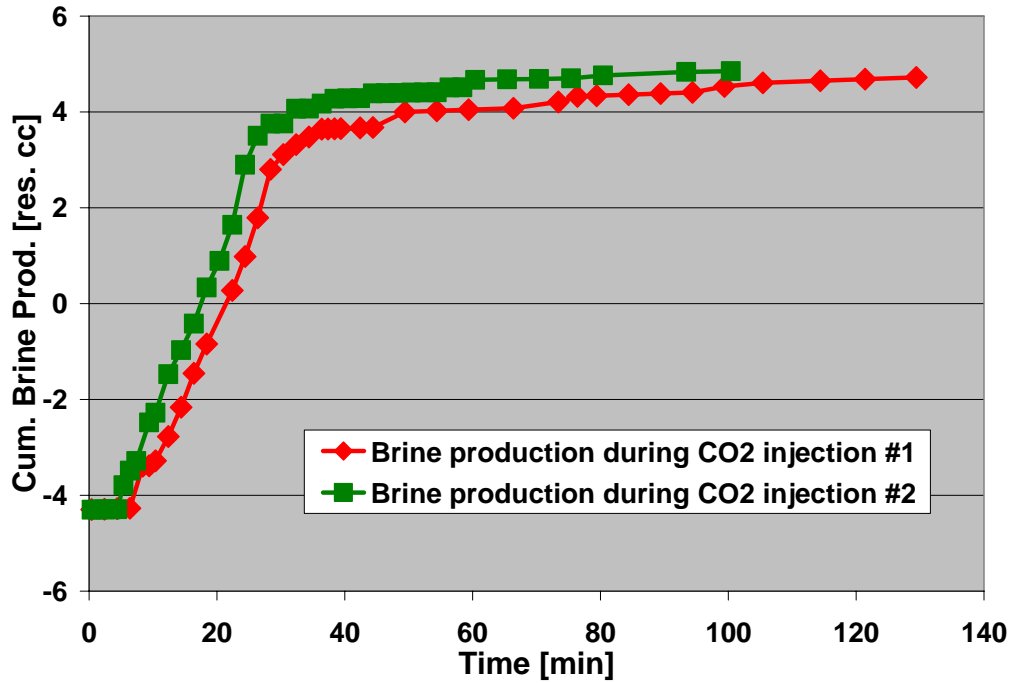


Fig. 10. Comparison of brine production versus time for both CO<sub>2</sub> injection Queen tests. One PV of injection is equal to about 38 minutes of injection.

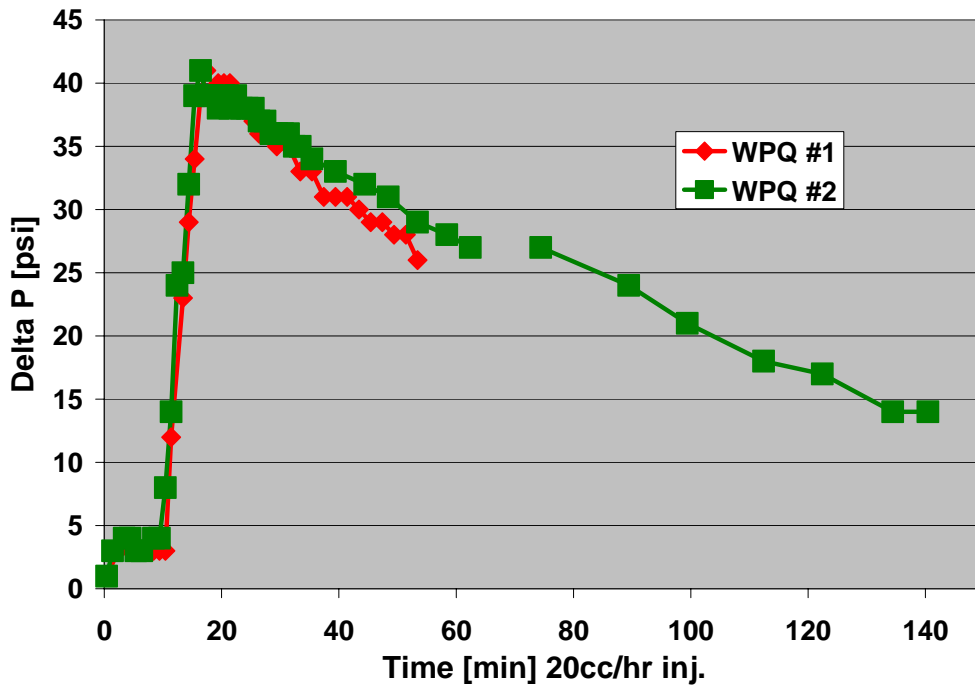


Fig. 11. Comparison of pressure drop across the core during CO<sub>2</sub> injection versus time during brine injection for both Queen tests. One PV of injection is equal to about 38 minutes of injection.

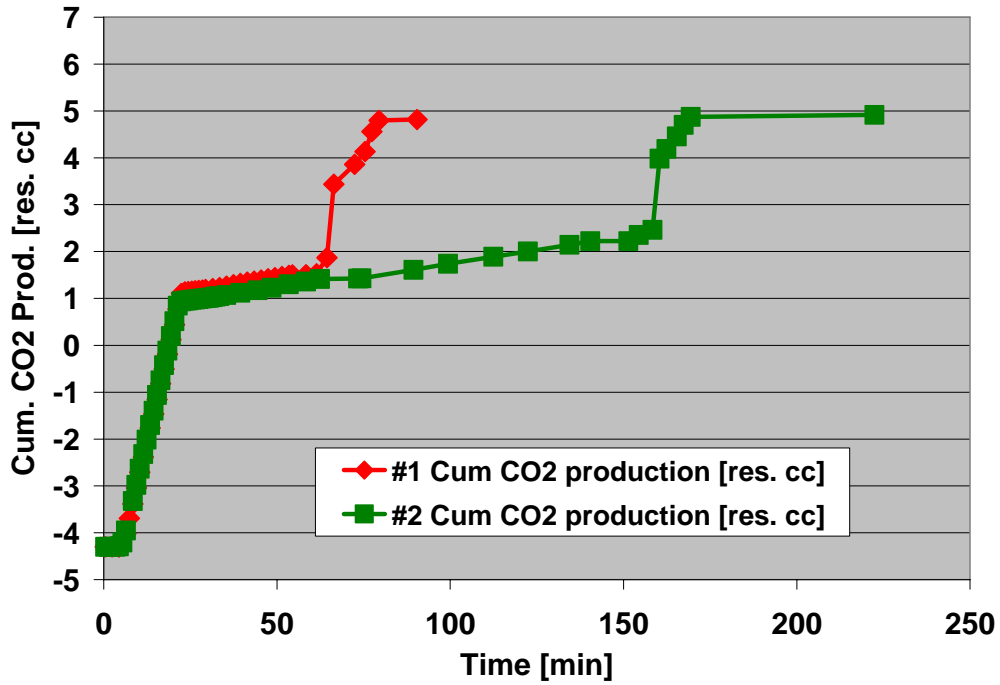


Fig. 12. Comparison of CO<sub>2</sub> cumulative production versus time during brine injection for both Queen tests. One PV of injection is equal to about 38 minutes of injection.

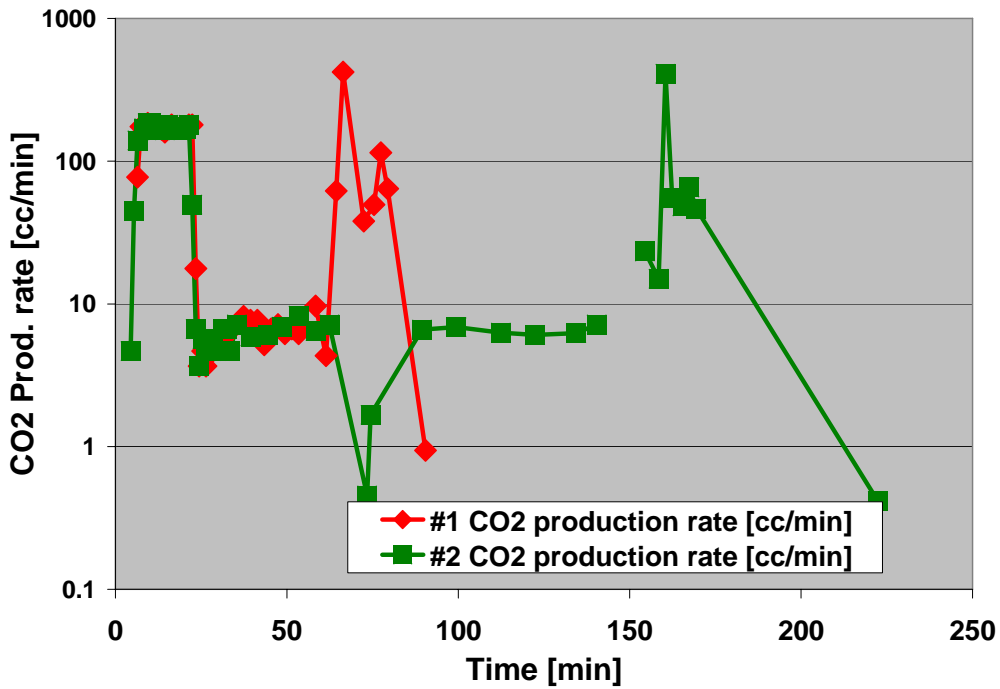


Fig. 13. Comparison of CO<sub>2</sub> production rate versus time during brine injection for both Queen tests. One PV of injection is equal to about 38 minutes of injection.

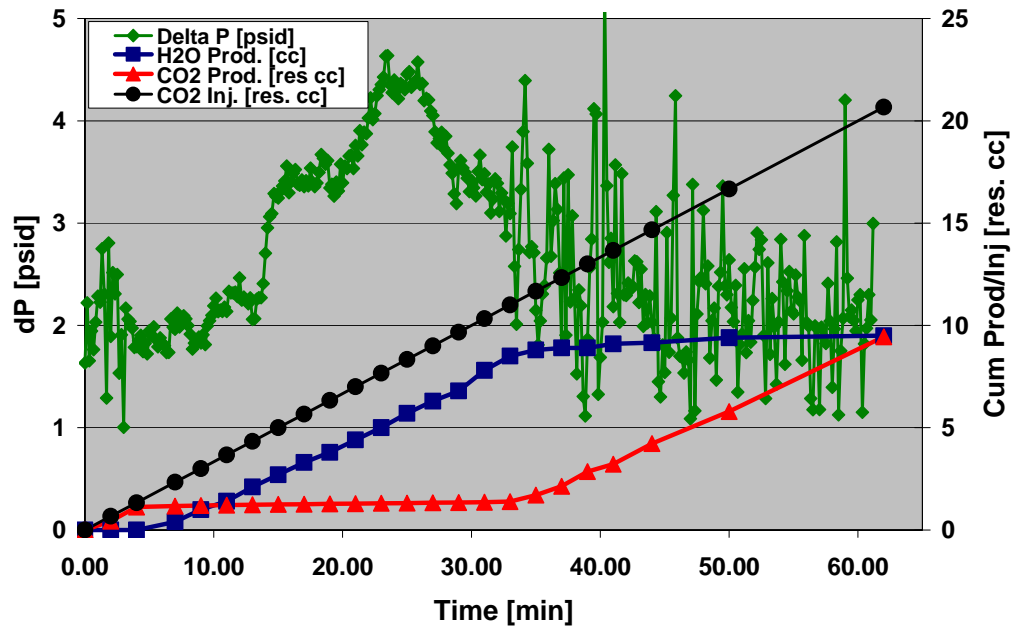


Fig. 14. Dolomite Flood 1 showing the injection and production of CO<sub>2</sub>, production of water, and differential pressure until CO<sub>2</sub> breakthrough.

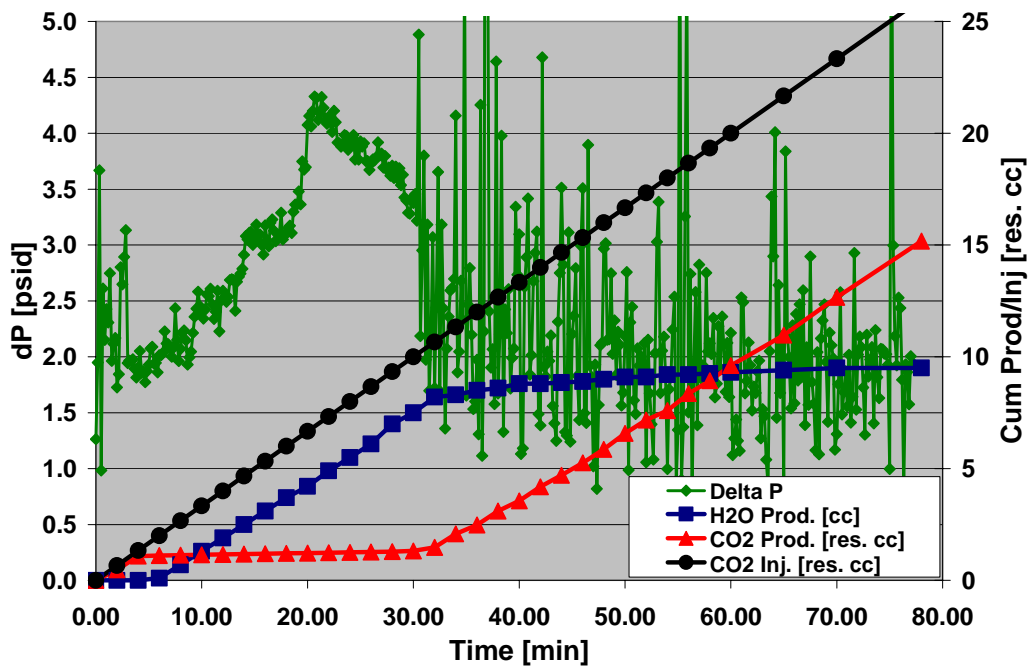


Fig. 15. Dolomite Flood 2 is similar to Flood 1 except production of CO<sub>2</sub> and water were recorded after CO<sub>2</sub> breakthrough.

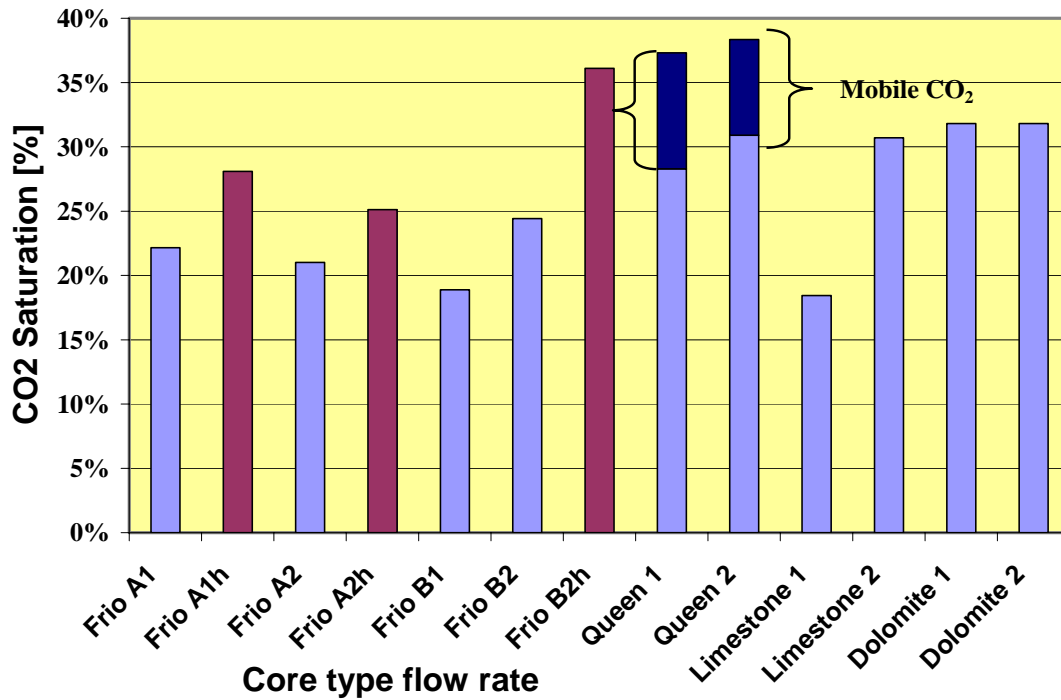


Fig. 16. CO<sub>2</sub> saturation in several core types. For all systems, the original injection rate was about 20 cc/hr; for each Frio system it was then increased to 100 cc/hr (200 cc/hr for Frio B2h) with the indicated increase in saturation indicated by the “h”. Only for Queen was there mobile CO<sub>2</sub>.

## Chapter 2: Effects of Flow Conditions and Surfactant Availability on Adsorption

### Introduction

Anionic surfactants, good foaming agents, can be used in CO<sub>2</sub> foam flooding to improve high-pressure, high-density CO<sub>2</sub> reservoir sweep efficiency. In this study, kinetics and equilibrium adsorption were investigated by examining adsorption behavior in a system of solid phase sandstone or limestone and of an aqueous phase of surfactant in 2% brine. Effects on surfactant adsorption density for different solid to liquid ratios as well as surfactant concentration, rock type and state, and flow conditions are presented. Three systems were used: batch tests on crushed rock, circulation tests through core samples, and nonflow, diffusion brine-saturated core tests. The density of an anionic surfactant adsorption on rock is best described as a function of surfactant available in the system (concentration plus volume), rather than by surfactant

concentration used by previous investigators. Experiments with solid rock were carried out to determine surfactant capacity of the porous media through flow and non-flow rock samples and crushed rock samples. Adsorption was similar for crushed sandstone and flow tests, while significantly higher in cubed, non-flow rock systems. For limestone the crushed rock and non-flow systems were similar while the flow system was significantly lower. The time to reach equilibrium required less than one hour (generally minutes) for the crushed rock, hours to days for the flow-through tests, and weeks to over a month for the non-flow rock systems. The rate of adsorption dependent on availability (delivery) that is generally much slower than the adsorption kinetics.

Surfactants are widely used in a large number of applications because of their remarkable ability to influence the properties of surfaces and interfaces. The applications of surfactants in petroleum industry are diverse and significant. Some of these areas include: in situ, wellbores, surface facilities, and environmental health and safety applications.<sup>51</sup> In each case appropriate knowledge and practices determine both the economic and technical successes of the industrial process concerned.

In-situ CO<sub>2</sub> flooding processes frequently experience poor sweep efficiency despite the favorable characteristics of CO<sub>2</sub> in recovery of oil. To mitigate this problem, significant research has focused on the use of foam in CO<sub>2</sub> flooding processes. It has been established that foam can improve sweep efficiency in CO<sub>2</sub> flooding processes by reducing the mobility of CO<sub>2</sub> and by diverting CO<sub>2</sub> flow to previously bypassed zones.<sup>3,52-57</sup>

Foam application involves injecting a surfactant along with water and gas into the reservoir. Normally, the surfactant is dissolved in the aqueous phase though surfactant dissolved in CO<sub>2</sub> are also being considered.<sup>58</sup> To aid in the selection of a suitable surfactant for the reservoir, laboratory data is collected to characterize the surfactant performance. The economics of foam flooding depend significantly on the quantity of surfactant required to generate and propagate foam. Surfactant loss through partitioning into the crude oil phase and through adsorption onto the rock surfaces often consumes more than 90% of the surfactant in the system.<sup>5</sup> Surfactant loss through partitioning into the crude oil can be responsible for surfactant losses of as much as 30%. However, for the very hydrophilic surfactants chosen for many foam flooding applications, the partitioning onto crude oil is near zero.<sup>51</sup>

More serious losses are demonstrated from the results of a number of studies of the adsorption properties of surfactants suitable for foam flooding.<sup>59-61</sup> These have shown that effective foam forming surfactant may exhibit adsorption levels from near zero to up to quite high levels on the order. For example one test determined adsorption rates of 2.5 mg/g (mg of adsorbed surfactant for each gram of rock in the system). A mile-square, 10-ft-thick reservoir saturated with surfactant would require 55,000 tons (50,000 tonnes) of surfactant at 2.5 mg of surfactant per g of rock. Adsorption does not depend on the nature of the surfactant alone, but also (though not inclusively) on temperature, brine salinity and hardness, rock type, wettability, and the presence of the residual oil phase. These factors will lead to vastly different distances of foam propagation into a reservoir, so selection of foam-forming surfactant formulation with acceptable adsorption levels at reservoir conditions is critical.

In this study the effect on surfactant adsorption for different solid to liquid ratios, surfactant concentration, rock type and state, and flow conditions are determined. The goal for this work is to quantify equilibrium values and kinetics in order to predict adsorption and desorption under reservoir conditions.

## **Material, Procedures, and Definitions**

### **Materials**

Anionic surfactant Chaser International CD 1045™ (CD), which has been identified as one of the best foaming agents,<sup>62-64</sup> was used in this study. It was supplied by Chaser International as 46.7 wt% active aqueous solution. The anionic surfactant indicator Dimidium Bromide–Disulphine Blue was used in this study to determine an unknown concentration of CD solution. The base stock was supplied by BDH Laboratory Supplies. The working solution was prepared as outlined in an earlier publication.<sup>65</sup> Chloroform with 1% ethanol was used in this study. The brine used to prepare the surfactant solution was 2 wt% synthetic brine composed of 1.5 wt% NaCl and 0.5 wt% CaCl<sub>2</sub>.

Two types of cores were used as porous adsorbents: Berea sandstone and Indiana limestone. The powdered or crushed rock was prepared in-house by crushing the corresponding solid core with a maximum size determined by passing the crushed rock through a standard Number 60 sieve (~0.4 mm diameter).

### **Quantitative analysis of CD solution**

A colorimetric method was used in this study, as in earlier studies, using procedures previously outlined<sup>16</sup> except for the calibration curve, which in this study was milligrams of CD available in the testing solution. The absorbance was measured at 295 nm using a spectrophotometer.

### **Description of test procedures**

All the adsorption experiments were performed at 40°C and atmospheric pressure. In the case of the flow-through test the outlet pressure of core was atmospheric and the inlet pressure dependent on the flow rate and system permeability. To determine CD adsorption density onto crushed limestone or sandstone for each concentration, surfactant solution and crushed rock were added together in a test tube. The test tube was then placed in the shaker and placed in the thermostatic air bath. Samples of surfactant solution were taken from test tubes after at least 24 hours of exposition to determine residual CD concentrations at equilibrium. Initial surfactant concentrations tested were 500, 750, 1000, 1250, 2000 ppm. The solid to liquid weight ratios ranged from 1:1 to 1:5. Usually, 1 gram of solid was used for each combination of surfactant concentration and solid to liquid ratio.

Dynamic adsorption experiments were performed to determine adsorption densities of limestone and sandstone brine-saturated cores via circulation of a fixed volume of surfactant solution through the core. Samples of solution were taken from the flask periodically until no change in surfactant concentration was observed. Initial surfactant concentrations tested were 1000 and 2000 ppm and the range for solid to liquid ratios was from 1:1 to 1:5. The amount of surfactant-free brine in each core at the start of the experiment was included in calculations when equilibrium adsorption was determined in the system. The flow rate of surfactant solution was 15 ml/hr for each circulation experiment. Details of the crushed and flow-through tests have been presented earlier.<sup>8,9,11</sup>

To measure adsorption by diffusion of surfactant from a CD solution to brine-saturated sandstone and limestone cubes, the following equipment was used: glass jars with a screw cap, magnetic stirrers, and thermostatic air bath. The CD adsorption density calculated during each diffusion test into limestone or sandstone brine-saturated cores was determined on cubes that were covered with epoxy on five sides, leaving one side of the cube exposed. After the epoxy

hardened, cubes were evacuated and saturated with surfactant-free brine. After determining by weight change the amount of brine imbibed into the core and the pore volume, each cube was immersed into surfactant solution in a glass jar that was then closed with a screw cap to prevent evaporation and put on magnetic stirrer in the air bath. Samples of the surfactant solution were taken periodically to determine residual CD concentration. Initial surfactant concentrations tested were 1000 and 2000 ppm and the range for solid to liquid weight ratios varied from 1:1 to 1:5. The initial brine in each cube was included when calculating the total amount of liquid and surfactant available in each system.

### **Formulas used to calculate adsorption density**

The amount of surfactant absorbed (adsorption density) was expressed as the unit mass of CD adsorbed per 1 gram of rock (mg/g). Adsorption density of crushed rock was calculated by the following formula:

$$Ads = (C_i - C_r) * M_s / (M_c * 1000), \quad [1]$$

where: Ads is CD adsorption density (mg surfactant/g rock);  $C_i$  and  $C_r$  are initial and residual CD concentration in solution (ppm), respectively;  $M_s$  is mass of the solution (g) and  $M_c$  is mass of the core sample (g). During an experiment when it was necessary to take several samples to measure residual concentration in surfactant solution, material balance and adsorption density were calculated using the following formula:

$$Ads_i = [(M_t - \sum \{m_{s_i}\}) - (M_s - \sum \{m_{l_i}\}) * C_{r_i} / 1000] / M_c, \quad [2]$$

where:  $Ads_i$  is adsorption density after i-number of measurements (mg/g);  $M_t$  is total initial mass of surfactant in the system (mg);  $M_s$  is total initial mass of surfactant solution (g);  $\sum \{m_{s_i}\}$  is sum of surfactant mass removed during sampling (mg);  $\sum \{m_{l_i}\}$  is sum of surfactant solution mass removed during sampling (g);  $C_{r_i}$  is residual concentration after i measurements (ppm); and  $M_c$  is mass of the core sample (g).

### **Surfactant availability in the system**

In this study, when adsorption isotherms were constructed as adsorption density versus amount of surfactant available in the system, availability of surfactant in the system was defined as the total amount in mg of CD in solution per 1 g of solid. The term “surfactant availability” is used in this paper in lieu of the approach for presenting adsorption isotherms as a function of surfactant adsorption density versus equilibrium surfactant concentration. This approach was selected because it has been shown that by increasing the volume of surfactant solution the adsorption density generally increases at a fixed equilibrium surfactant concentration; thus the adsorption density might have different values for a given equilibrium concentration.

### **Presentation of Data and Results**

#### **CD adsorption onto crushed rock**

The first set of tests was performed on crushed limestone and sandstone. These are essentially small chunks of rock at or less than 0.4 mm in diameter (No. 60 sieve). From a previous study the crushed rock pieces are shown to be in the order of one to three grain diameters in size.<sup>66</sup> These tests were designed to determine adsorption kinetics in porous media with minimal diffusion.

The results from the experiments with crushed limestone indicate that CD adsorption was near completion in about 10 minutes for initial CD concentration of 1000 ppm and solid to liquid ratios from 1:1 to 1:5 and completed in less than one hour for initial concentration of 2000 ppm (Fig. 17). For sandstone the crushed rock reached 95 % of maximum adsorption within one hour for an initial CD concentration of 2000 ppm (Fig. 17). The adsorption experiments with a weight ratio of 1:1 between surfactant solution and crushed limestone showed that with a linear increase of surfactant concentration the CD adsorption density increases linearly from 0.450 mg/g to 1.796 mg/g over the range of initial CD concentrations from 500 ppm to 2000 ppm (available surfactant of 0.5 to 2.0 mg/g) (Fig. 18). Crushed sandstone demonstrated a similar trend. Adsorption density for crushed sandstone in the range of initial concentration 500 to 2000 ppm (available surfactant of 0.5 to 2.0 mg/g) and solid to liquid ratio of 1:1 increased linearly from 0.107 mg/g to 1.35 mg/g (Fig. 19).

It was found that CD adsorption density increases when the available volume of surfactant solution increases while holding the initial CD concentration constant. The results are plotted in Fig. 18 where the availability of CD per gram of rock varies from 0.5 mg/g (1:1 @ 500 ppm) to 10mg/g (1:5 @ 2000 ppm). The increase in adsorption is independent of concentration and approximately linear until about 4 mg/g of surfactant is available. After reaching an adsorption density of 3.0 mg/g at 4 mg/g of surfactant available, adsorption increases only slightly with increasing availability of surfactant. Over the tested CD concentrations and solid to solution ratios, CD adsorption density on crushed limestone is a function of CD available in the system rather than a function of surfactant concentration.

Figure 19 shows a number of adsorption isotherms plotted as a function of availability of surfactant with an apparent dependence on initial surfactant concentration. Adsorption density for crushed sandstone in the range of initial concentrations of 500 to 2000 ppm and solid to liquid ratio from 1:1 to 1:5 increased with availability of surfactant with a significant change of slope at 4 mg/g of surfactant available. The maximum adsorption was above 3 mg/g. The plotted curves of CD available versus adsorption density have an increasing slope with increasing CD concentration (Fig. 19). The slope increases from about 0.3 to 0.7 going from CD concentrations of 500 ppm to 2000 ppm. For the lower concentrations the availability (liquid to solid ratio) was not high enough to reach a plateau. Thus, further tests are required to determine if the plateau would be similar for all concentrations, though it appears that the plateau for 1250 ppm is lower than for 2000 ppm, etc.

In general, crushed limestone demonstrated higher CD adsorption densities compared to crushed sandstone for all corresponding initial CD concentrations and solid to liquid ratios, (see Figs. 17 and 18).

### **CD adsorption by diffusion into brine saturated cores.**

In the second series of tests there was no injection into the test cubes, thus fluid within the core was static and diffusion should play the major role in adsorption rates. The only mechanical mixing was in the bulk solution to maintain a homogeneous solution, as explained in an earlier section. Adsorption dynamic and equilibrium tests data for brine saturated cubes of limestone and sandstone are summarized in Tables 4 and 5, respectively. Time required for CD adsorption to reach equilibrium by diffusion into brine saturated rock was about three orders of magnitude

longer than in the crushed rock (400-600 hours for brine saturated cubes versus one or less hours for the crushed rock, see Fig. 1).

Figure 4 compares the final values of CD adsorption density on crushed and non-flow solid cubes for limestone. The two systems types had similar adsorptions at the same surfactant availability. Figure 21 compares the final values on crushed and non-flow solid cubes for sandstone. There is a higher adsorption for the cubed non-flow systems. The difference might be due to the fact that the Berea sandstone rock samples used to prepare the crushed and cubes samples were from different blocks. All tests were performed at CD concentrations of either 1000 or 2000 ppm.

There is a similar point in both the limestone (Fig. 20) and sandstone (Fig. 21) that are significantly lower than adjacent points. They were both at a solid to liquid ratio of 1:3 and initial surfactant concentration of about 2000 ppm (6 mg/g surfactant availability). The two tests were performed concurrently and when compared with tests that preceded and followed them had significant differences in their adsorption isotherms (Fig. 22). Their final adsorption densities were lower than systems with both less and more available surfactant. Also, the initial 100 hours had an unusual “S” shaped curve in the isotherm. It is suggested that these two points be weighted less when determining adsorption density trends and at a future date be retested.

### **Effect of flow conditions on CD adsorption**

The third set of tests comprised flow tests similar to tests that have traditionally been performed to determine adsorption onto rock. During the flow test surfactant solution is circulated through the core until equilibrium or steady state is achieved. One difference from traditional tests was that not only were surfactant concentrations varied, but the amount of solution or as explained earlier the solid (rock) to liquid mass ratios were varied. Tables 6 and 7 summarized the CD adsorption values and conditions measured in the circulation experiments with limestone and sandstone cores.

Time for CD adsorption to achieve equilibrium by circulation through brine-saturated cores was at least one order of magnitude greater compared to the crushed rock (20–50 hours for brine-saturated cores versus one hour or less for the crushed rock) and an order of magnitude less compared to nonflow brine-saturated core tests (Fig. 17).

Values of CD adsorption density on limestone were significantly lower in the circulation experiments compared to those measured in crushed rock and nonflow saturated core tests (Fig. 23). Since these were prepared from samples of the same rock, the differences might be explained from the energy required for mono- versus multi-layer adsorption. The electrostatic interaction between surfactant molecules and solid surface as well as the lateral chain-chain interactions between the adsorbed surfactant molecules contribute to the driving force of adsorption.<sup>67</sup> Energy due to hydrophobic attraction of the surfactants to form surface aggregates is of the same order of magnitude as the energy of micellization of surfactants (~1 kcal/mol) while energy of electrostatic interaction between surfactant molecules and solid surface is around 20-30 kcal/mol, which is an order of magnitude greater than the energy of hydrophobic interaction. Therefore the difference in CD adsorption densities due to the flow conditions, shown in Fig. 23, might be interpreted as the inability of surfactant aggregates formed outside the near-surface adsorption on the solid to resist surface washing by the flow of liquid in porous space. This result will be significant when determining adsorption in nonflow regions of the rock compared to flow paths. This may imply varying adsorption capacity versus flow rate. Thus an understanding of flow and diffusion rates are required for accurate adsorption density calculations onto limestone.

The results for the sandstone systems had similar equilibrium time compared to the limestone, but found little difference in the total adsorption in flow versus nonflow systems (Fig. 24). Unlike the solid cube sandstone samples, the flow tests were prepared from the same lot as the crushed samples. In earlier studies it was found that the adsorption onto pure silica was less than onto sandstone.<sup>9</sup> The increase was dependent on the amount of clays in the system, which generally have a much higher adsorption capability than sandstone due to increased surface area and composition.<sup>9</sup> This and the discussion from the last paragraph indicates that different CD adsorption mechanisms and adsorption energy levels that occur on sandstone and limestone surfaces should affect adsorption density and result in adsorption density as a function parameters such as flow conditions, rock type, and rock impurities (clays etc).

## Conclusions and Implications

1. Values of CD adsorption density on crushed and non-flow solid limestone cubes were found to be the same and are best described as a function of surfactant availability (mass of surfactant available per mass of solid) in the system.
2. The shape of the adsorption isotherms on crushed sandstone, comparing surfactant availability with adsorption density, suggests the slopes and possibly the density plateau depend on surfactant concentration and availability.
3. Adsorption time dynamic depends on the state of solid and flow conditions. Time to reach equilibrium in nonflow core volumes was an order of magnitude greater compared to circulation experiment, and 3 orders of magnitude greater compared to the crushed rock. Thus the rate of adsorption is dependent on the availability of surfactant with the kinetics and equilibrium being comparably very rapid.
4. When comparing flow versus nonflow systems in cube or core samples, the adsorption density on limestone underwent a significant decrease due to the flow in porous media while adsorption density on sandstone remained the same. This might be an indication of different adsorption mechanisms and/or energy levels that occur on limestone and sandstone surfaces. Tests such as heats of adsorption that are planned for the future should shed some light on the cause of these differences.
5. The results should be considered when determining reservoir adsorption requirements.

**Table 4. CD Adsorption by Diffusion into Brine Saturated Limestone Cubes**

Test #	Ratio S:L	CD available [mg/g]	Core mass [g]	Pore Volume [cc]	Mass of Surfactant Solution [g]	Initial CD Conc. [ppm]	Duration of the experiment [hrs]	Residual CD Conc.* [ppm]	CD Ads. density* [mg/g]
1	1:1	1	146.3	6.2	140.4	1021	167	94	0.850
2	1:2	2	141.6	8.9	274.2	1012	167	74	1.796
3	1:3	3	147.5	8.2	434.2	999	600	202	2.330
4	1:4	4	142.5	8.5	561.4	1016	743	158	3.356
5	1:5	5	121.9	7.5	601.9	1013	644	356	3.163
6	1:1	2	162.6	9.5	153.0	2126	166	441	1.585
7	1:2	4	142.5	8.5	276.4	2062	576	604	2.821
8	1:3	6	157.7	9.1	463.9	2040	360	1338	2.094
9	1:4	8	138.0	8.4	543.5	2031	431	1112	3.643
10	1:5	10	129.1	7.8	637.6	2025	547	1273	3.738

(\* at the end of experiment)

**Table 5. CD Adsorption by Diffusion into Brine Saturated Sandstone Cubes**

Test #	Ratio S:L	CD available [mg/g]	Core mass [g]	Pore Volume [cc]	Mass of Surfactant Solution [g]	Initial CD Conc. [ppm]	Duration of the experiment [hrs]	Residual CD Conc.* [ppm]	CD Ads. Density* [mg/g]
1	1:1	1	105.8	9.6	96.2	1023	167	25	0.886
2	1:2	2	108.1	10.7	205.4	1032	167	67	1.809
3	1:3	3	109.2	11.2	316.3	1015	600	264	2.158
4	1:4	4	105.5	11.5	410.4	1028	743	148	3.392
5	1:5	5	103.5	11.1	506.3	1022	644	284	3.584
6	1:1	2	107.0	11.3	95.6	2239	166	501	1.537
7	1:2	4	107.2	11.6	202.7	2115	576	429	3.158
8	1:3	6	105.8	11.6	305.7	2077	360	1177	2.590
9	1:4	8	102.9	11.5	400.0	2058	431	708	5.241
10	1:5	10	105.9	11.3	518.1	2044	547	1262	3.823

(\* at the end of experiment)

**Table 6. CD Adsorption by Circulation of Surfactant Solution through Limestone Cores**

Test #	Ratio S:L	CD available [mg/g]	Core mass [g]	Pore Volume [cc]	Mass of Surfactant Solution [g]	Initial CD Conc. [ppm]	Duration of the experiment [hrs]	Residual CD Conc.* [ppm]	CD Ads. density* [mg/g]
1	1:1	1	141.6	8.9	132.6	1046	22	524	0.488
2	1:2	2	141.6	8.9	274.2	1012	70	544	0.898
3	1:3	3	144.4	9.9	443.0	980	103	665	0.952
4	1:4	4	115.8	7.7	455.4	997	71	692	1.193
5	1:5	5	110.0	7.9	542.0	1015	30	781	1.148
6	1:1	2	125.5	8.0	117.4	2096	24	1251	0.792
7	1:2	4	120.6	8.7	232.4	2118	35	1351	1.484
8	1:3	6	114.4	8.5	334.6	2052	21	1575	1.396
9	1:4	8	115.8	8.3	454.8	2037	44	1531	1.988
10	1:5	10	112.6	8.7	540.0	2086	18	1672	1.982

(\* at the end of experiment)

**Table 7. CD Adsorption by Circulation of Surfactant Solution through Sandstone Cores**

Test #	Ratio S:L	CD available [mg/g]	Core mass [g]	Pore Volume [cc]	Mass of Surfactant Solution [g]	Initial CD Conc. [ppm]	Duration of the experiment [hrs]	Residual CD Conc.* [ppm]	CD Ads. density* [mg/g]
1	1:1	1	137.2	9.8	127.4	1055	50	492	0.515
2	1:2	2	138.2	10.0	266.1	1017	46	533	0.923
3	1:3	3	115.0	10.2	345.0	980	103	532	1.335
4	1:4	4	108.3	9.1	424.0	1001	71	587	1.611
5	1:5	5	103.0	9.2	505.7	1018	50	700	1.558
6	1:1	2	112.1	8.3	103.7	2120	24	729	1.277
7	1:2	4	115.6	9.3	221.8	2128	35	1076	2.013
8	1:3	6	107.2	8.5	313.0	2055	21	1380	1.966
9	1:4	8	110.3	9.9	431.2	2046	22	1436	2.385
10	1:5	10	104.8	9.9	514.0	2039	18	1553	2.382

(\* at the end of experiment)

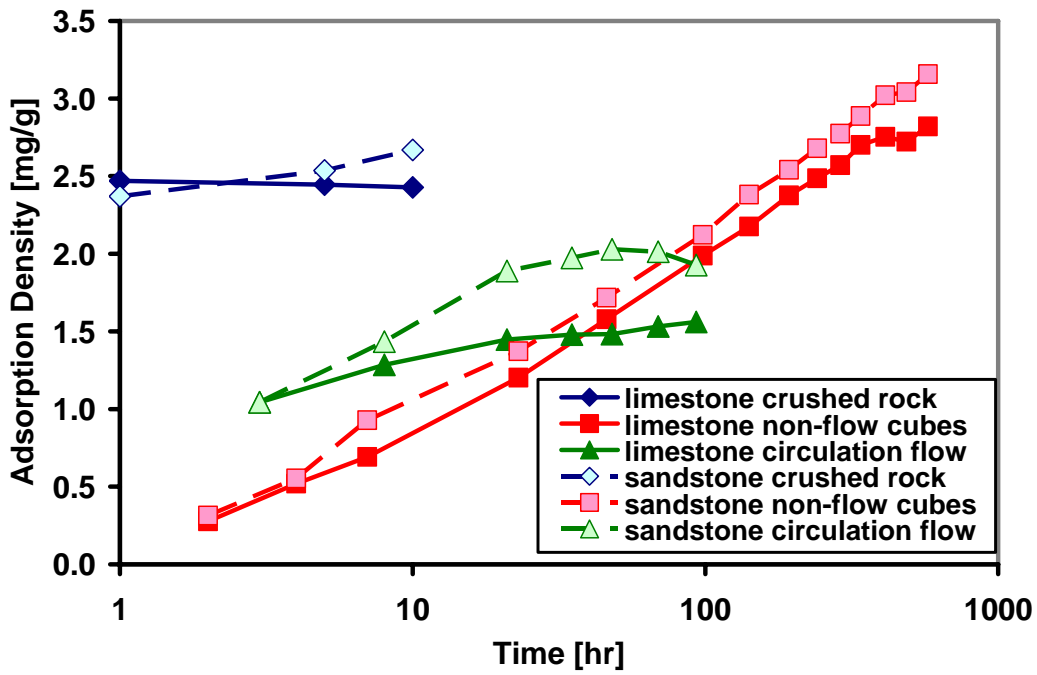


Fig. 17. Comparison of equilibrium time versus adsorption density for crushed rock, non-flow cubes, and flow-through core for limestone and sandstone systems.

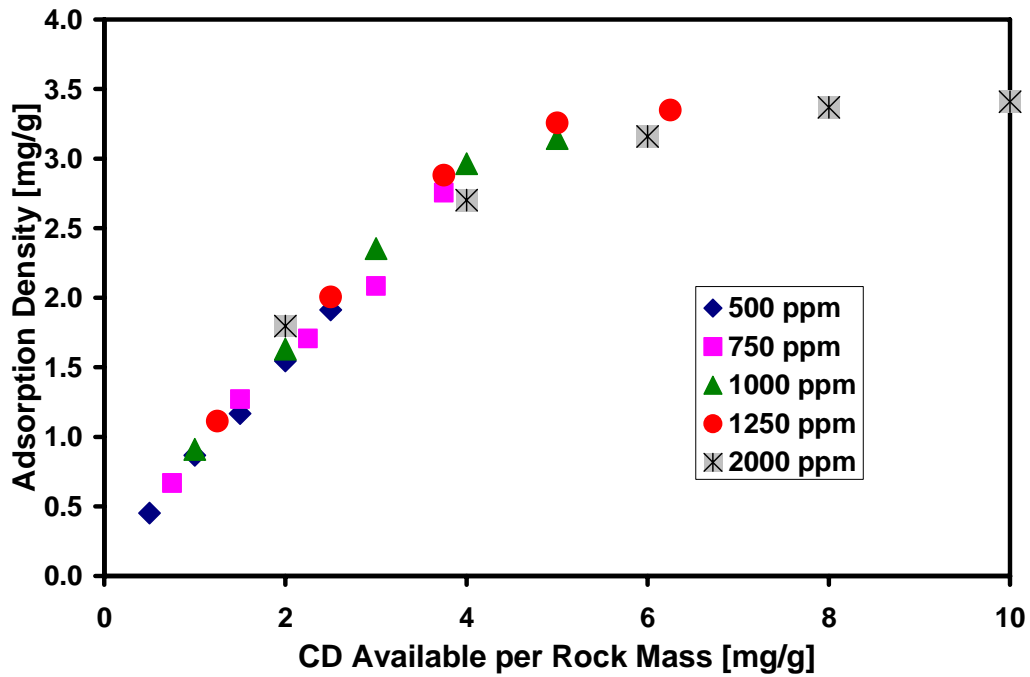


Fig. 18. CD adsorption density versus mass of CD available per gram of crushed limestone.

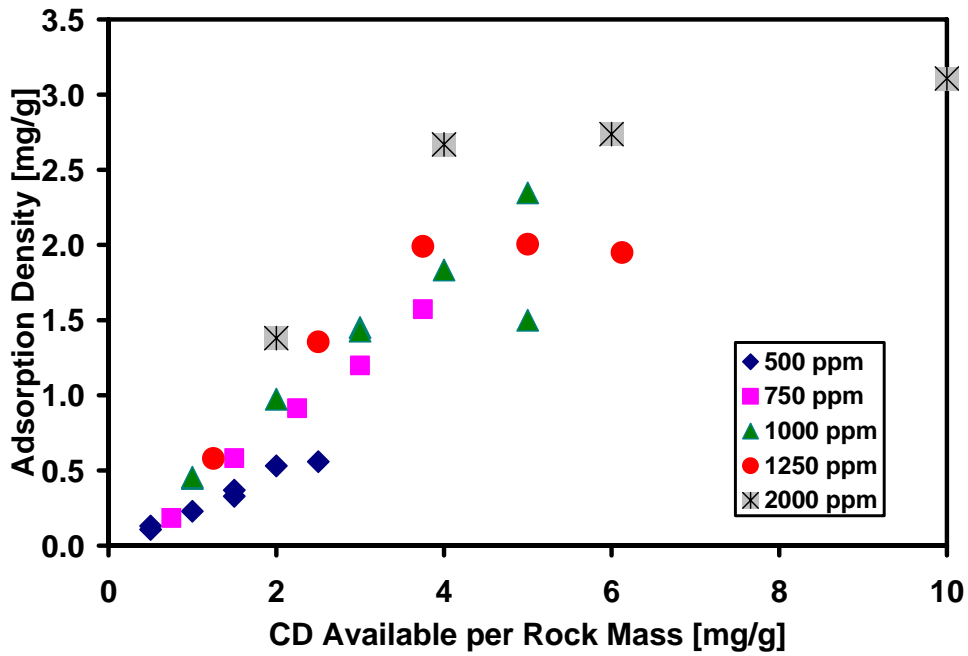


Fig. 19. CD adsorption density versus mass of CD available per gram of crushed sandstone.

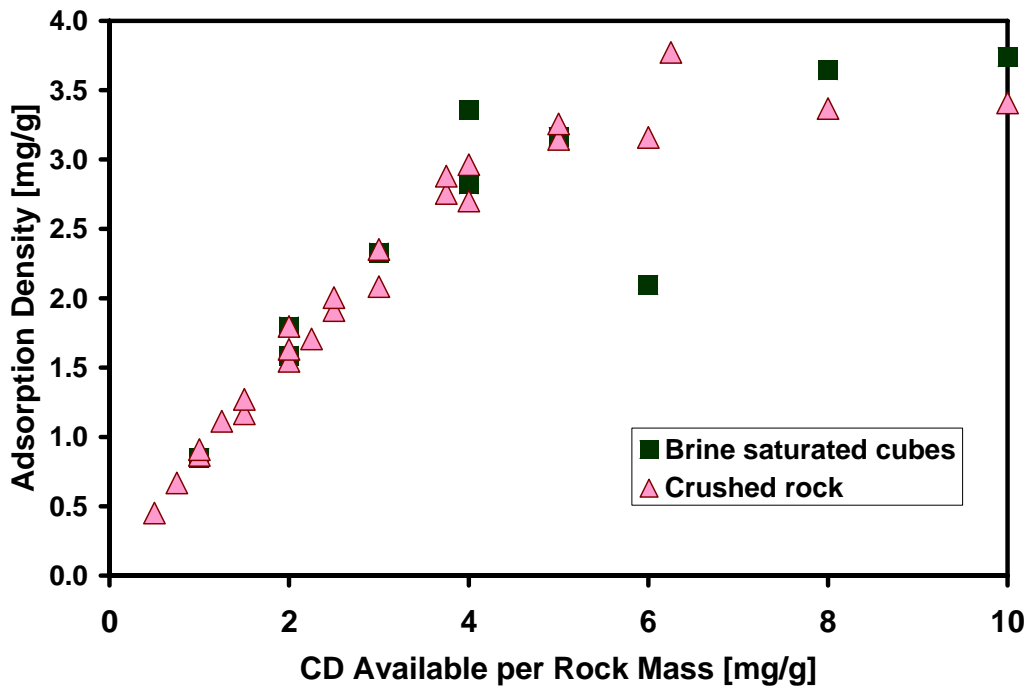


Fig. 20. Comparison of CD adsorption density onto crushed limestone and solid limestone cubes, both non-flow tests.

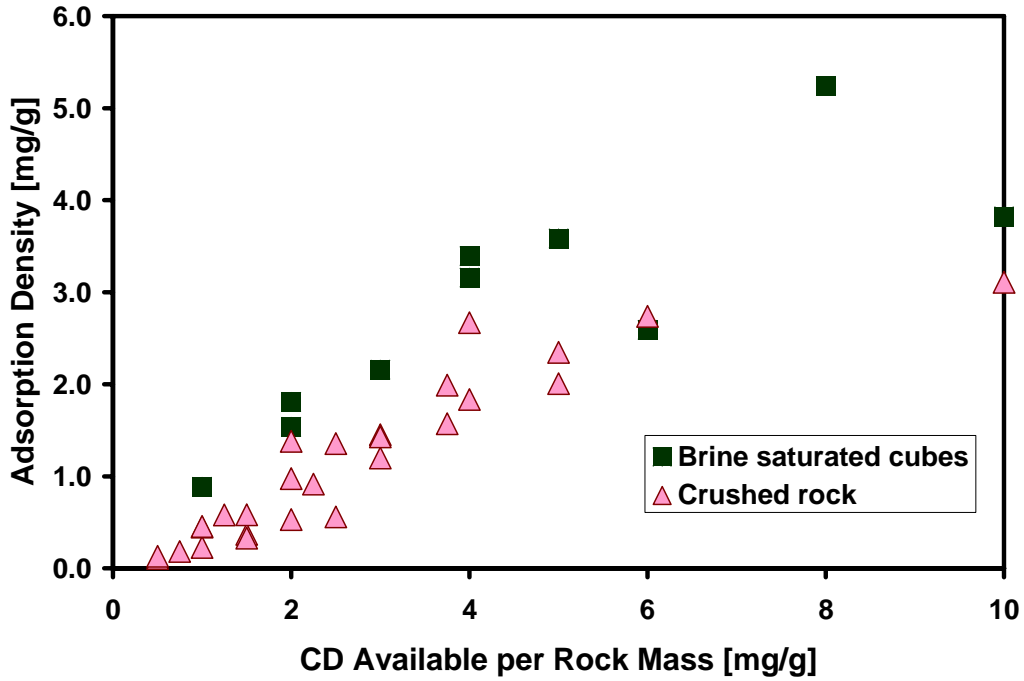


Fig. 21. Comparison of CD adsorption density onto crushed sandstone and solid sandstone cubes, both non-flow.

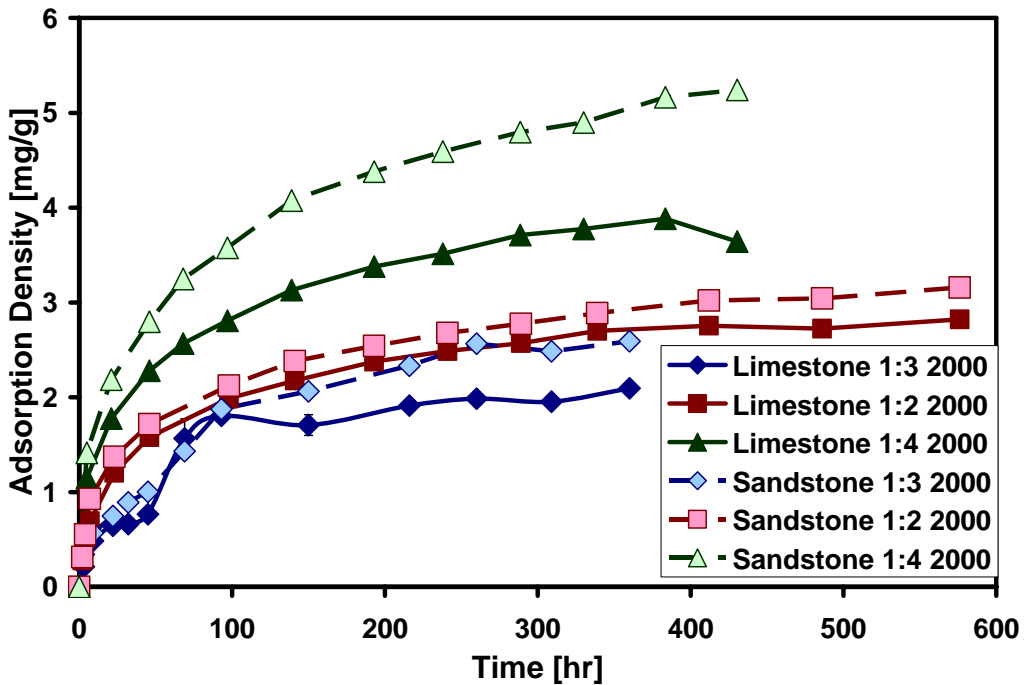


Fig. 22. Comparison of equilibrium time for several limestone and sandstone non-flow cube tests at 2000 ppm CD concentration.

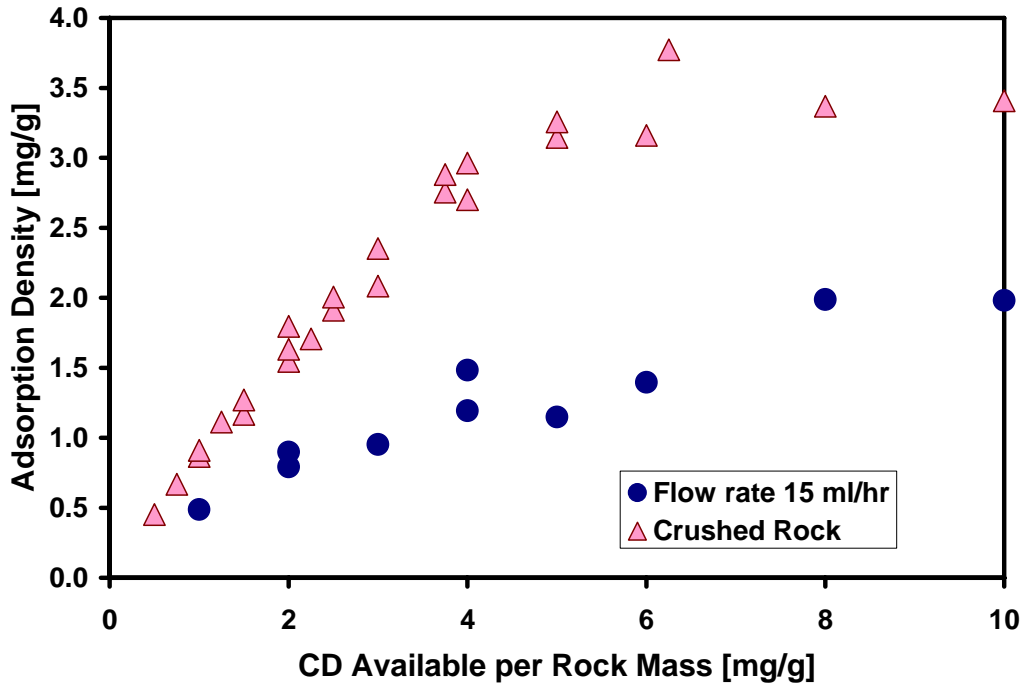


Fig. 23. Comparison of CD adsorption density for crushed limestone and flow-through limestone core tests.

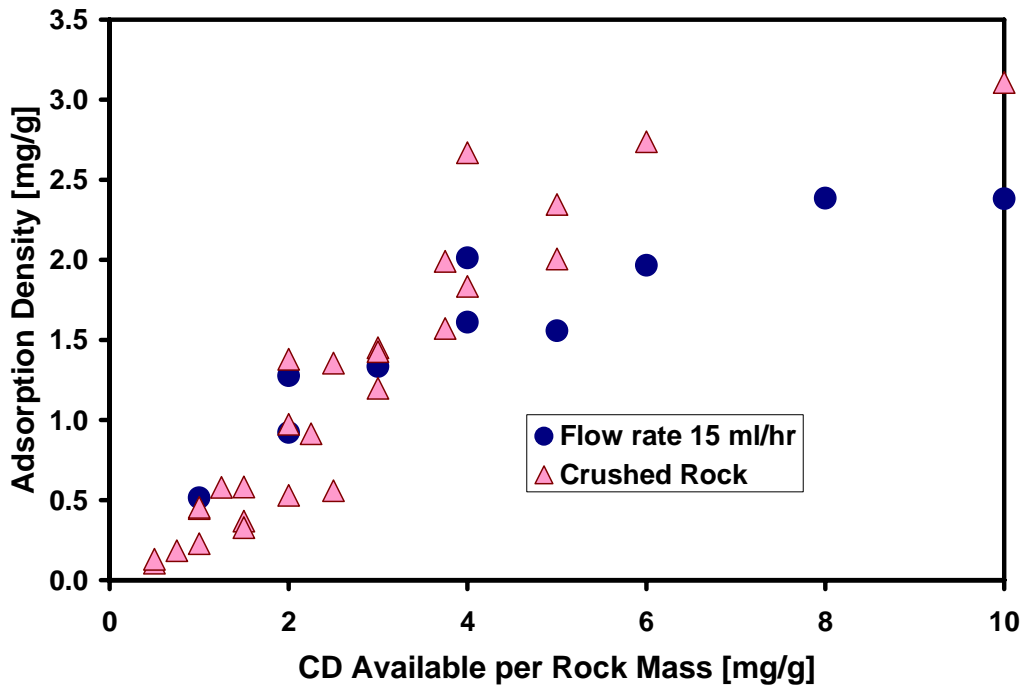


Fig. 24. Comparison of CD adsorption density for crushed sandstone and flow-through sandstone core tests.

### Chapter 3: Development of Kinetic Models of a CO<sub>2</sub>-foaming Surfactant onto Berea Sandstone from Sorption Experiments

#### Introduction

This chapter presents the results of eight series of adsorption and seven series of desorption experiments of CO<sub>2</sub> foaming surfactant CD1045 onto and from Berea sandstone, each with a different initial concentration. Nonlinear pseudo- first and second order kinetic models for adsorption and desorption processes were derived. A simplex optimization method was adapted for the calculation of kinetic parameters of these models. This method can be used for calculating not only the kinetic model parameters, but also the absolute errors between the model and the measurements, and thus the fitness of the model. Using this simplex method and the experimental results, the adsorption and desorption processes of CD1045 onto and from Berea sandstone were found to follow the pseudo- second order adsorption model and the pseudo-first order desorption model, respectively.

The history of US oil production shows that one-third to half of the original oil in place (OOIP) is recovered using primary and secondary production technologies.<sup>68,69</sup> Enhanced oil recovery (EOR) thus targets the remaining half to two-thirds of reserves that are usually isolated and trapped. There are many different EOR technologies, among which CO<sub>2</sub> flooding has the advantage of high effectiveness in recovering trapped oil, but its drawback of low sweep efficiency due to high mobility and gravity override restricts its applications.<sup>70,71</sup>

One effective method to increase sweep efficiency is to increase the viscosity of the CO<sub>2</sub> by generating CO<sub>2</sub> foam through adding surface-active agents, *surfactants*, during the injection.<sup>72</sup> A routinely used technique in CO<sub>2</sub> flooding is water-alternating-gas (CO<sub>2</sub>), or WAG, injection in which water and CO<sub>2</sub> are alternatively injected into the formation. In the CO<sub>2</sub> injection cycle, surfactant solution and liquid CO<sub>2</sub> are injected alternatively. The process is sometimes called surfactant-alternating-gas (SAG). During the CO<sub>2</sub> injection cycle, foam will be formed when the CO<sub>2</sub> phase mixes with the surfactant solution.<sup>73</sup>

A proper surfactant concentration is the key to CO<sub>2</sub> foam efficiency and durability. Laboratory and field experiences have shown that foaming capability depends on such factors as surfactant type and concentration, oil composition, rock wettability, flow rate, pressure and temperature.<sup>74</sup> For each specific reservoir, a specific surfactant type and concentration is chosen based on laboratory screening experiments and field pilot tests. While the formation and oil

conditions stay relatively stable, surfactant concentration may change during injection and flooding due to adsorption onto and desorption from the formation rocks. In order to take proper counter measures to keep the surfactant concentration at the right level, it is essential to understand the surfactant sorption kinetics.

The study of surfactant sorption kinetics has a long history in many different disciplines.<sup>75,76</sup> In petroleum engineering, surfactant sorption studies have been related to chemical flooding and foam flooding.<sup>77</sup> Recently, pseudo-first and second order models have been proposed.<sup>40,78</sup> However, equations cited in the literature included several variables on both sides of the equations. In addition, linear equations have been obtained through simplification of the original pseudo-first and second order sorption equations based on some unrealistic assumptions. These assumptions have, in fact, jeopardized the physics foundation of the kinetics model itself, and thus the kinetic parameters determined cannot fully describe the real sorption processes.

Our studies intend to improve upon our previous work through the following: (1) to derive the pseudo-first and second order sorption kinetics models in a mathematically complete format, (2) to develop a simplex nonlinear optimization method applicable for calculating kinetic parameters in both linear and nonlinear equations, and (3) to determine the kinetic parameters of CD1045 onto and from Berea sandstone using this simplex method and previous experimental results.

## **Experimental Study**

### ***Experimental Design***

The experiment design was reported in a previous paper.<sup>8</sup> Two methods, circulation and flow-through, were used to study adsorption and desorption, respectively. The circulation experiment was used to simulate adsorption during the injection of surfactant solution. The flow-through experiment was intended to study desorption during water injection.

### ***Circulation Experiment***

The circulation experimental apparatus comprised a solution flask, a magnetic stirrer, a pump and the core (Fig. 25). The core was first flushed by a certain volume of brine at a constant flow rate. After circulating a designed period of time, the brine was replaced with the same volume of

surfactant solution with known concentration. At predetermined intervals, surfactant solution was sampled from the flask for analysis.<sup>40</sup>

### ***Flow-through Experiment***

The flow-through experiment setup is shown in Fig. 26. It was composed of a solution beaker, a pump, the core, and an effluent collector. The effluent sample was sampled at designed intervals for surfactant analysis using spectro-photometer.

### ***The Materials***

The surfactant was CD1045 provided by Chaser International as 46.7 wt% active aqueous solution. Surfactant solution was prepared by adding 2 wt% synthetic brine to the original CD 1045. The synthetic brine was composed of 1.5 wt% NaCl and 0.5 wt% CaCl<sub>2</sub>. This synthetic brine was also used as the flush fluid in the desorption experiment.

The core specimen was Berea sandstone of 3.81 cm in diameter and 6.2 cm in length with porosity of 21.05%, and permeability of 224 mD. In this study, eight series of circulation experiments for adsorption and seven series of flow-through experiments for desorption were conducted. Tables 8 and 2 show the adsorption and desorption experimental conditions. In Table 8 the surfactant concentration refers to the initial value in the circulation solution; in Table 9 this value is used to relate desorption and adsorption experiments.

### ***Adsorption Density in Adsorption Process***

The measured adsorption density during the adsorption and desorption processes was calculated from the results of these experiments. The measured adsorption density in the circulation experiment is calculated according to the following equation:

$$q_i = \frac{\sum_{i=1}^N (C_{i-1} - C_i) \cdot V_i}{W} \quad 3]$$

where  $q_i$  is the surfactant adsorption density at the  $i^{th}$  step, mg/g;  $W$  is the mass of the rock specimen, g;  $C_i$  is the surfactant concentration at the  $i^{th}$  step, mg/l;  $V_i$  is the total surfactant solution volume at the  $i^{th}$  step, l; and  $N$  is the total steps at present.

The surfactant solution was sampled and tested more often at the beginning. Table 10 shows the results of Ads. Test 1, for which initial surfactant concentration was 196 mg/g.

### ***Adsorption Density in Desorption Process***

For the desorption process, the adsorption density at each step was calculated using the following equation group:

$$\left\{ \begin{array}{l} A_1 = q_0 \cdot W + C_0 \cdot PV \\ A_i = A_{i-1} - C_{i-1} \cdot Ve_{i-1} \quad (i = 2, \dots, N) \\ M_i = C_{i+1} \cdot PV \\ B_i = A_i - M_i \\ q_i = \frac{B_i}{W} \end{array} \right. \quad [4]$$

where  $A_i$  is the surfactant in the rock and tubing at the  $i^{th}$  step, mg;  $q_0$  is the initial surfactant adsorption density in the desorption process, mg/g;  $W$  is the mass of the rock specimen, g;  $C_0$  is the initial surfactant solution concentration in the desorption process, mg/l;  $PV$  is the volume of the pore space and the tubing, l;  $Ve_i$  is the effluent volume at the  $i^{th}$  step, l;  $M_i$  is the surfactant left in the pore space and the tubing at the  $i^{th}$  step, mg; and  $N$  is the total steps at present.

Similarly, the effluent was analyzed more frequently at the beginning. Table 11 shows the results of Des Test 1, corresponding to Ads Test 1.

In total, eight series of circulation experiments for adsorption were conducted, and seven series of flow-through experiments for desorption were performed. From the measured adsorption density at different steps during the adsorption and desorption processes, the adsorption and desorption kinetics of the surfactant can be determined.

### **Derivation of Kinetic Equations**

Assuming rate dependence of surfactant sorption, the pseudo-first and second order kinetic models for adsorption and desorption are derived as follows.

#### ***Pseudo First Order Adsorption Model***

If the adsorption process obeys pseudo-first order adsorption model, it can be written in the following differential equation:<sup>78</sup>

$$\frac{dq}{dt} = k_{a1}(q_e - q) \quad [5]$$

where  $q$  is the surfactant adsorption density, mg/g;  $t$  is the time, h;  $k_{a1}$  is the pseudo-first order kinetic coefficient of adsorption, h<sup>-1</sup>; and  $q_e$  is the surfactant adsorption density at equilibrium, mg/g.

The initial condition is  $q = 0$  at  $t = 0$ . Using this condition, the solution for Eq. 3 is obtained as follows:

$$q = q_e(1 - e^{-k_{a1}t}) \quad [6]$$

### ***Pseudo Second Order Adsorption Model***

The differential equation for the pseudo-second order adsorption model can be written as:<sup>78</sup>

$$\frac{dq}{dt} = k_{a2}(q_e - q)^2 \quad [7]$$

where  $k_{a2}$  is the pseudo-second order kinetic coefficient of adsorption, g/(mg •h); and  $t$ ,  $q$ , and  $q_e$  are the same as in Eq. 5.

Integrating Eq. 7 at the initial condition of  $q = 0$  at  $t = 0$ , the following solution is obtained:

$$\frac{1}{q_e - q} - \frac{1}{q_e} = k_{a2}t \quad [8]$$

Rearranging Eq. 8 leads to:

$$q = \frac{k_{a2} \cdot q_e^2 t}{1 + k_{a2} \cdot q_e t} \quad [9]$$

### ***Pseudo-First Order Desorption Model***

The differential equation of the pseudo-first order kinetic model for desorption process can be defined as:<sup>40</sup>

$$\frac{dq}{dt} = k_{d1}(q - q_r) \quad [10]$$

where  $k_{d1}$  is the pseudo-first order kinetic coefficient of desorption, h<sup>-1</sup>; and  $q_r$  is the residual surfactant adsorption density at the end of the desorption process.

The initial condition is  $q = q_0$  at  $t = 0$ , where  $q_0$  is the adsorption density at the start of the desorption process. Solving Eq. 10 based on this initial condition gives:

$$q = (q_0 - q_r)e^{k_{d1}t} + q_r \quad [11]$$

### ***Pseudo-Second Order Desorption Model***

The differential equation of the pseudo-second order kinetic model for the desorption process can be defined as:

$$\frac{dq}{dt} = k_{d2}(q - q_r)^2 \quad [12]$$

where  $k_{d2}$  is the pseudo-second order kinetic coefficient of desorption, g/(mg •h). With the initial condition  $q = q_0$  at  $t = 0$ , Eq. 12 is solved as follows:

$$\frac{1}{q - q_r} = \frac{1}{q_0 - q_r} - k_{d2}t \quad [13]$$

It can be further simplified as:

$$q = \frac{q_0 - q_r}{1 - k_{d2} \cdot (q_0 - q_r) \cdot t} + q_r \quad [14]$$

Using the experimental data obtained in last section, Eqs. 6, 9, 11 and 14 can be used to test if the adsorption and desorption processes can be described by these models; and if a specific model is applicable, what the kinetics parameters' values are. In return, when the kinetic model and their parameters are known the change of the surfactant concentrations in the solution can be predicted, and thus the foaming processes.

### **Simplex Nonlinear Optimization**

It can be seen that in Eqs. 6, 9, 11 and 14, adsorption density and time are related nonlinearly. Previous efforts to test nonlinear models through simplification and linearization have limitations. For instance, only two unknown parameters can be determined. For nonlinear equations with three and more unknown parameters, the linear correlation method does not apply. The correlation coefficient,  $R^2$ , is a relatively relax condition. No absolute errors are given in this type of correlation. In order to overcome these limitations, simplex method for nonlinear optimization is adapted here for testing the models and determining their parameters.

The simplex method refers to two different mathematical optimization approaches: simplex linear programming<sup>79</sup> and simplex nonlinear optimization.<sup>80</sup> While sharing the same

name, these two approaches are completely different.<sup>81</sup> This paper focuses on the method of simplex nonlinear optimization.

### ***Function Definition***

A properly defined function is the basis of simplex nonlinear optimization. An objective function is assumed to be defined by  $n$  variables as:

$$\begin{aligned} f &= f(X) \\ &= f(x_1, x_2, \dots, x_n) \end{aligned} \quad [15]$$

Now the task is to find a set of variables,  $X^0(x_1^0, x_2^0, \dots, x_n^0)$  minimizing the simplex function  $f$ .

### ***Mathematical Procedures***

The general idea of the simplex method is to minimize the simplex function of the  $n$  variables by comparing function values at  $(n+1)$  points, which forms a polyhedron, or simplex, in the  $n$ -dimensional space. In each step of iteration the point that makes the function maximum and minimum are termed as the worst point,  $W$ , and the best point,  $B$ . The worst point is replaced by a new point calculated through the simplex operation. The procedures are as follow:

- Step 1. Initialize  $(n+1)$  feasible solutions to define the initial simplex.
- Step 2. Calculate the function value at each point. Find the best and the worst point which makes the function value minimum and maximum, respectively.
- Step 3. Calculate the possible new point to substitute for the worst point.
- Step 4. Substitute the worst point by a new point according to the simplex operation rules.
- Step 5. Repeat Step 2 through Step 4 until a previously defined criterion is satisfied.

These procedures are achieved by four basic operations: reflection ( $R$ ), expansion ( $E$ ), contraction ( $C$ ) and shrinking ( $S$ ), as demonstrated in Fig. 27 by a two-variable simplex. In Fig. 27,  $BMW$  is the initial simplex, in which  $B$  represents the best point,  $W$  the worst, and  $M$  the intermediate. The dashed lines represent the simplex operations,  $R$  refers to the reflected point of  $W$ ,  $E$  the expanded point of  $R$ ,  $C$  the contracted point of  $W$ , and  $S_1$  and  $S_2$  the shrunk points of both  $M$  and  $W$ . Whether the initial simplex  $BMW$  becomes  $BMR$ ,  $BME$ ,  $BMC$  or  $BS_1S_2$  is decided by the following simplex operations.

### **Simplex Operations**

**Initialize the Simplex.** Assuming the initial simplex is composed of the following  $(n+1)$  points:

$$X_i = (x_{1i}, x_{2i}, \dots, x_{ni}) \quad (i = 1, 2, \dots, n+1) \quad [16]$$

Each of the  $X_i$  must be both mathematically and physically valid to Eq. 15. The simplex function value at each point is:

$$f_i = f(X_i) \quad (i = 1, 2, \dots, n+1) \quad [17]$$

**Rank the Function Values.** The function value of each point is calculated. Then the best point,  $B(X_B)$ , and the worst point,  $W(X_W)$ , are determined by the following formula:

$$\begin{cases} f_B = f(X_B) = \min(f_i) \\ f_W = f(X_W) = \max(f_i) \end{cases} \quad (i = 1, 2, \dots, n+1) \quad [18]$$

**Calculate the Reflection Point.** The reflection point,  $R(X_R)$ , of the worst point,  $W(X_W)$ , is calculated as follows:

$$\begin{cases} X_R = 2X_F - X_W \\ X_F = \frac{1}{n} \sum_{\substack{i=1 \\ i \neq W}}^{n+1} X_i \end{cases} \quad [19]$$

**Substitute the Worst Point.** The substitution of the worst point is conducted according to the following simplex rules:

a. If  $f_R < f_B$ , then  $R(X_R)$  is expanded to  $E(X_E)$ , by the following formula:

$$X_E = (1 + \mu)X_R - \mu X_F \quad [20]$$

where  $\mu$  is the expanding coefficient,  $1.2 < \mu < 2$ . Now if  $f_E < f_B$ , then  $W(X_W)$  is substituted by  $E(X_E)$ ; otherwise,  $W(X_W)$  is substituted by  $R(X_R)$ .

b. Else, if  $f_B < f_R < f_W$ , then  $W(X_W)$  is substituted by  $R(X_R)$ .

c. Otherwise, if  $f_R \geq f_W$ , then  $R(X_R)$  is contracted to  $C(X_C)$ , by the following formula:

$$X_C = \lambda X_W + (1 - \lambda)X_F \quad [21]$$

where  $\lambda$  is the contracting coefficient,  $0.0 < \lambda < 1.0$ .

Now if  $f_C < f_W$ , then  $W(X_W)$  is substituted by  $C(X_C)$ ; otherwise, the whole simplex is shrunk by half toward the best point,  $B(X_B)$ , to form a new simplex by the following formula:

$$X'_i = \frac{1}{2}(X_i + X_B) \quad (i = 1, 2, \dots, n + 1) \quad [22]$$

where  $S_i(X'_i)$  is the new points of the simplex.

After the above substitution steps, a new simplex is formed. The function value of each point of this new simplex is again calculated by Eq. 15, and the simplex operations from ranking to substitution are repeated until a predefined criterion is satisfied.

### **Simplex Algorithm for Sorption Kinetics**

In the previous section, equations of the pseudo-first and second order adsorption and desorption models were derived. From Eqs 6, 9, 11 and 14, it is seen that adsorption models have two unknown parameters, and desorption models have three unknown parameters. Using the above simplex method and the experimental data of Ads. Test 1 and Des. Test 1 shown in Tables 10 and 11, this section will demonstrate the testing of the models and determination of the kinetic parameters.

#### ***Test of Pseudo-Second Order Adsorption Model***

**Defining the Function.** The pseudo-second order adsorption model, Eq. 9, has two unknown parameters,  $k_{a2}$  and  $q_e$ . Thus the simplex will have three points,  $(k_{a2i}, q_{ei})$  ( $i = 1, 2, 3$ ). In Table 3, there are 12 measurements,  $(t_j, q_{tj})$  where ( $j = 1, 2, \dots, 12$ ). On the other hand, for each measurement time,  $t_j$ , a theoretical adsorption density,  $q_{cj}$ , can be calculated using Eq. 7 with each assumed value of  $(k_{a2i}, q_{ei})$ . Now the goal is to find the best point  $(k_{a2b}, q_{eb})$  that can minimize the cumulative difference between the measured and the calculated adsorption densities. With these considerations, the function is defined as:

$$f_i = \sum_{j=1}^M \left| q_{tj} - \frac{k_{a2i} \cdot q_{ei}^2 \cdot t_j}{1 + k_{a2i} \cdot q_{ei} \cdot t_j} \right| \quad [23]$$

where  $j$  is the index of measurements;  $i$  is index of simplex points; and  $M$  is the total number of measurements,  $M=12$  in Ads Test 1.

**Initiated Simplex.** Theoretically, the simplex algorithm is independent of the initial values of  $(k_{a2i}, q_{ei})$  where ( $i = 1, 2, 3$ ). However, a reasonable set of initial values would speed up the search for the solution. In order to give reasonable initial values for  $(k_{a2i}, q_{ei})$  where ( $i = 1, 2, 3$ ),

a rough estimate of the ranges of these parameters is helpful. If the adsorption process is rate-independent,  $k_{a2}$  would be zero; otherwise,  $k_{a2}$  could be any positive value. If there is no adsorption,  $q_e$  would be zero. From Table 10,  $q_e$  could be very well constrained within 0 and 1. Based on this rough estimation, three pairs of initial values are given in Table 12. Initial values in a larger range have been tested and same results have been repeated.

**Solution Criterion.** Two criteria were applied: the absolute error and the maximum iteration of simplex operations. The first is the function value defined by Eq. 23 divided by the number of measurements. It is the error between the measured and calculated values. This criterion was set at  $0.005 \text{ mg/g}$  for Ads Test 1. The second criterion was set to avoid dead loop in case of incorrect model or unrealistic error level. A maximum iteration of 1000 was set in this case.

**Results of Ads. Test 1.** Using the above defined function, initial simplex and criteria, a computer program was developed for the simplex operation. Table 13 shows part of the results. The same results were repeated by changing the initial simplex values and the criteria. This proves that the algorithm is robust, and the results are reliable. It can be seen that the solution was obtained by the 200<sup>th</sup> iteration. After that, the solution and the error did not change. It is also seen that error criterion of  $0.005 \text{ mg/g}$  has not been met. Instead, the program stopped when the maximum iteration is reached and was not changed after 100 iterations.

Applying the  $k_{a2}$  and  $q_e$  of Table 13 and the time of Table 10 into Eq. 9, the calculated adsorption density at each time can be obtained. Figure 28 compares the measured and modeling results for this case. The model matches the test results well except the third test point that was taken at 6 hours. The experimental results are more erratic in the time period of rapid transition. This is where the experimental and modeled results deviate. This occurred and was probably due to the experimental accuracy where adsorption rate changes rapidly.

**Results of Ads. Tests 2–8.** Following the same procedure, Ads. Tests 2–8 were analyzed. Table 14 summarizes the final results of all the tests. Fitness of the measured and modeled results is shown in Fig. 29. The low absolute error, the close match between the measurements and the modeled results indicate that pseudo-second order model can describe the adsorption kinetics of the CD1045 onto the Berea sandstone under the specific conditions.

### ***Test of Pseudo-First Order Desorption Model***

Desorption experiments shown in Table 9 were found to be best fitted by the pseudo-first order desorption model. The simplex procedure is similar to that for the test of the pseudo-second order adsorption model. Applying Eq. 11 to replace the counterpart in Eq. 23, the simplex function for the desorption model is defined as:

$$f_i = \sum_{j=1}^M \left| q_{ij} - \left[ (q_{0i} - q_{ri}) e^{k_{d1i} t_j} \right] + q_{ri} \right| \quad [24]$$

In Eq. 24, there are three unknowns,  $k_{d1}$ ,  $q_0$ , and  $q_r$ . Therefore, the simplex is a three-dimensional tetrahedron. The initial simplex has four points, each with three values for each of the three unknowns. Table 15 shows the initial values for Des. Test 1.

With the above modifications of the simplex computer program, the parameters of the pseudo-first order model for Des. Test 1 are obtained as shown in Table 16. The fitness of the measured data and the modeling results are shown in Fig. 6. Des. Tests 2–7 in Table 9 were also processed in the same way. Table 17 summarizes the final results of all the desorption tests. The fitness of the model to the measured results for Des. Tests 2–7 is shown in Fig. 31. It can be seen that all desorption tests can be well-fitted by the pseudo-first order model except for Des. Test 6. This is because Des. Test 6 had three different flow rates, as shown in Table 9.

### ***Test of Pseudo-First Order Adsorption and Pseudo Second Order Desorption Models***

The adsorption and desorption experimental results were also tested with the pseudo-first order adsorption model, Eq. 6, and pseudo-second order desorption model, Eq. 14. The models did not converge, and there was no indication that they would do so, even though the iteration limit of 10,000 was used. Therefore, these experimental data cannot be described by these models.

## **Conclusions**

Through the work described in this chapter, the following conclusions were arrived:

1. The pseudo-first and second order kinetic models for adsorption and desorption were derived in a mathematically complete format. These models are nonlinear. The adsorption models have two unknown parameters, and the desorption models have three unknown parameters.
2. A simplex nonlinear optimization method was adapted for the determination of the unknown parameters for these kinetics models. This algorithm can be applied to determine not only the

parameters of these nonlinear models, but also the absolute error between the model and the measured results.

3. The adsorption and desorption processes of surfactant CD1045 onto and from Berea sandstone were found to obey the pseudo-second order adsorption model and the pseudo-first order desorption models, respectively. More experimental work under different conditions will be carried out to better understand the influences of different factors on the sorption processes.

**Table 8. Adsorption Experiment Conditions**

Ads. Test	Surf. conc. (mg/g)	Flowrate (cm <sup>3</sup> /h)	Temp. (°C)	Pressure (kPa)
1	196	15	40	101.3
2	493	15	40	101.3
3	727	15	40	101.3
4	1034	15	40	101.3
5	1627	15	40	101.3
6	2114	15	40	101.3
7	3123	15	40	101.3
8	485	15	23	101.3

**Table 9. Desorption Experiment Conditions**

Des. Test	Surf. conc. (mg/g)	Flow rate (cm <sup>3</sup> /h)	Temp. (°C)	Pressure (kPa)
1	196	15	40	101.3
2	727	15	40	101.3
3	1627	15	23	101.3
4	3123	15	40	101.3
5	493	30	40	101.3
6	1034	30	40	101.3
7	2114	60→4→60	40	101.3

**Table 10. Measurements of Ads. Test 1**

Step	Time (h)	Adsorption density (mg/g)
1	1	0.009
2	3	0.046
3	6	0.109
4	24	0.106
5	30	0.115
6	36	0.122
7	48	0.121
8	72	0.138
9	96	0.138
10	120	0.139
11	144	0.139
12	168	0.137

**Table 11. Measurements of Des. Test 1**

Step	Time (h)	Adsorption density (mg/g)
1	0.5089	0.1089
2	0.9749	0.0918
3	1.4368	0.0907
4	1.8972	0.0906
5	2.5097	0.0903
6	3.3083	0.0903
7	4.3241	0.0895
8	5.3496	0.089
9	5.6694	0.0888
10	9.9094	0.0868
11	18.2027	0.0842

**Table 12. Initials for Ads. Test 1**

I	$k_{a2}$ (g/(mg·h))	$q_e$ (mg/g)
1	0	0
2	0	1
3	5	0

**Table 13. Simplex Operation Results of Ads Test 1**

Iteration	$k_{a2}$ (g/(mg·h))	$q_e$ (mg/g)	Error (mg/g)
100	0.9782	0.1458	0.007
200	0.9781	0.1458	0.007
400	0.9781	0.1458	0.007
600	0.9781	0.1458	0.007
800	0.9781	0.1458	0.007
1000	0.9781	0.1458	0.007

**Table 14. Simplex Results of Ads. Tests1–8**

Ads. Test	Surf. conc. (mg/g)	Iteration	$k_{a2}$ (g/(mg·h))	$q_e$ (mg/g)	Error (mg/g)
1	196	200	0.9781	0.1458	0.007
2	493	100	0.6145	0.2691	0.014
3	727	200	0.7866	0.4254	0.006
4	1034	100	0.7940	0.5581	0.009
5	1627	100	0.2462	0.7578	0.012
6	2114	200	0.1386	0.9847	0.026
7	3123	200	0.3061	1.376	0.040
8	485	200	1.3826	0.3174	0.011

**Table 15. Initials for Des. Test 1**

I	$k_{d1}$ (h <sup>-1</sup> )	$q_0$ (mg/g)	$q_r$ (mg/g)
1	0.1	0.15	0.5
2	5	0.3	0.1
3	1	0.5	0.1
4	5	0.5	0.5

**Table 16. Simplex Operation Results of Des. Test 1**

Iteration	$k_{d1}$ (h <sup>-1</sup> )	$q_0$ (mg/g)	$q_r$ (mg/g)	Error (mg/g)
100	-4.5458	.2856	0.0895	0.001
200	-4.5759	.2886	0.0895	0.001
400	-4.5759	.2886	0.0895	0.001
600	-4.5759	.2886	0.0895	0.001
800	-4.5759	.2886	0.0895	0.001
1000	-4.5759	.2886	0.0895	0.001

**Table 17. Simplex Results of Des Tests 1–7**

Des. Test	Surf. conc. (mg/g)	Iteration	$k_{d1}$ (h <sup>-1</sup> )	$q_0$ (mg/g)	$q_r$ (mg/g)	Error (mg/g)
1	196	200	-4.5759	0.2886	0.0895	0.001
2	493	1000	-2.9550	0.2821	0.0903	0.002
3	727	500	-0.0881	0.3476	0.3017	0.001
4	1034	200	-0.0476	0.5738	0.3042	0.002
5	1627	1300	-0.0805	0.8204	0.3035	0.005
6	2114	300	-0.5127	0.9306	0.4858	0.028
7	3123	3100	-0.0664	1.0595	0.7215	0.013

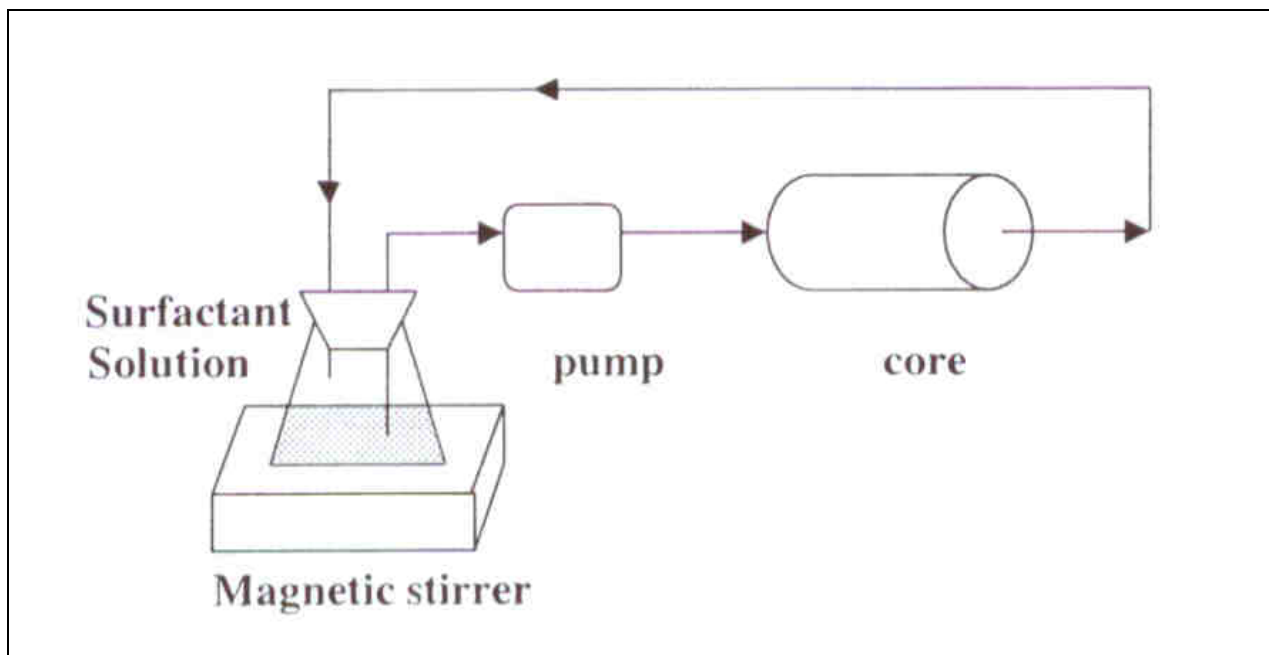


Fig. 25. Circulation experiment setup.

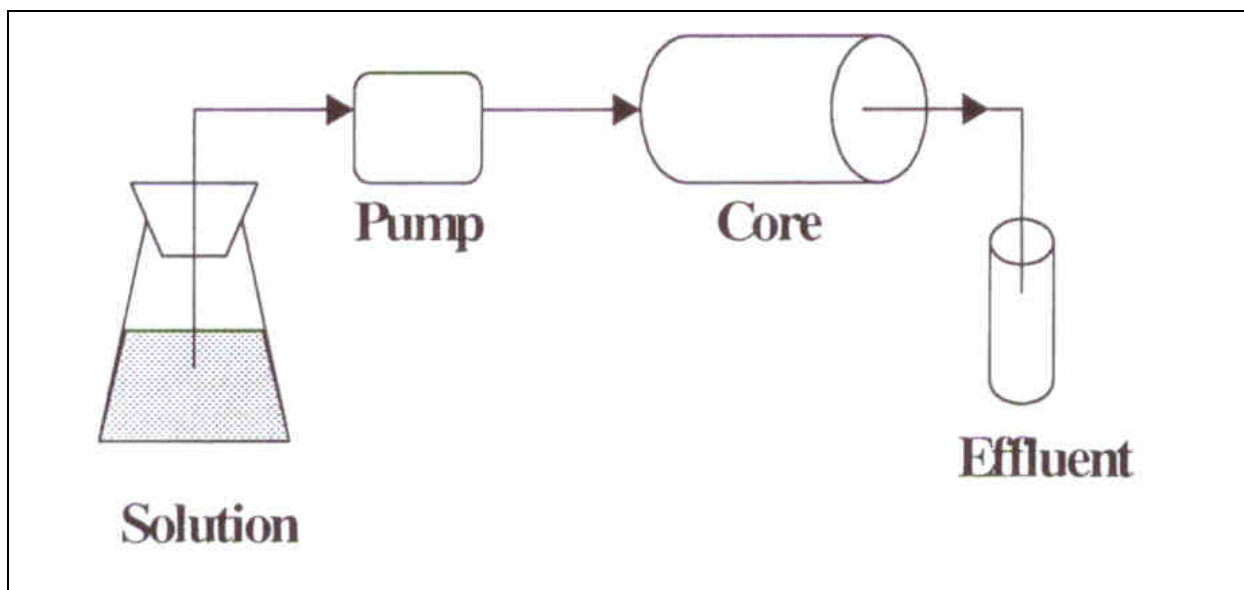


Fig. 26. Flow-through experimental set up.

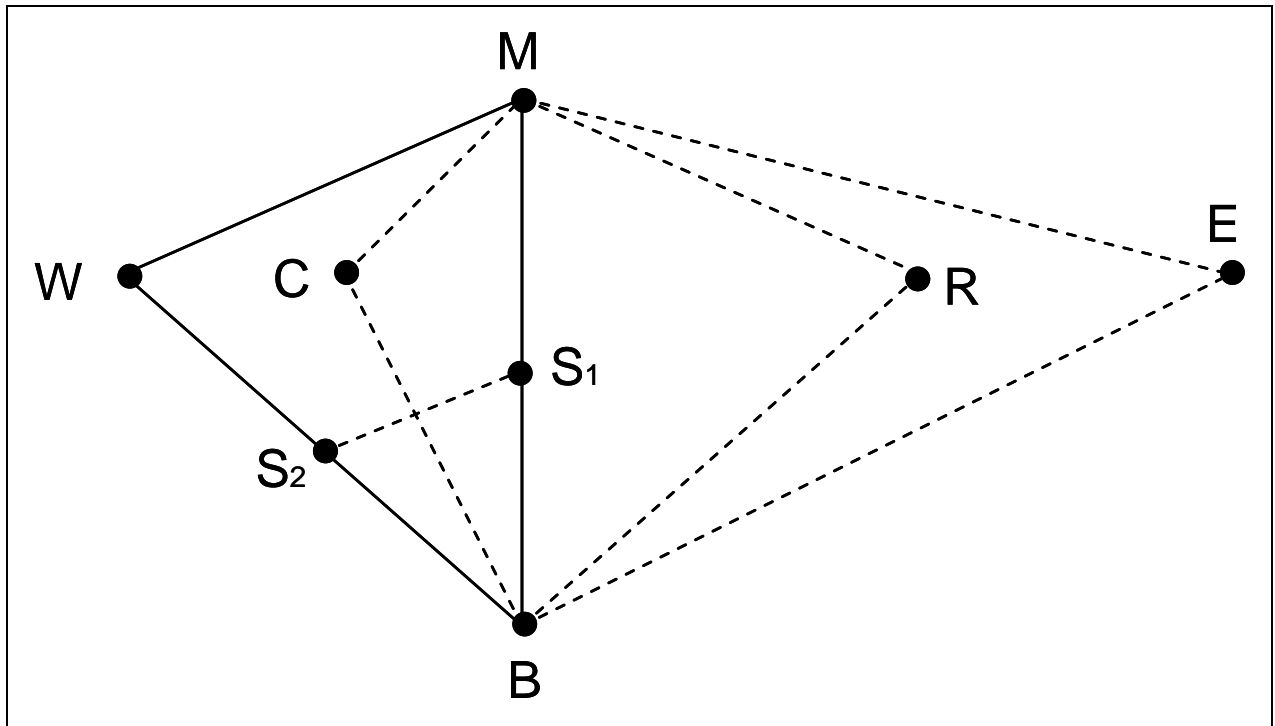


Fig. 27. Simplex operations in a 2-variable case.

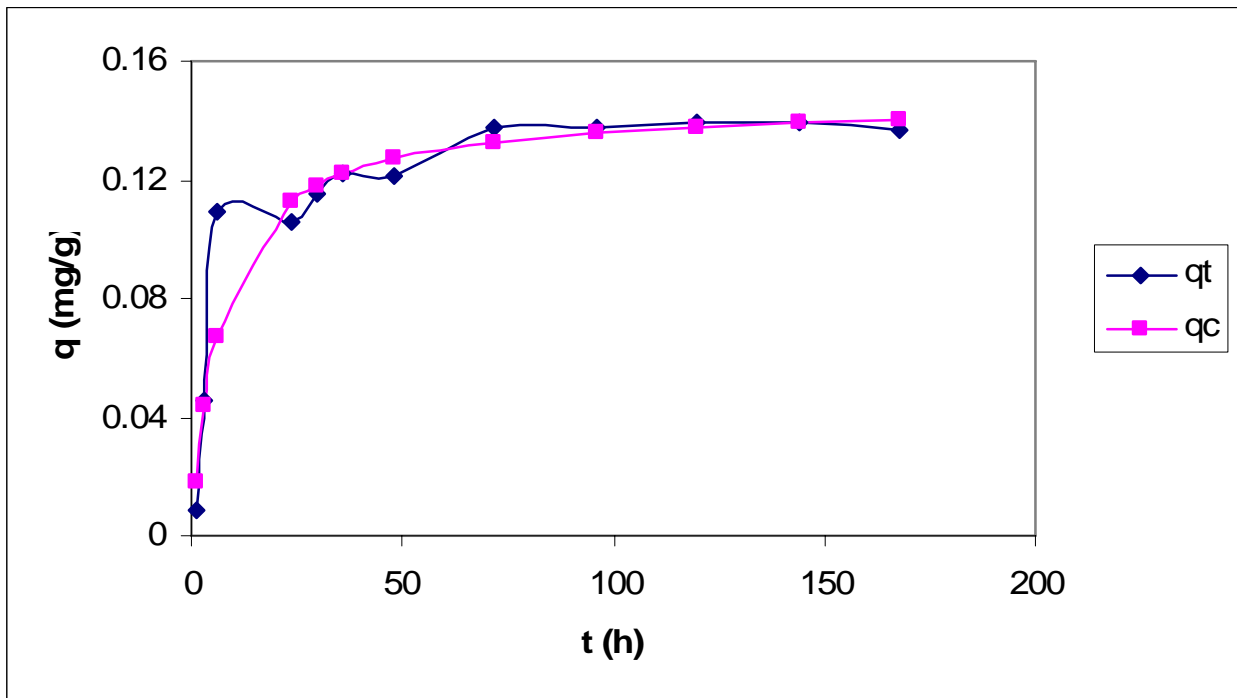
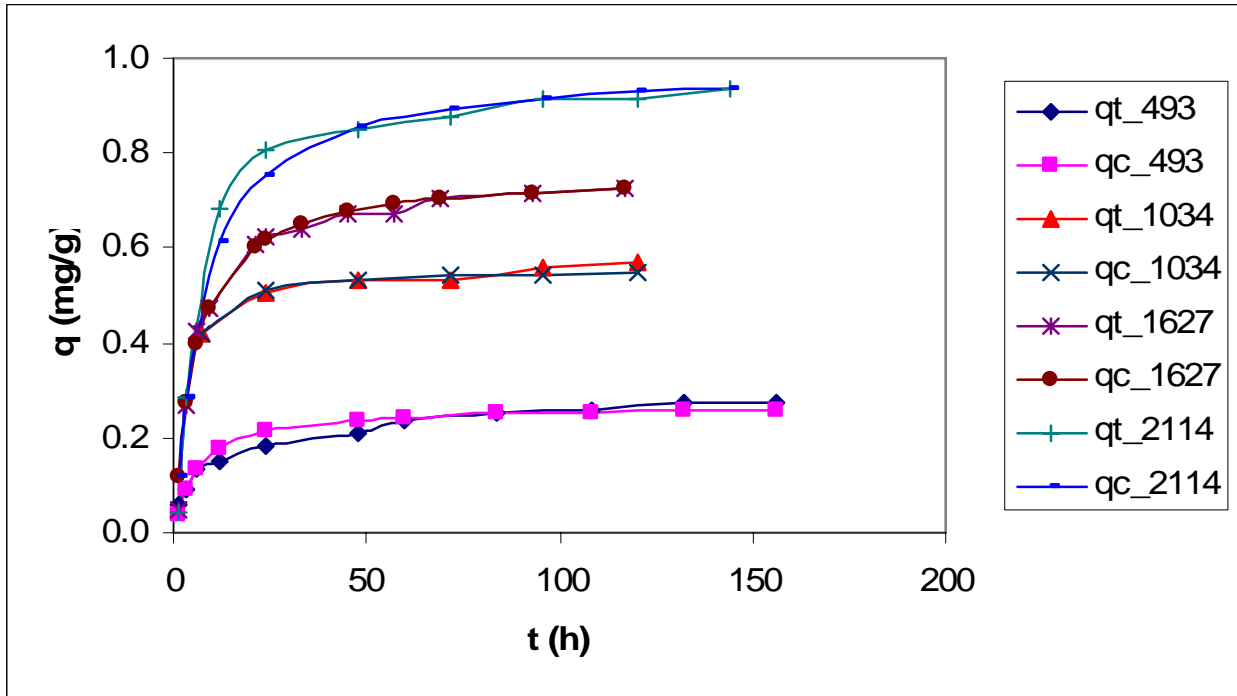
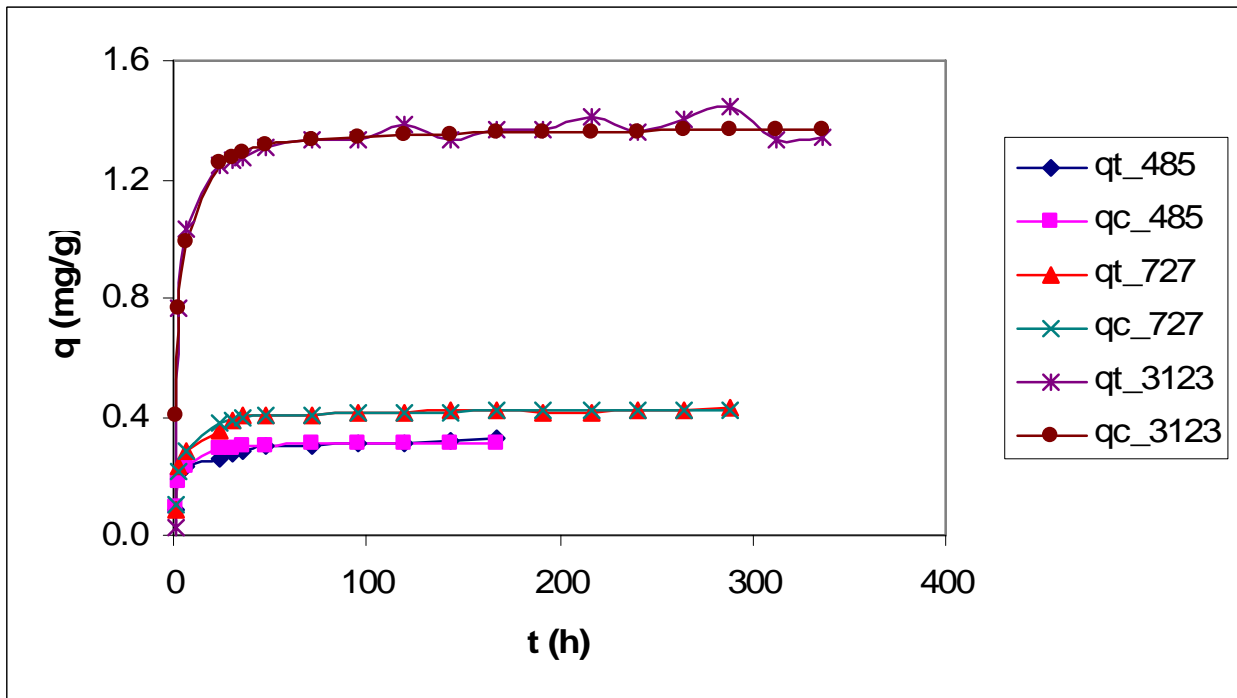


Fig. 28. Comparison of Ads. Test 1 and pseudo-second order modeled adsorption.



(a)



(b)

Fig. 29. Experimental results,  $q_t$ , compared to pseudo second order model calculated adsorption density,  $q_c$ , in Ads Test 2-8: (a) Ads Test-2, -4, -5, and -6; (b) Ads Test-3, -7, and -8.

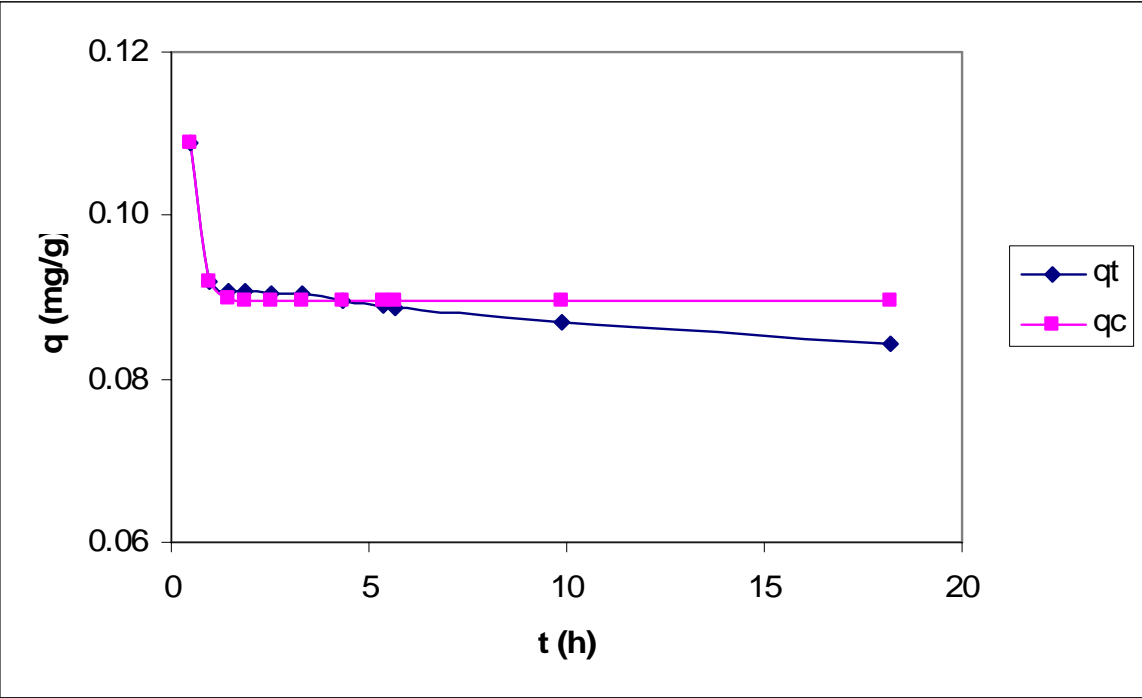
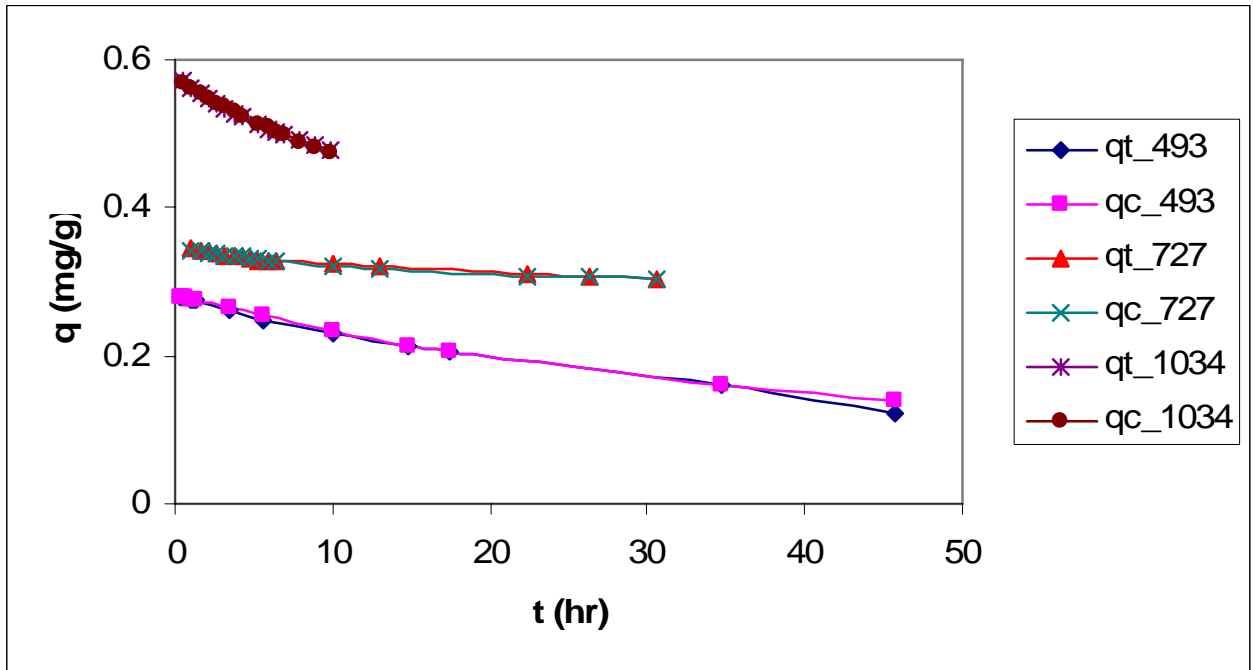
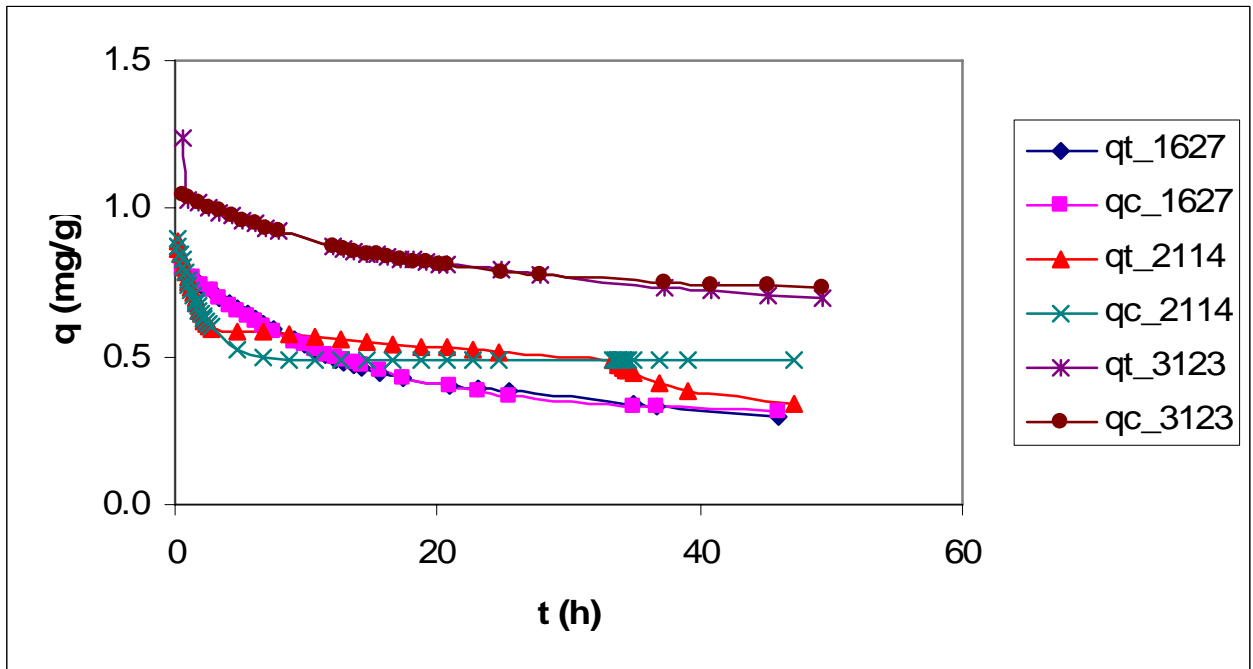


Fig. 30. Comparison of measured  $q_t$  and modeled  $q_c$  results of Des Test 1.



(a)



(b)

Fig. 31 Experimental results,  $q_t$ , compared to pseudo first order model calculated adsorption density,  $q_c$ : (a) Des Test-2, 3 and 4; (b) Des Test-5, 6 and 7.

## Chapter 4: Gas Mobility of CO<sub>2</sub>/brine at Reservoir Conditions

### Introduction

This chapter describes how gas fractional flow,  $f_g$ , is used to determine how foam flow behavior is affected by different parameters. Khatib et al.<sup>82</sup> showed that at a given gas flow rate,  $q_g$ , foam mobility decreases slightly with increasing  $f_g$  ranging from 50% to 98%. But for  $f_g > 98\%$ , foam mobility increases with increasing  $f_g$ . Similarly, De Vries and Wit<sup>83</sup> reported that, at a constant total flow rate,  $q_t$ , foam mobility decreases as  $f_g$  increases until the break point (where the pressure gradient reaches the maximum), and increases beyond that point. Also, Patton et al.,<sup>84</sup> Hirasaki and Lawson,<sup>85</sup> Marsden and Khan,<sup>86</sup> and Chang and Grigg<sup>87</sup> found that foam mobility decreases with increasing  $f_g$ . On the other hand, Lee and Heller<sup>88</sup> reported that foam mobility increases with increasing  $f_g$ . Yaghoobi and Heller<sup>89</sup> found that foam mobility increases slightly as  $f_g$  increases up to about 85%; thereafter, foam mobility increases rapidly.

Flow rate is another parameter that affects foam flow behavior. Persoff et al.<sup>90</sup> found that, at a fixed gas flow rate ( $q_g$ ), foam mobility decreases with increasing liquid flow rate ( $q_l$ ) and at a fixed  $q_l$ , foam mobility is independent of gas flow rate. Hu et al.<sup>91</sup> showed that foam mobility increases with increasing  $q_l$  at a given  $q_g$ . The results by Lee et al.<sup>92</sup> demonstrated that, at a fixed gas fractional flow ( $f_g$ ), foam mobility increases with increasing  $q_t$  (total flow rate). Khatib et al.,<sup>82</sup> de Vries and Wit,<sup>83</sup> and Yaghoobi and Heller<sup>89</sup> reported foam mobility increases with increasing  $q_t$  at a fixed  $f_g$ . Chang and Grigg<sup>93</sup> also showed that foam mobility increases with increasing  $q_t$ , and at the constant  $q_t$ , the total mobility decreases with increasing  $q_g$ .

The destabilizing effect of crude oil on foam was first examined by Bernard and Holm.<sup>94</sup> They reported that foam's effectiveness in reducing gas mobility greatly diminished when crude oil was present. More recently, Jensen and Friedmann<sup>95</sup> studied the propagation rates of nitrogen and steam foams at 149°C in partially oil-saturated Berea sandstone cores. They found that the oil must be displaced below 15% residual oil saturation before oil-sensitive foam could propagate. They also concluded that the type of oil had little effect on the overall propagation rate of the different foams, but that the type of surfactant had dramatic effects. The "oil-insensitive" surfactant produced foam that propagated through the medium more rapidly than the "oil sensitive" surfactants. The pressure drop associated with the foam created with the oil-insensitive surfactant responded more rapidly. Raterman<sup>96</sup> investigated the oil destabilization of

nitrogen in porous media and concluded that the destabilization of foams by oil in a porous media correlates strongly to the inherent probability of pseudo-emulsion film drainage and oil penetration of the gas/liquid interface. When Yang and Reed<sup>97</sup> examined mobility control using CO<sub>2</sub> foams and decane in Berea sandstone, they found there was no partitioning of surfactants into the oil phase, but one viscous and long-lived oil emulsion with decane formed for the surfactant (DPEDS and NES-25) solution. Manlowe and Radke<sup>98</sup> visually studied foam in an etched-glass, porous-medium micromodel containing residual oil and demonstrated that foam decays as a result of breakage of pseudoemulsion films between foam bubbles and oil. Foam films collapse whenever nearby thin aqueous films separating gas bubbles and oil rupture.

Due to the different results for the foam flooding discussed above, it is necessary to clarify the nature of the problem. Meanwhile, most of the investigations for the interaction between oil and foam mainly focused on nitrogen foam. To advance the field application of CO<sub>2</sub> foam, it is essential to perform a systematic laboratory study such as that described in this chapter.

For this study, the experiments were divided into two groups. In the first group, a total of six displacement experiments were performed with CO<sub>2</sub> and CD surfactant (@0.05wt % and 0.25 wt %) at three different flooding modes (changing  $f_g$  with gas flow rate, CD aqueous flow rate and total flow rate fixed, respectively) in two fired Berea sandstone cores. There were two objectives for this part of study. The first was to examine the non-oil CO<sub>2</sub> foam flow behavior in the fired Berea sandstone and further verify the effect of gas fractional flow ( $f_g$ ) and flow rate on foam mobility. The second was to determine an optimum  $f_g$  value with the highest CO<sub>2</sub> foam mobility reduction. In the second group, six oil recovery experiments were conducted based on the optimum  $f_g$  obtained in the first group of experiments. The purposes was to investigate the CO<sub>2</sub> foam behavior when oil is present.

### **Literature on CO<sub>2</sub>-foam flooding experimental study**

The flow behavior and the displacement mechanism of CO<sub>2</sub>-foam were investigated by several researchers.<sup>99,100</sup> In 1980, Bernard et al. performed CO<sub>2</sub> flooding with three types of surfactants (anionic, cationic and nonionic).<sup>99</sup> The oil recovery efficiency increased when the surfactant was injected with CO<sub>2</sub>. Wang investigated the flow behavior of CO<sub>2</sub>-foam and the displacement mechanism in glass bead pack porous media using SACROC and Rock Creek crude oils.<sup>100</sup>

With varying CO<sub>2</sub> slug injection sequences and surfactant concentration, he showed that CO<sub>2</sub>-foam flooding slightly improved oil recovery and delayed gas breakthrough.

Several researchers have reported that some surfactants generate foams, which selectively reduced mobility of CO<sub>2</sub> by a greater fraction in higher than in lower permeability regions.<sup>97,101,102</sup> The main objective of injecting CO<sub>2</sub>-foam is to divert the injection fluid into the lower permeability region. Yaghoobi et al. conducted CO<sub>2</sub>-foam core flooding in core plug without oil.<sup>89</sup> The experiment was performed in composite core samples with two different permeability regions in capillary contact. Sweep efficiency was found to be improved. The experiment was later continued on one composite core of a known heterogeneity with oil present.<sup>102</sup> The composite core system consisted of two coaxial permeability layers in capillary contact. They observed that foam was diverted to lower permeability regions and delayed CO<sub>2</sub> breakthrough, thus improving oil recovery efficiency for both regions. Additional experiments were performed with oil saturation<sup>103</sup> and compared well with earlier work.<sup>102</sup>

The idea of using foam for mobility control was proposed and patented by Bond and Holbrook in 1958.<sup>104</sup> Fried conducted foam drive experiments and reported a sharp pressure drop across the foam bank and reduced gas mobility through porous media.<sup>105</sup> Since then, there have been several reviews on foam research.<sup>93,106-110</sup> The results of these studies indicate that CO<sub>2</sub> foam will increase the apparent viscosity of displacing fluid and improve the oil recovery by decreasing mobility. Compared to CO<sub>2</sub> gas and water, CO<sub>2</sub> foam has the potential of reducing viscous fingering, improving sweep efficiency and oil recovery.

Many published studies have indicated that the presence of foam did not affect the wetting phase relative permeability.<sup>83,94,111-114</sup> Darcy's law can be applied to calculate the water relative permeability. Steady-state water saturations are different between foam and surfactant-free two-phase flow under identical flow rate conditions, while the relationship between the aqueous phase relative permeability,  $k_{rw}$ , and the aqueous saturation remains the same. However, the relative permeability of the nonwetting gas phase is drastically reduced when foam is present in the porous media. Therefore, gas mobility can be used as a measure for foam flow resistance in porous media. Also, steady-state pressure gradients are the same in both the wetting and the nonwetting phases. The gas mobility,  $\lambda_g$ , in md/cp, can be calculated using Eq. 25 and is defined as the ratio of the gas Darcy (or superficial) velocity,  $u_g$ , or volume per time period per cross-sectional area of the core,  $q_g/A$ , divided by the average pressure gradient,  $dp/dl$ , across the core

after a steady state is achieved. With the regular engineering unit, we can get the equation for gas mobility as shown in Eq. 25.:

$$\lambda_g = 1.60717 \cdot (q_g / A) / (dp / ds) \quad [25]$$

where  $\lambda_g$  is gas mobility (md/cp),  $q_g$  is gas injection rate in the core (cc/hr),  $A$  is average cross section area of the core (in<sup>2</sup>),  $dp$  is pressure drop across the entire core (psi), and  $ds$  is length of the entire core (in.).

### **The limiting capillary pressure and two foam regimes**

Capillary pressure is the pressure differential across the interface between a gas phase and a liquid phase. The capillary pressure imposed on a lamella yields an attraction between two charged interfaces. Based on DLVO theory,<sup>115</sup> the double layer repulsion must balance the van der Waals attraction plus the capillary pressure. The work required to break the film decreases as the capillary pressure increases.<sup>116</sup> Thus, capillary pressure affects foam stability outside porous media. Many published studies<sup>82,117,118</sup> verify capillary pressure effect on foam stability and illustrate that the lifetimes of lamellae decreased with capillary increase.

Similarly, foam stability in porous media depends on capillary pressure. Capillary pressure will increase with gas fractional flow at a constant gas flow rate. However, the capillary pressure,  $P_c$  will increase up to a limiting value as  $f_g$  increases. This limiting value is defined as the limiting capillary pressure,  $P_c^*$  (Fig. 32). The foam texture becomes coarser because the capillary pressure cannot exceed its  $P_c^*$  with further increase of  $f_g$ . Khatib *et al.*,<sup>82,119</sup> Persoff *et al.*,<sup>90</sup> Ettinger and Radke,<sup>120</sup> and de Vries and Wit<sup>83</sup> reported a sharp transition from stable foam to a weak foam or even no foam at  $P_c^*$  in different porous media. When  $P_c$  reaches  $P_c^*$ , foam bubbles change size as needed to maintain foam at  $P_c^*$ . As a result, liquid saturation,  $S_w$ , is constant and equal to  $S_w^*$  at  $P_c^*$  (Fig. 32). If  $P_c^*$  and  $S_w^*$  are independent of flow rates, then  $k_{rw}$  ( $S_w$ ) is constant during foam flow. This leads to the pressure gradient being proportional to the liquid flow rate, or liquid superficial velocity,  $u_w$ , and independent of the gas flow rate.

Figure 33 is a plot for two foam-flow regimes.<sup>122</sup> The vertical  $dp/ds$  contours define the high gas fractional flow regime, which is also known as the coarse foam regime. The horizontal contours define the low gas fractional flow regime or stable foam regime. In the high foam gas fractional flow regime, the pressure drop is independent of gas flow rate at constant liquid flow rate, which is controlled by  $P_c^*$  when  $P_c$  reaches  $P_c^*$ . In the low gas fractional flow regime, the

pressure gradient remains constant with changing liquid flow rate at constant gas flow rate. The transition zone between the two regimes is characterized by a specific value  $f_g^*$ , which corresponds to the critical gas fractional flow.

### **Effect of gas fractional flow and flow rate on foam mobility**

In this study, foam mobility refers to the total mobility of gas (CO<sub>2</sub> or N<sub>2</sub>)/surfactant solution. The total mobility is calculated as a single fluid and is defined as the ratio of the total injection rate per unit superficial area to the pressure gradient required for simultaneous flow of gas (CO<sub>2</sub> or N<sub>2</sub>) and brine/surfactant through the core.<sup>92</sup> That is,

$$\lambda_t = 1.60717 \cdot [(q_g + q_l) / A] / (dp / ds) \quad [26]$$

where  $\lambda_t$  is total mobility (md/cp) and  $q_l$  is liquid (surfactant solution or brine) injection rate in the core (cc/hr). Gas fractional flow ( $f_g$ ), a term conventionally called foam quality or gas quality, refers to the fraction ratio of gas injection rate in the core to the total gas-liquid injection rate, which can be expressed in Eq. 27:

$$f_g = q_g / (q_g + q_l) \quad [27]$$

where  $f_g$  is gas fraction flow. Gas fractional flow affects foam flow behavior. Khatib et al.<sup>82</sup> showed that, at a given gas flow rate,  $q_g$ , foam mobility decreases slightly with increasing  $f_g$  ranging from 50% to 98%. But for the case  $f_g > 98\%$ , foam mobility increases with increasing  $f_g$ . Similarly, De Vries and Wit<sup>83</sup> reported that, at a constant total flow rate,  $q_t$ , foam mobility decreases as  $f_g$  increases until the break point; beyond that point it increases. Also, Patton et al.,<sup>84</sup> Hirasaki and Lawson,<sup>85</sup> Marsden and Khan,<sup>86</sup> and Chang and Grigg<sup>87</sup> found that foam mobility decreases with increasing  $f_g$ . On the other hand, Lee and Heller<sup>88</sup> reported that foam mobility increases with increasing  $f_g$ . Yaghoobi and Heller<sup>89</sup> found that foam mobility increases slightly as  $f_g$  increases up to about 85%; thereafter, foam mobility increases rapidly.

Flow rate is another parameter that affects foam flow behavior. Persoff et al.<sup>90</sup> found that, at a fixed  $q_g$ , foam mobility decreases with increasing  $q_l$  (liquid flow rate); at a fixed  $q_l$ , foam mobility is independent of gas flow rate. Hu et al.<sup>91</sup> showed that, foam mobility increases with increasing  $q_l$  at a given  $q_g$ . The results by Lee et al.<sup>92</sup> demonstrated that, at a fixed  $f_g$ , foam mobility increases with increasing  $q_t$  (total flow rate). Khatib et al.,<sup>82</sup> de Vries and Wit<sup>83</sup> and Yaghoobi and Heller<sup>89</sup> reported foam mobility increases with increasing  $q_t$  at a fixed  $f_g$ . Chang

and Grigg<sup>87</sup> also showed that foam mobility increases with increasing  $q_t$ , and at a constant  $q_t$ , the total mobility decreases with increasing  $q_g$ .

## **EXPERIMENTAL APPROACHES**

### **Materials**

Chaser CD1045<sup>TM</sup> (CD) was the primary surfactant selected for this study. CD1045<sup>TM</sup> was identified as one of the best foaming agents in several other studies.<sup>89,92,123</sup> It was supplied by Chaser International as 46.8 wt% active aqueous solution. The critical micelle concentration (CMC) of the CD is approximately 0.06 wt%. Unless otherwise stated, the CD concentration used in this paper is 0.25 wt%. Calcium lignosulfonate (CLS) was obtained from Tricon Commodities International Inc. This product was produced by sulfonation of softwood lignin and provided in a yellow powder with a melting point of 266°F .

Unless otherwise stated, all aqueous solutions were 2 wt% brines with NaCl:CaCl<sub>2</sub> weight ratio of 3:1. The crude oil used in this study is dead crude with API gravity of 33.3, average molecular weight of 237 g/mol, and viscosity of 15.80 cp @ 68°F. The CO<sub>2</sub> is 99.9% purity. Dimidium Bromide-Disulphine Blue Indicator was supplied by BDH Laboratory Supplies and chloroform, HPLC grade, containing approximately 1.0% ethanol as a preservative, were used to determine unknown CD concentrations. Tetrahydrofuran (THF), 99+%, with density of 0.88 g/cm<sup>3</sup>, freeze point of -6°F and boiling point of 151°F, supplied by Acros Organics Company, was used as a strong solvent to remove the residual oil and clean the core between oil recovery experiments.

Berea sandstone from the Michigan Basin was used. Both core plugs used in this study are fired Berea sandstones (fired at ~1000°F for 5 hours), which are relatively uniform and homogeneous cores quarried in Amherst, Ohio by the Cleveland Quarries Company. Each core is 6 in. long and 2 in. in diameter. A detailed description of the two fired Berea sandstones are listed in Table 18.

### **Core flooding apparatus setup**

The CO<sub>2</sub>-foam core flooding experiments were performed by using a high pressure coreflood apparatus, which is shown in Fig. 34. Six series of CO<sub>2</sub> foam flooding experiments were conducted in this part. Two fired Berea sandstone core plugs, designated SS-1 and SS-2, were

utilized, the former plug being used in first three series and the latter plug used in last three. The fired Berea sandstone core was surrounded by an outlayer with both ends open and installed into a molded viton rubber sleeve without any pressure taps outside. The outlayer for Core SS-1 is a heat shrink plastic, but for Core SS-2, it was changed to epoxied lead foil, which can provide a more reliable seal to prevent CO<sub>2</sub> communication between the core and annulus under high overburden pressure.

The core sample body composed of core and rubber sleeve was horizontally positioned inside a Hassler-type 304-grade stainless steel core holder, which can accommodate a core up to 2 in. in diameter and 24 in. long with a maximum working pressure of 10,000 psi. The annulus between the rubber sleeve and the core holder was refilled with distilled water and kept at 3100 psi overburden pressure.

Three filters were placed in front of the core to act as a foam generator and filter; the final and smallest aperture was 0.5  $\mu\text{m}$ . One pressure transducer was incorporated in the design to measure differential pressures,  $dp_1$ , across the total core. A heater with an electric fan installed inside the air bath provided the heat and maintained the constant temperature desired for the experiment. The final equilibrium temperature of the air bath could be manually preset on a thermal adjustment box.

Two syringe pumps, Pump A and Pump B, provided the power for the coreflooding. To avoid corrosion damage, the fluid used in these two precision pumps was distilled water only. As shown in Fig. 34, pump A was used to drive flow for either of the aqueous floating piston accumulators and pump B was used to drive flow for the gas floating piston accumulator. Two backpressure regulators (BPR) with 5000 psi working pressure, were installed downstream of the accumulators to control the flow rate of CO<sub>2</sub> and aqueous solution. The two BPR valves were filled with N<sub>2</sub> gas, maintaining a dome pressure of 3100 psi at 105°F. The core was maintained at a 1540 psi pressure with one outlet BPR.

The system tubing was designed to minimize volume and eliminate possible storage of solution, which could strongly effect the effluent measurements. According to the tubing design, the fluid could flood through/bypass the core and flow out of the system with/without passing core outlet BPR. The effluent was recovered in the first trap flask, and then the CO<sub>2</sub> gas would pass through the second flask trap and enter a wet test meter through which the amount of

produced CO<sub>2</sub> can be recorded. The CO<sub>2</sub> gas passing from the wet test meter finally was released to air through a flask of fresh water for the purpose of gas visualization.

The pressures and temperatures were recorded by a computerized data acquisition system. This system consisted of a personal computer and a demodulator, receiving voltage signals from the three pressure transducers and three other temperature transducers positioned on a core holder surface, inside and outside the air bath. The voltage signals, produced by each transducer, were transformed through a designated channel into the demodulator and then to the computer for data acquisition. The time delay between two recorded data in this study was set to 1.0 min. The data were collected and finally averaged.

### **Core flooding experimental procedures**

The core was prepared in the following sequence: cut and cored cylindrical, measured and recorded dimensions, dried in an oven at 248°F temperature for 24 hrs, and evacuated and measured pore volume at 2000 psi pressure with a 3000 psi overburden pressure. Finally, the core was redried and installed horizontally into the coreholder as the procedures for apparatus setup in Fig. 34.

All the brines used in these experiments were filtered and degassed before refilling the aqueous accumulator. Assuming the compressibility due to the change of pressure and temperature was negligible; the injection rate for Pump A was equal to the flooding rate in the core. The pressure drop obtained by changing the injection rate from 10 cm<sup>3</sup>/hr to 200 cm<sup>3</sup>/hr in 10 cm<sup>3</sup>/hr intervals was used to determine the mobility of the core. The permeability to brine can be computed from viscosity times the mobility. This permeability would be used as the baseline value to evaluate changes in the core plug by comparing it with the subsequent baseline value determined between experiments.

Brine and CO<sub>2</sub> coinjection (CWG) was used as the baseline to acquire the foam mobility reduction factor (MRF) in the subsequent CD–CO<sub>2</sub> foam flooding experiments. The CWG baseline experimental methods utilized in this study are listed in Table 19.

During the brine-CO<sub>2</sub> coinjection, assuming the solubility of the CO<sub>2</sub> into the brine and brine into the CO<sub>2</sub> is negligible, efficiency of the ISCO syringe pump B is 100%, the injection flow rate is:

$$q_b \cdot \frac{\rho_a}{\rho_c} + q_a \approx q_{c1} + q_{c2} \quad [28]$$

where  $\rho_a$  is CO<sub>2</sub> density in the accumulator (g/cm<sup>3</sup>),  $\rho_c$  is CO<sub>2</sub> density in the core plug (g/cm<sup>3</sup>),  $q_a$  is injection flow rate of pump A (cm<sup>3</sup>/hr),  $q_b$  is injection flow rate of ISCO pump B (cm<sup>3</sup>/hr),  $q_{c1}$  is flow rate of CO<sub>2</sub> in the core (cm<sup>3</sup>/hr), and  $q_{c2}$  is flow rate of brine aqueous solution in the core (cm<sup>3</sup>/hr). For the experiments in this study, the average temperature was 105°F, and the pump and gas accumulator pressures were 3170 psig and the core pore pressure  $P_c \sim 1540$  psig. The densities,  $\rho_c$  and  $\rho_a$ , were obtained using an equation of state software.<sup>124</sup> During the CO<sub>2</sub>-brine coinjection flooding, the total flow rate was fixed and the flow fraction ratios between brine and CO<sub>2</sub> were varied. For each ratio, the flooding was continued until the pressure drop steady state was established.

### **CO<sub>2</sub>-CD coinjection foam flooding**

The CD aqueous solution was filtered and degassed. To start the experiment, the desired gas and aqueous solution flow rates were set, and the computerized data acquisition system was started to collect pressure drop data ( $dp_1$ ), pressure of inlet and outlet of core ( $P_{in}$  and  $P_{out}$ ), core holder temperature, room temperature and air bath (inside) temperature. The experiments performed are listed in Table 20. Normally, each test interval was stopped after the pressure drop across the core reached steady state. In the CD-CO<sub>2</sub> foam flooding, three general types of injection models were performed. One was to change the fraction flow ratio between the CD solution and CO<sub>2</sub> with fixed total flow rate. Second was to change the CD solution flow rate with fixed CO<sub>2</sub> flow rate. And third was to change the CO<sub>2</sub> flow rate with fixed CD solution flow rate. At the end of each test, the core was flushed with CD-free brine until the pressure drop through the core was close to the value obtained at the core initial conditions at the same flow rate. The effluent out of the core was collected to analyze the concentration of CD to determine the adsorption and desorption at HPHT in the CO<sub>2</sub> foam system. Finally, the brine baseline would be tested and the core damage status evaluated.

## Results and Discussion

### Brine base permeability tests

The brine base permeability results for Cores SS-1 and SS-2 are shown in Figs. 35 and 36, respectively. Figures 35 and 36 show that, even though Cores SS-1 and SS-2 are both fired Berea sandstone, their permeabilities are quite different. Brine base permeability for Core SS-1 is 26 md, while for Core SS-2 it is 450 md.

### CO<sub>2</sub>-brine coinjection base mobility tests

A series of baseline experiments were carried out by coinjecting CO<sub>2</sub> and brine into a brine-saturated core until a steady-state pressure drop across the core was achieved. The total mobility of CO<sub>2</sub>/brine and the gas mobility were determined by regression based on the constant total flow rate. These values are listed in Table 21. The results of the total mobility of CO<sub>2</sub>/brine and gas mobility as a function of  $f_g/(1-f_g)$  are shown in Figs. 37 and 38. Apparently, for both Berea sandstones, gas mobility of CO<sub>2</sub>/brine increased with increasing  $f_g$ . The total mobility increased with increasing  $f_g$  ranging from 0.6 to 0.9, but decreased with increasing  $f_g$  when  $f_g$  was less than 0.6. This observation was consistent with the results of Chang and Grigg,<sup>87</sup> which indicated that the total mobility of CO<sub>2</sub>/brine increased with increasing  $f_g$  ranging from 0.333 to 0.8, but decreased with increasing  $f_g$  when  $f_g$  is less than 0.333. The difference of value may be due to the core difference.

### Three foam flow zones and determination of $f_g^*$

**Strategies to determine  $f_g^*$ .** The effect of capillary pressure is important for any type of multiphase flow in porous media, especially when flow rates are low and the heterogeneity in the core is high. Gas fractional flow,  $f_g$ , will alter the water or gas saturation in the reservoir. Capillary pressure varies with water saturation and thus the capillary pressure will be a function of  $f_g$  with the limiting capillary pressure dividing the foam into a stable regime from unstable foam in porous media. The limiting capillary pressure determines  $f_g^*$ . A foaming agent should have a higher  $f_g^*$ , which is an essential consideration when screening surfactants for foam applications.

In order to determine  $f_g^*$ , a series of coreflooding experiments were conducted for both core plugs. For Core SS-1, the 0.05 wt% CD aqueous phase flow rate was varied from 0.20 to

1250 cc/hr at a constant CO<sub>2</sub> gas flow rate of 20 cc/hr. For Core SS-2, keeping a constant gas flow rate of 40cc/hr, two sets of experiments were performed, respectively, with CD concentration of 0.05 wt% and 0.25 wt% CD and flow rates ranging from 1.12 cc/hr to 1250 cc/hr. The experimental values are listed in Table 21. The relationships for Core SS-1 and Core SS-2 between gas mobility,  $\lambda_g$ , and  $f_g/(1-f_g)$  at the constant gas flow rate are shown in Fig. 39.

Some previous studies showed the relationship between the gas mobility and  $f_g^*$ , at a constant gas flow rate. Khatib *et al*<sup>82</sup> reported  $f_g^*$  of 0.98 for 1 wt% sodium dodecyl benzene sulfonate surfactant (Siponate DS-10) in a sand pack. Liu, et al<sup>125</sup> reported  $f_g^*$  of  $0.85 \pm 0.05$  for foam 0.25 wt% CD surfactant with a constant N<sub>2</sub> flow rate of 22 cc/hr in an Indiana limestone core. They also showed that the plot for the relationship between the gas mobility and  $f_g$  is characterized by two straight lines intersecting at  $f_g^*$ .<sup>125</sup> At lower values of  $f_g$ , gas mobility slightly decreases or remains constant with increasing  $f_g$ , while at higher  $f_g$  the foam mobility increases with increasing  $f_g$  (see Fig. 40). The solid lines in Fig. 40 represent the trend obtained from their experimental data, while the dashed lines represent the estimated trends from limited experimental data at lower constant gas flow rates. Their results obtained with different gas flow rate indicated similar  $f_g^*$ .

The effect of permeability on  $f_g^*$  was also discussed by Liu et al.<sup>125</sup> With the same core, they determined different permeability and  $f_g^*$  for different sections of core. As shown in Fig. 41, the  $f_g^*$  values corresponding to 21 md (B-the middle segment), 29 md (the entire core) and 53 md (C-the ending segment) are 0.84, 0.85 and 0.85 respectively. In Segment A (inlet section), gas mobility values are scattered because Segment A permeability increased over time presumably due to erosion and/or dissolution. The increased scatter in gas mobility for Segment C at high  $f_g/(1-f_g)$  is probably due to capillary end effects at low aqueous flow rates. The difference of permeability did not have a drastic effect on the  $f_g^*$  values.

**Three recognized foam flow zones.** The results obtained from the experiments for  $f_g^*$  determination are shown in Fig. 39. The plot for the relationship between the gas mobility and  $f_g$  can be characterized by three straight lines intersecting at  $f_g^*$  and  $f_g^0$  ( $f_g^0$  was denoted as the inflexion between single phase zone to the lower gas fractional flow zone). When  $f_g < f_g^0$ , the gas mobility increases with increasing  $f_g$ . When  $f_g \geq f_g^0$ , the foam flow demonstrated behavior similar to the results obtained by Liu, et al.,<sup>125</sup> specifically, when  $f_g^0 \leq f_g \leq f_g^*$ , gas mobility decreases

with increasing  $f_g$ . When  $f_g \geq f_g^*$ , the gas mobility increases with increasing  $f_g$ . Thus, the foam flow regime can be divided into three zones: single-phase zone ( $f_g < f_g^0$ ), low gas fractional flow zone ( $f_g^0 \leq f_g \leq f_g^*$ ) and high gas fractional flow zone ( $f_g \geq f_g^*$ ).

The reasons for the existence of  $f_g^*$  in foam flow due to the limiting capillary pressure have been elucidated in detail in the previous literature.<sup>82,97,125</sup> However, the region of the single-phase zone ( $f_g < f_g^0$ ) for the foam flow has not been mentioned previously in the literature. When the aqueous phase (CD surfactant) flow rate becomes very high, the CO<sub>2</sub> gas flow portion is nearly negligible (even though the gas is still flowing at a constant flow rate). In this case, the flow can be considered to be a single-phase flow. According to Darcy's law, the pressure drop across the core should be proportional to the aqueous flow rate. With a constant gas flow rate  $q_g$ , when increasing  $f_g$  in this zone, the aqueous flow rate will decrease, leading to a lower pressure drop gradient across the core ( $dp/ds$ ). The gas mobility, which can be expressed as  $\lambda_g = 1.60717 \cdot (q_g / A) / (dp / ds)$ , will increase linearly.

**Factors that affect the critical gas fractional flow value ( $f_g^*$ ).** Table 23 lists the results obtained from this study and an earlier study to determine  $f_g^*$ .<sup>125</sup> Surprisingly, with different core, gas (CO<sub>2</sub> and N<sub>2</sub>), core permeability, and gas flow rate, we obtained the same  $f_g^*$  as that of Liu et al. It appeared that the same type of surfactant (CD 1045) with same formulation (0.25 wt%) is the reason for the same  $f_g^*$  attained for two different experiments. With only limited results, even though we cannot conclude that  $f_g^*$  is independent of core type, core permeability, foam type and gas flow rate, at least we can predict that the surfactant is a dominant factor in determining  $f_g^*$ . This was further supported with the results for Core SS-2, shown in Table 23. Having the same conditions except that the CD concentration are 0.05 wt% and 0.25 wt%, the higher CD concentration leads to a higher  $f_g^*$  and  $f_g^0$ .

With comparison of  $f_g^*$  value, permeability and gas flow rate obtained with the same 0.05 wt% CD solution and CO<sub>2</sub> gas, for both core plugs, it was found that the higher the permeability and flow rate, the higher the  $f_g^*$  value. Without adequate experimental data, it cannot be verified which of the two parameters (permeability and flow rate) plays an important role in determining the gas fractional flow value. However, one conclusion that can be drawn is that the permeability and flow rate do affect  $f_g^*$ . Alvarez et al.<sup>121</sup> studied the relationships between the

effect of permeability and flow rate on the  $f_g^*$ . They demonstrated that whether increasing flow rate or permeability,  $f_g^*$  will increase. The results of this work are consistent with theirs.

### **Effect of $f_g$ on foam mobility**

**Effect of  $f_g$  on foam mobility with constant total flow rate.** Experiments for Core SS-1 and SS-2 were performed with CD concentration of 0.05 wt% at a constant flow rate of 20 cc/hr and 100cc/hr, respectively, with varying  $f_g$ . The experimental results are listed in Table 24. Even though there were several variables such as permeability (26.22 md and 450md) and total flow rate (20cc/hr and 100 cc/hr), the same relationships for both core plugs between the total motility and  $f_g$  were obtained. As shown in Fig. 42,  $f_g^*$  for the two core plugs are different, for Core SS-1  $f_g^*$  is 0.6 and for Core SS-2  $f_g^*$  is 0.7. Both are in a flat total mobility values region; therefore, the difference may be insignificant. When  $f_g \leq f_g^*$ , the total mobility decreases with increasing  $f_g$ , when  $f_g > f_g^*$ , the total mobility increases with increasing  $f_g$ .

The mobility reduction factor (MRF)<sup>127</sup> is an expression used to assess the magnitude of the mobility reduction in laboratory foam tests. The MRF is defined as the total mobility of CO<sub>2</sub>/brine divided by the foam mobility (total mobility of CO<sub>2</sub>/surfactant solution), where both mobility measurements are conducted at the same CO<sub>2</sub>-liquid volumetric injection ratio. Figure 43 show the changing tendency of MRF for Core SS-1 and SS-2 with variable  $f_g$  at different total flow rates. With the same CD surfactant solution (0.05 wt% concentration) but different permeabilities, the maximum MRF for Core SS-1 is 50.92 at  $f_g=0.6$  but for Core SS-2 it is 103.61 at  $f_g=0.8$ . This embodies the characteristics of foam to reduce the foam mobility selectively, that is, the higher the permeability of the core, the more the foam mobility will be reduced.

The results above are similar to those from Chang and Grigg,<sup>87</sup> who also studied the relationship between CO<sub>2</sub> foam mobility and  $f_g$  in fired Berea sandstone using solutions with 0.25 wt% CD concentration. They determined that total mobility of CO<sub>2</sub>/surfactant solution decreases with increasing  $f_g$ . Meanwhile, they also showed that the MRF increases with increasing  $f_g$  ranging from 33.3% to 80%; there appeared to be a minimum MRF between  $f_g$  value of 20% and 33.3%. The value difference may result from the varying properties of the cores used. Nevertheless, this study shares one thing with theirs, that no matter the surfactant concentration, either 0.05 wt% or 0.25 wt%, the maximum MRF was realized at about  $f_g=0.8$ .

This was considered the optimum  $f_g$  and was used to perform the subsequent oil recovery experiments.

**Effect of  $f_g$  on foam mobility with a constant CO<sub>2</sub> gas flow rate.** A schematic plot of relationship between total mobility and ratio of gas to liquid fractional flow is shown in Fig. 44, which uses the data in Table 25. For Core SS-1, one series of experiment was conducted with CD concentration of 0.05 wt% at a constant CO<sub>2</sub> flow rate of 20cc/hr, while for Core SS-2, two series of experiments were performed with CD concentration of 0.05 wt% and 0.25 wt% at a constant CO<sub>2</sub> flow rate of 40 cc/hr. The plot for the relationship between the total mobility and  $f_g/(1-f_g)$  was also characterized as three intersected straight lines with two cross points of  $f_g^0$  and  $f_g^*$ . It shows that, at a constant CO<sub>2</sub> gas flow rate, the total mobility was independent of  $f_g$  when  $f_g < f_g^0$ , decreased with increasing  $f_g$  when  $f_g^0 \leq f_g \leq f_g^*$  and increased with increasing  $f_g$  when  $f_g > f_g^*$ . The results for  $f_g \geq f_g^0$  are consistent with those of Khatib et al.<sup>82</sup> and Liu.<sup>126</sup>

The total mobility and  $f_g$  can be expressed as  $\lambda_t = 1.60717 \cdot [(q_g + q_l) / A] / (dp / ds)$  and  $f_g = q_g / (q_g + q_l)$ . When  $f_g < f_g^0$ , the aqueous flow rate is so high that the gas flow rate  $q_g$  in this region can be negligible, so the flow is an aqueous single phase. According to Darcy's law, the pressure gradient is proportional to the liquid flow rate. As a result, the total mobility is independent of gas flow rate. When  $f_g > f_g^*$ , foam bubbles change size as needed to maintain foam at the limiting capillary pressure. Consequently, liquid saturation,  $S_w$ , is constant and equal to  $S_w^*$ , at limiting capillary pressure  $P_c^*$ . If  $P_c^*$  and  $S_w^*$  are independent of gas flow rates, then  $K_{rw}(S_w)$  is constant during foam flow; as a result, the pressure gradient is proportional to the liquid flow rate and independent of gas flow rate. With a constant  $q_g$ , when the  $f_g$  increases,  $q_l$  will decrease. At the same time,  $(q_l / A) / (dp / ds)$  is constant, therefore, with increasing  $f_g$ , the total mobility will increase linearly. When  $f_g^0 \leq f_g \leq f_g^*$ , more bubbles are produced with increasing  $f_g$ . Schramm,<sup>127</sup> pointed out that snapoff is the dominant foam generation mechanism under coinjection of surfactant solution and gas. The produced foam is either transported in the porous media or trapped in the pore throat, either of which leads to an increase in pressure drop across the core. Based on the total mobility equation above, when  $f_g$  increases with a constant  $q_g$ ,  $q_l$  decreases and the  $dp/ds$  increases, the total mobility will gradually decrease as a result. In addition, another observation was found for the three series of experiments above. Foam

mobility for Core SS-1 was much less than that of Core SS-2, possibly due to the lower pressure gradient owing to the larger pores and pore throats in Core SS-2.

**Effect of  $f_g$  on foam mobility with constant CD flow rate.** The effect of gas fractional flow on foam mobility with a constant CD aqueous solution flow rate was also studied with Core SS-1 only. The results are presented in Table 25, with the relationship between the total mobility and  $f_g/(1-f_g)$  plotted in Fig. 45. The foam flow region under this condition can also be divided into three zones. The characteristics of the plot for the relationship between total mobility and  $f_g/(1-f_g)$  is similar to that when  $\text{CO}_2$  gas flow rate was constant. It was noticed that  $f_g^*$  is lower compared to the values in the previous experiments. This may be due to the lower total flow rate.

#### **Effect of surfactant concentration on $f_g^*$ and foam mobility**

Two experiments were conducted using Core SS-2 at a constant  $\text{CO}_2$  flow rate of 40 cc/hr with CD concentration of 0.25 wt% and 0.05 wt%, respectively. Figure 46 shows that the reduction of surfactant concentration below the CMC (CD CMC is 0.06 wt%) caused a shift of the transition zone to lower values of  $f_g^*$ , from 0.754 for 0.25 wt% CD to 0.689 for 0.05 wt% CD. The reduction in surfactant concentration reduced the foam strength. The weaker foam would result in the reduction of the  $f_g^*$ .<sup>121</sup> Similarly, increasing surfactant concentration will result in a higher  $f_g^*$ , and the foam will withstand a higher capillary pressure. In practice, a higher  $f_g^*$  means a higher ratio of gas and less surfactant, which will be a savings in the amount of surfactant required.

Figure 46 shows that in the high gas fractional flow region, the total mobility for the foam produced by 0.25 wt% is much lower than that produced by 0.05 wt%. A higher surfactant concentration brings about a higher limiting capillary pressure. In turn, a higher capillary pressure will allow more bubbles to exist, though some bubbles coalesce at the limiting capillary pressure. As a result, more pore throats were blocked by the trapped gas bubbles, leading to a higher pressure drop and a lower total mobility. When  $f_g < f_g^*$ , according to the model of Rossen and Wang,<sup>128</sup> the bubble size was fixed and the pressure gradient was independent of surfactant concentration dependent only on the porous medium and surface tension. Therefore, when  $f_g < 0.689$ , the higher total mobility for the foam produced by 0.25 wt% CD can not be

attributed to the high surfactant concentration. The lower pressure gradient may cause this result because some of the minerals were dissolved by the acidic, carbonated water and the pore and pore throats may become larger as foam flooding proceeds.

### **Effect of total flow rate on mobility**

The effect of total flow rate,  $q_t$ , on mobility in the application of CO<sub>2</sub> foam for oil recovery is also of great interest. A number of previous researchers<sup>47,88,93,121,125</sup> have conducted studies on this aspect and unanimously agreed that foam mobility increased with increasing  $q_t$ . Yang and Reed<sup>97</sup> investigated mobility control using CO<sub>2</sub> foam and found that when the flow velocity is higher than 1.0 ft/day, the foam was shear thinning and the foam mobility increased with increasing  $q_t$ . A transition zone was found at velocities between 0.5 and 1.0 ft/day, in which the mobility is constant. When flow velocity was less than 0.5 ft/day, the foam was shear thickening and foam mobility decreased with increasing  $q_t$ .

According to Yang and Reed,<sup>97</sup> both “shear thickening” and “shear thinning” can be interpreted in terms of relative effects of flow rate on bubble snap-off and coalescence. The driving force for bubble coalescence increases as the flow rate increases. The bubble coalescence time decreases with increasing driving force. Therefore, thin films are shorter-lived, resulting in less resistance to CO<sub>2</sub> flow. The snap-off time is negligible compared with the coalescence time for effective foam. The fact that snap-off time is probably more efficient at high rates cannot offset the effect of rate on bubble coalescence. This is consistent with a “shear thinning” trend. When the rate decreases, in the transition zone, snap-off becomes less effective. At the same time, bubble coalescence is slower. The effect of low rate on snap-off offsets that of coalescence. Thus, foam mobility seems constant. As the rate further decreases, the effect of flow rate on snap-off is greater than that on coalescence. Probably snap-off completely stops, and bubble generation may rely on some secondary mechanisms. CO<sub>2</sub> foam flow demonstrates shear thickening behavior.

In this study, one experiment was performed to investigate the effect of  $q_t$  on the mobility. CO<sub>2</sub> and CD(@ 0.25 wt%) were coinjected into Core SS-2 at constant flow rate of 20, 40, and 80 cc/hr with a fixed  $f_g=0.8$ . Figure 49 shows that the total mobility and gas mobility increase with increasing  $q_t$  when the  $f_g$  is fixed in the Berea sandstone. When the  $f_g$  is variable, the data for the mobility vs  $q_t$  in this study was not available. The results are compared to the

earlier work of Liu,<sup>125,126</sup> where tests were performed in limestone with N<sub>2</sub>/CD co-injection at constant flow rates of 6, 10, 16 cc/hr and the results are shown in Fig. 50. Figures 47 and 48 show that the base line results obtained in this study and in hers are similar. Liu<sup>126</sup> showed that the gas mobility and total mobility increase with increasing total flow rate in Indiana limestone (see Figs. 50 and 51), and the N<sub>2</sub> foam demonstrates a shear-thinning behavior, which agrees with the results in a Berea sandstone core.<sup>88</sup> Due to the similar base line results, CO<sub>2</sub> gas mobility and total mobility will increase with increasing total flow rate in this study.

### **Surfactant adsorption and desorption at reservoir conditions**

During the process of foam flooding in this study, the adsorption and desorption behavior of the foam were also investigated. The experimental strategies are outlined in Table 26.

In this study, Cores SS-1 and SS-2 were utilized. The adsorption process was studied with 0.05 wt% CD solution and CO<sub>2</sub>. Unfortunately, the desorption data was lost when the core was damaged in the experiment. For Core SS-2, both the adsorption and desorption test results were obtained. The adsorption stage for this core can be divided into two phases. First was the adsorption phase with 0.05 wt% CD solution and CO<sub>2</sub>. Second, with the previous CD pre-slug remaining in the core, the 0.25 wt% CD solution was directly injected into the core with CO<sub>2</sub> until the end of foam flooding, then a one-time desorption process followed.

The effluent was collected during all adsorption and desorption tests. Desorption was determined by injecting surfactant-free solution after coinjection flooding of surfactant and gas (CSG). The relationship between effluent CD concentrations normalized to the initial injected CD solution concentration versus pore volumes (PV) of injected CD solution are shown in Figs. 52 and 53.

Each adsorption process was characterized by a rapid short period of adsorption followed by a longer period of slower adsorption. This is consistent with the results of Bai et al.<sup>129</sup> In the case of coinjection without a CD pad, when CD solution with 0.05 wt% concentration was adopted, no CD adsorption equilibrium was achieved throughout the experimental process even though the foams were observed after 116 PV of CD injection for Core SS-1 and 67 PV CD injection for Core SS-2. The final maximum CD effluent concentration detected was 60% of the initial injected solution concentration (0.05 wt%) for Core SS-1 and 70% of the initial injected solution concentration (0.05 wt%) for Core SS-2.

Liu et al<sup>125</sup> studied adsorption with N<sub>2</sub> and CD of 0.05 wt% concentration in an Indiana limestone core where the CD adsorption equilibrium was detected only after 6~7 PV of CD injection. To understand this problem, two samples were taken from Core SS-1 effluent during the coinjection foam flooding with CO<sub>2</sub> and 0.05 wt% CD. One sample (#1) was foaming as expected but the other sample (#2) had little foam after shaking. The IFT tests were carried out for these two samples; the results are shown in Fig. 54. The IFT value for the foaming effluent sample (#1) was only a little lower than the nonfoaming effluent sample (#2), but the foaming results were different (as indicated in the two photos in Fig. 54). The foaming delay in this study might have resulted from the inadequate CD surfactant supply. There are two possibilities that might cause this. One is that perhaps as a consequence of the size of the pore walls of the Berea sandstone core, adsorption equilibrium is not immediate but requires more time. Schramm<sup>127</sup> had pointed out that even though surfactant molecules could be expected to adsorb onto the internal walls of the porous rock according to an equilibrium isotherm, in many laboratory experiments and at the displacement front in the field such equilibrium may not be attained. The other possibility is the loss of surfactant due to some other mechanisms. Novosad<sup>130</sup> studied surfactant retention in Berea sandstone and put forward the idea that when the overall retention is much higher than expected, the surfactant losses caused by unfavorable phase behavior or some other mechanisms should be suspected. Here, the unfavorable phase behavior refers to the surfactant entrapment in an immobile hydrocarbon phase that remains within the core following a surfactant flood. Other mechanisms may include surfactant precipitation by divalent ions, surfactant precipitation caused by a separation of the cosurfactant from the surfactant and surfactant precipitation resulting from chromatographic separation of different surfactant species. During this study, some minerals in the effluent were indeed observed, which were oxidized after being exposed to the atmosphere for a couple hours and the solution color had changed from colorless to red. One speculation was that the CO<sub>2</sub> light acid solution eroded the internal walls of the Berea sandstone and scraped the surface layers. The new exposed surface would restart the adsorption process, leading to more adsorption of the surfactant.

The third observation was that the high initial concentration CD (@0.25 wt%) propagated through the core faster than the low initial concentration CD (0.05 wt%), which can be seen in Fig. 53. It was found that the foam started after only 7 PV of CD injection at a 0.25 wt% concentration, while this process for CD of 0.05 wt% required more than 67 PV injection in the

same core (SS-2). Additionally, the adsorption equilibrium was established for CO<sub>2</sub> foam produced by a 0.25 wt % CD concentration after 65 PV of CD solution was injected. This observation was further verified by the surfactant retention process, shown in Fig. 55. With the injection of CD solution, the surfactant retention density (for this stage alone, ignoring any previous CD pad effect) increased until steady state was accomplished after 65 PV CD solution injection.

Another interesting observation for three adsorption tests (see Figs. 52 and 53) was that, once the foam started to be produced, there was one flooding interval in which the detected CD concentration in the effluent was lower than that obtained prior to foaming, which indicates the surfactant adsorption onto the core would further increase. This might be due to the larger surface area of the foam contacting the rock surface and the higher surfactant concentration in the lamella.

The behavior of CD desorption compared to adsorption for the (0.05 wt% + 0.25 wt%) CD system is shown in Figs. 56 and 57. The effluent CD concentration drops rapidly after switching to the injection of CD-free solution. This rapid drop in produced CD followed by a long tail of low concentration corresponds to earlier studies in which desorption was not 100% reversible, at least in a comparable time frame to the adsorption.<sup>129</sup> The final recovered CD mass divided by the initial mass of rock produced an equivalent core retention density of 1.82 mg/g, which can be observed in Fig. 58 below. 1.12 mg/g density was obtained in the process of 0.05 wt% CD injection, which leaves the incremental retention density during 0.25 wt% CD injection of 0.70 mg/g. Based on the test data, the equivalent retention density loss during the injection of 160 PV 0.05 wt% CD solution was approximately 3.45 mg/g. Considering the 1.12 mg/g retention density recovered in the effluent, the remaining 2.34 mg/g was retained in the core. Exploration of the real mechanism for surfactant retention in the core should be one important task for the future work

## Summary/Conclusions

1. Gas mobility of CO<sub>2</sub>/brine increases with increasing of  $f_g$ . The total mobility of CO<sub>2</sub>/brine increases with increasing  $f_g$  ranging from 0.6 to 0.9; but decreases with increasing  $f_g$  when  $f_g$  is less than 0.6.

2. Total mobility (and or gas mobility) as a function of  $f_g$  is characterized by three intersecting straight lines with two crossed points  $f_g^o$  and  $f_g^*$ . Three foam flow regions are described in this study: a single-phase region, a low gas fractional flow region and a high gas fractional region. In the single-phase region, with fixed CO<sub>2</sub> gas flow rate, the gas mobility increases with increasing  $f_g$ . But the total mobility is independent of  $f_g$  no matter what the fixed CO<sub>2</sub> gas flow rate or the fixed CD aqueous flow rate. In the low gas fractional flow region, the gas mobility and total mobility decreases with increasing  $f_g$ . In the high gas fractional flow region, the gas mobility and total mobility increases with increasing  $f_g$ .
3. In different cores, the  $f_g^*$  is generally different. Even in the same core, due to different flow rates and different foam flow modes,  $f_g^*$  may also vary. The higher the permeability and flow rate, the higher the  $f_g^*$ .
4. The mobility reduction factor for Cores SS-1 and SS-2 reaches maximum at  $f_g=0.6$  and  $f_g=0.8$ , respectively.
5. Gas mobility and foam mobility increases with increase in total flow rate if the foam flow is shear-thinning.
6. During CO<sub>2</sub> foam flooding, with CD solution of 0.05 wt% concentration, it was difficult to establish adsorption equilibrium. Exploration of the reason for this would be an important task for future work.
7. The adsorption/desorption of the surfactant are characterized as a rapid short period of adsorption/desorption to/from the rock surface followed by a long period of slow adsorption/desorption. The adsorption of surfactant onto rock increases with the occurrence of foam.
8. A CD surfactant solution with a higher concentration will reach adsorption equilibrium in the core faster than a CD surfactant solution with a lower concentration.

**Table 18. The Properties of Berea Sandstone**

Core ID	OD, in	Length, in	Initial Pore Volume, cm <sup>3</sup>	Initial Porosity, %	Initial water permeability, md
SS-1	2.003	5.998	49.75	16.06	26.22
SS-2	2.028	5.785	68.25	22.29	450

**Table 19. Experimental Methods Used in the CO<sub>2</sub>/Brine Coinjection Flooding Baseline Test**

Core	Flow Rate	Foam Flooding Mode	Brine Description
SS-1	$q_t=20\text{cm}^3/\text{hr}$	fixed total flow rate $q_t$ , change $q_g/q_l$ to realize variable $f_g$	2.0 wt% total, 1.5 wt % of NaCl and 0.5 wt% of CaCl <sub>2</sub>
SS-2	$q_t=100\text{ cm}^3/\text{hr}$		
	$q_t=40\text{ cm}^3/\text{hr}$		

**Table 20. Experimental Methods used in CO<sub>2</sub> Foam Flooding**

Core ID	Concentration of CD surfactant used	Foam Flooding Mode	Flow Rate
SS-1	0.05 wt%	fixed CD $q_l$ , change $q_g$ to realize variable $f_g$	$q_l=10\text{cm}^3/\text{hr}$
		fixed $q_g$ , change $q_l$ to realize variable $f_g$	$q_g=20\text{ cm}^3/\text{hr}$
		fixed $q_t$ , change $q_g/q_l$ to realize variable $f_g$	$q_t=20\text{ cm}^3/\text{hr}$
SS-2	0.05 wt%	fixed $q_g$ , change $q_l$ to realize variable $f_g$	$q_g=40\text{ cm}^3/\text{hr}$
		fixed $q_t$ , change $q_g/q_l$ to realize variable $f_g$	$q_t=100\text{ cm}^3/\text{hr}$
	0.25 wt%	fixed $q_g$ , change $q_l$ to realize variable $f_g$	$q_g=40\text{ cm}^3/\text{hr}$

**Table 21. Summary of CO<sub>2</sub>/Brine Coinjection Baseline Experiments**

Core	CO <sub>2</sub> Fraction Flow, $f_g$	Gas to liquid fractional flow, $f_g/(1-f_g)$	Pressure Drop psig	Total Mobility (md/cp)	Gas Mobility (md/cp)	Gas Interstitial Velocity (ft/day)
SS-1*	0.00	0.00	1.8900	43.85 <sup>#</sup>	0.00 <sup>#</sup>	0.00
	0.10	0.11	1.4940	40.41	4.04	0.48
	0.20	0.25	1.6367	36.89	8.30	0.96
	0.30	0.43	1.6203	30.25	9.07	1.45
	0.40	0.67	2.0940	24.81	9.92	1.93
	0.50	1.00	2.6035	23.19	11.59	2.41
	0.60	1.50	2.5419	23.75	14.25	2.89
	0.70	2.33	2.4459	24.68	17.28	3.38
	0.80	4.00	2.1686	27.84	22.27	3.86
	0.90	9.00	1.9738	30.59	27.53	4.34
	1.00	n/a	1.5751	38.33 <sup>#</sup>	38.33 <sup>#</sup>	4.82
SS-2**	0.00	0.00	0.3604	315.20 <sup>##</sup>	0.00 <sup>##</sup>	0.00
	0.10	0.11	0.5033	225.69	22.57	0.68
	0.20	0.25	0.6102	186.16	37.23	1.36
	0.30	0.43	0.6485	175.18	52.55	2.03
	0.40	0.67	0.6682	170.01	68.00	2.71
	0.50	1.00	0.6923	164.09	82.04	3.39
	0.60	1.50	0.6988	162.57	97.54	4.07
	0.70	2.33	0.6955	163.34	114.34	4.75
	0.80	4.00	0.6735	168.67	134.93	5.42
	0.90	9.00	0.6269	181.20	163.08	6.10

Note:

- \* Flow rate 20 cc/hr which is an interstitial flow rate of 4.82 ft/day
- \*\* Flow rate of 40 cc/hr which is an interstitial flow rate of 6.78 ft/day
- # data obtained with CO<sub>2</sub> injection at brine saturation;
- ## data obtained with brine injection without CO<sub>2</sub> in the core.

**Table 22. Experimental Strategy for  $f_g^*$  Determination**

Core with CD con.	Run Sequence	$\Delta P$ [psi]	CO <sub>2</sub> Flow Rate [cc/hr]	CD Flow rate (cc/hr)	Gas Fraction flow [ $f_g$ ]	$f_g/(1-f_g)$	Total Mobility [md/cp]	Gas Mobility [md/cp]
SS-1 0.05 wt% CD	1	51.54	20	0.20	0.990	99.000	1.18	1.17
	2	97.17	20	1.12	0.947	17.868	0.66	0.62
	3	102.40	20	2.50	0.889	8.009	0.66	0.59
	4	114.66	20	4.78	0.807	4.184	0.65	0.53
	5	123.67	20	6.52	0.754	3.067	0.65	0.49
	6	144.20	20	9.99	0.667	2.003	0.63	0.42
	7	152.71	20	13.33	0.600	1.500	0.66	0.40
	8	156.66	20	16.36	0.550	1.222	0.70	0.39
	9	168.03	20	20.00	0.500	1.000	0.72	0.36
	10	156.07	20	30.00	0.400	0.667	0.97	0.39
	11	133.40	20	40.06	0.333	0.499	1.36	0.45
	12	92.72	20	80.00	0.200	0.250	3.26	0.65
	13	74.00	20	150.00	0.118	0.133	6.93	0.82
	14	60.39	20	300.00	0.063	0.067	15.99	1.00
	15	127.66	20	889.09	0.022	0.022	21.49	0.47
	16	162.60	20	1250	0.016	0.016	23.58	0.37
Core SS-2 CD 0.05 wt%	1	41.02	40	1.12	0.973	35.714	3.03	2.94
	2	43.21	40	2.24	0.947	17.868	2.95	2.79
	3	52.59	40	4.99	0.889	8.009	2.58	2.30
	4	74.61	40	13.04	0.754	3.067	2.15	1.62
	5	73.14	40	19.97	0.667	2.003	2.47	1.65
	6	71.14	40	26.66	0.600	1.500	2.83	1.70
	7	68.48	40	32.72	0.550	1.222	3.21	1.76
	8	56.12	40	60.00	0.400	0.667	5.38	2.15
	9	46.07	40	80.12	0.333	0.499	7.87	2.62
	10	35.88	40	160.00	0.200	0.250	16.83	3.37
	11	21.99	40	300.00	0.118	0.133	46.67	5.49
	12	11.14	40	889.09	0.043	0.045	251.78	10.84
	13	14.98	40	1250	0.031	0.032	259.90	8.06
Core SS-2 CD 0.25 wt%	1	120.34	40	1.12	0.973	35.714	1.03	1.00
	2	133.41	40	2.24	0.947	17.868	0.96	0.91
	3	152.33	40	4.99	0.889	8.009	0.89	0.79
	4	141.97	40	9.56	0.807	4.184	1.05	0.85
	5	127.29	40	13.04	0.754	3.067	1.13	0.95
	6	116.23	40	19.97	0.667	2.003	1.56	1.04
	7	96.99	40	26.66	0.600	1.500	2.07	1.24
	8	84.19	40	32.72	0.550	1.222	2.61	1.43
	9	67.80	40	40.00	0.500	1.000	3.56	1.78
	10	45.27	40	60.00	0.400	0.667	6.67	2.67
	11	43.08	40	80.12	0.333	0.499	8.42	2.80
	12	23.36	40	160.00	0.200	0.250	25.85	5.17
	13	18.22	40	300.00	0.118	0.133	56.32	6.63
	14	12.55	40	600.00	0.063	0.067	153.87	9.62
	15	12.10	40	889.09	0.043	0.045	231.85	9.98
	16	16.17	40	1250	0.031	0.032	240.83	7.47

**Table 23. Comparison of Test Results with Earlier Results<sup>125,126</sup>**

Core ID	Gas Type used	Gas Flow Rate, cc/hr	Core Permeability K, md	CD Surfactant Conc.	Inflexion between Single Phase region and low gas fractional flow region, $f_g^o$	Critical Gas Fractional Flow, $f_g^*$	Gas flow rate	Remarks
ss-1	CO <sub>2</sub>	20	26.22	0.05wt%	0.063	0.50±0.05		Two sandstones used in this study
ss-2	CO <sub>2</sub>	40	450	0.05wt%	0.043	0.754±0.05		
ss-2	CO <sub>2</sub>	40	450	0.25wt%	0.054	0.85±0.05		
Ls-2	N <sub>2</sub>	22	25.61	0.25wt%	none	0.85±0.05		Limestone core used in Liu et al's research

**Table 24. Coreflood Results used in Determining Optimum  $f_g$  at Constant Total Flow Rate**

Core ID	Running #	Total Flow rate (cc/hr)	Pressure Drop, psig	CO <sub>2</sub> Gas Fraction flow, $f_g$	CO <sub>2</sub> /CD Total Mobility (md/cp)	Total Interstitial Velocity, (ft/day)	CO <sub>2</sub> /Brine base total mobility, md/cp	MRF
SS-1	9	20	1.46	0.00	41.39*	4.82	43.85 <sup>@</sup>	n/a
	10	20	24.44	0.10	2.47	4.82	40.41	16.36
	1	20	44.93	0.20	1.34	4.82	36.89	27.45
	2	20	70.56	0.30	0.86	4.82	30.25	35.36
	3	20	99.52	0.40	0.61	4.82	24.81	40.89
	4	20	119.80	0.50	0.50	4.82	23.19	46.02
	5	20	129.44	0.60	0.47	4.82	23.75	50.92
	6	20	117.55	0.70	0.51	4.82	24.68	48.06
	7	20	91.09	0.80	0.66	4.82	27.84	42.00
	8	20	52.64	0.90	1.15	4.82	30.59	26.67
	11	20	21.23	1.00	2.84 <sup>#</sup>	4.82	38.33 <sup>&amp;</sup>	n/a
SS-2	1	100	0.45	0.00	673.76*	16.95	0.47 <sup>@</sup>	n/a
	2	100	7.36	0.10	41.01	16.95	444.10	10.83
	3	100	29.34	0.20	10.29	16.95	336.68	32.73
	4	100	47.45	0.30	6.36	16.95	312.03	49.05
	5	100	64.62	0.40	4.67	16.95	309.39	66.23
	6	100	78.29	0.50	3.86	16.95	308.94	80.13
	7	100	87.97	0.60	3.43	16.95	294.11	85.72
	8	100	95.45	0.70	3.16	16.95	301.74	95.41
	9	100	95.35	0.80	3.17	16.95	328.01	103.61
	10	100	80.16	0.90	3.77	16.95	338.00	89.76
	11	100	9.89	1.00	30.51 <sup>#</sup>	16.95	9.89 <sup>&amp;</sup>	n/a

Note: \* CD injection with CO<sub>2</sub> saturation; <sup>#</sup> CO<sub>2</sub> injection with CD saturation; <sup>@</sup> Brine injection with CO<sub>2</sub> saturation; <sup>&</sup> CO<sub>2</sub> injection with brine saturation;

**Table 25. Experimental Results to Determine the Relationship between Total Motility and  $f_g/(1-f_g)$  with CD Concentration of 0.05 wt% for Core SS-1**

Running Sequence	CD Flow rate (cc/hr)	Pressure Drop, psig	$f_g$	$f_g/(1-f_g)$	Total Mobility (md/cp)	Total Interstitial Velocity, (ft/day)
1	10	1.43	0.02	0.02	21.50	2.41
2	10	1.36	0.06	0.07	23.59	2.41
3	10	2.43	0.12	0.13	14.10	2.41
4	10	141.27	0.40	0.67	0.36	2.41
5	10	150.85	0.50	1.00	0.40	2.41
6	10	151.37	0.60	1.50	0.50	2.41
7	10	161.58	0.75	3.07	0.76	2.41
8	10	159.43	0.89	8.01	1.71	2.41
9	10	59.07	0.20	0.25	0.64	2.41
10	10	99.06	0.33	0.50	0.46	2.41
11	10	190.05	0.95	17.87	3.00	2.41
12	10	163.70	0.972	35.20	6.67	2.41

**Table 26. The Experimental Sequence for Adsorption and Desorption**

Core ID	Displacing fluid sequence	Determination	Injection strategy
SS-1	(1)0.05 wt% CD and CO <sub>2</sub>	CD adsorption with CO <sub>2</sub> present	CSG without CD pre-slug
SS-2	(1)0.05 wt% CD and CO <sub>2</sub>	CD adsorption and CO <sub>2</sub> present	CSG without CD pre-slug
	(2) 0.25 wt% CD and CO <sub>2</sub>	Partially saturated CD adsorption prior to 0.25 wt% CD and CO <sub>2</sub> co-injection	CSG with CD pre-slug
	(3) CD free brine	Desorption	

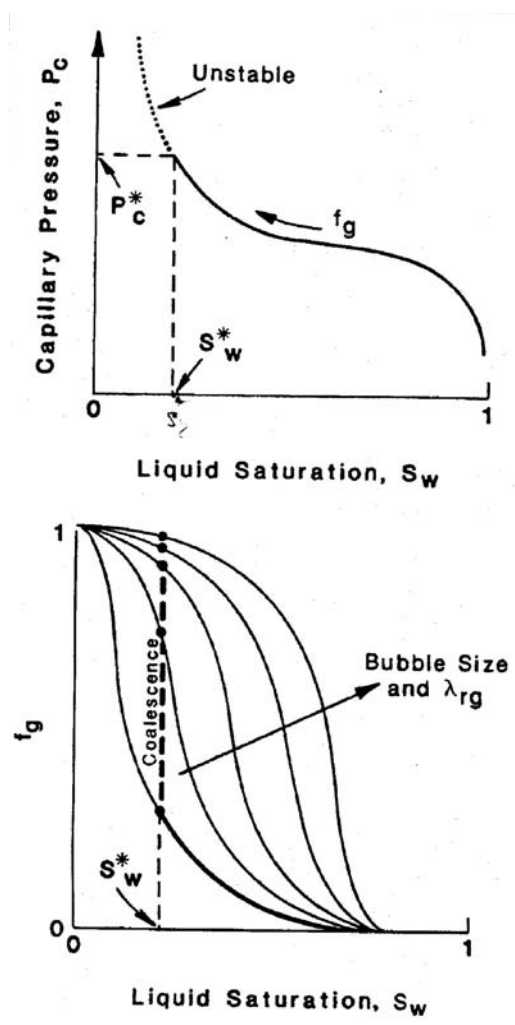


Fig. 32. Sketches of capillary pressure and fractional-flow curves operating during a two-phase displacement.<sup>82</sup>

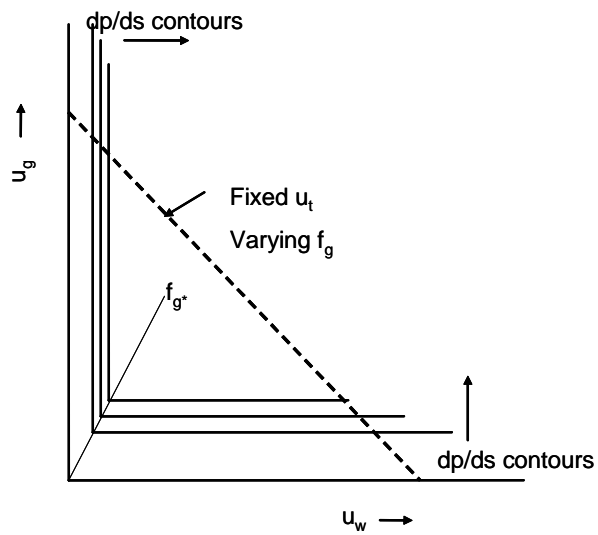


Fig. 33. Two foam-flow regime.<sup>121,122</sup>

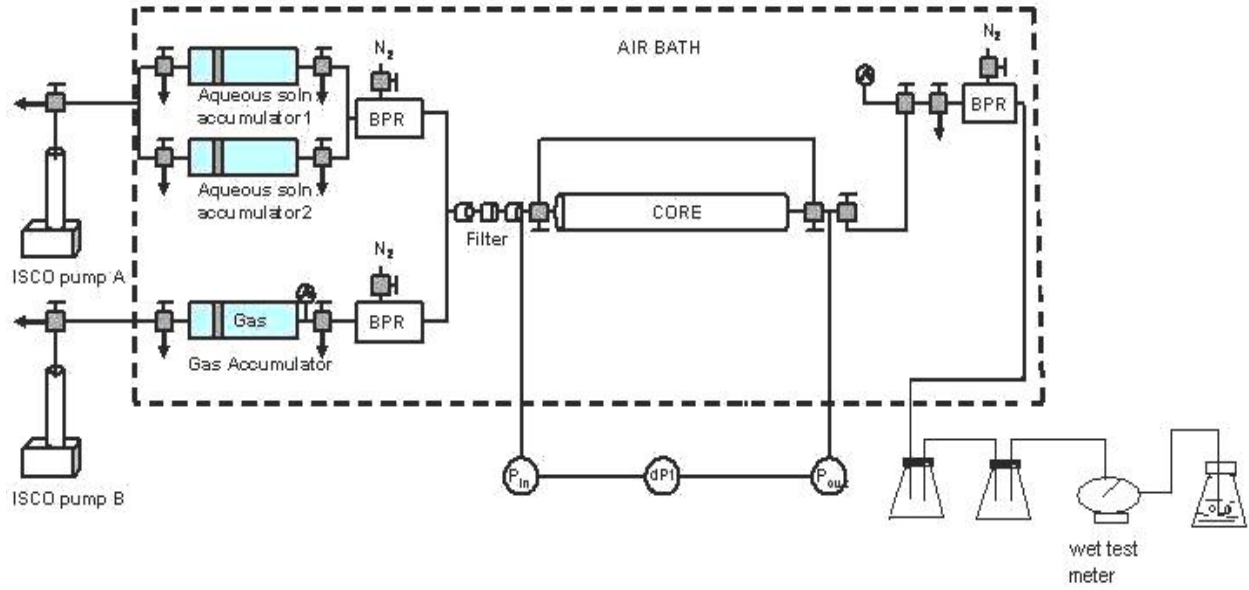


Fig. 34. Schematic diagram of oil free core flooding setup.

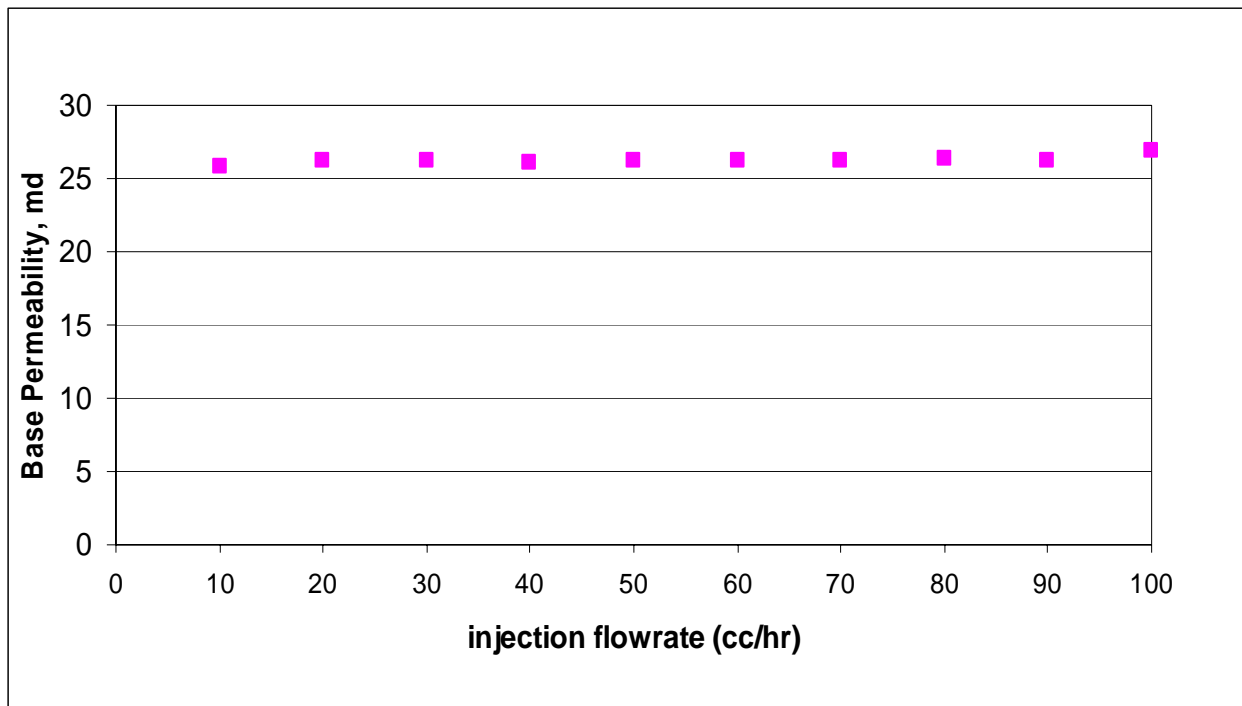


Fig. 35. Core SS-1 initial permeability with brine.

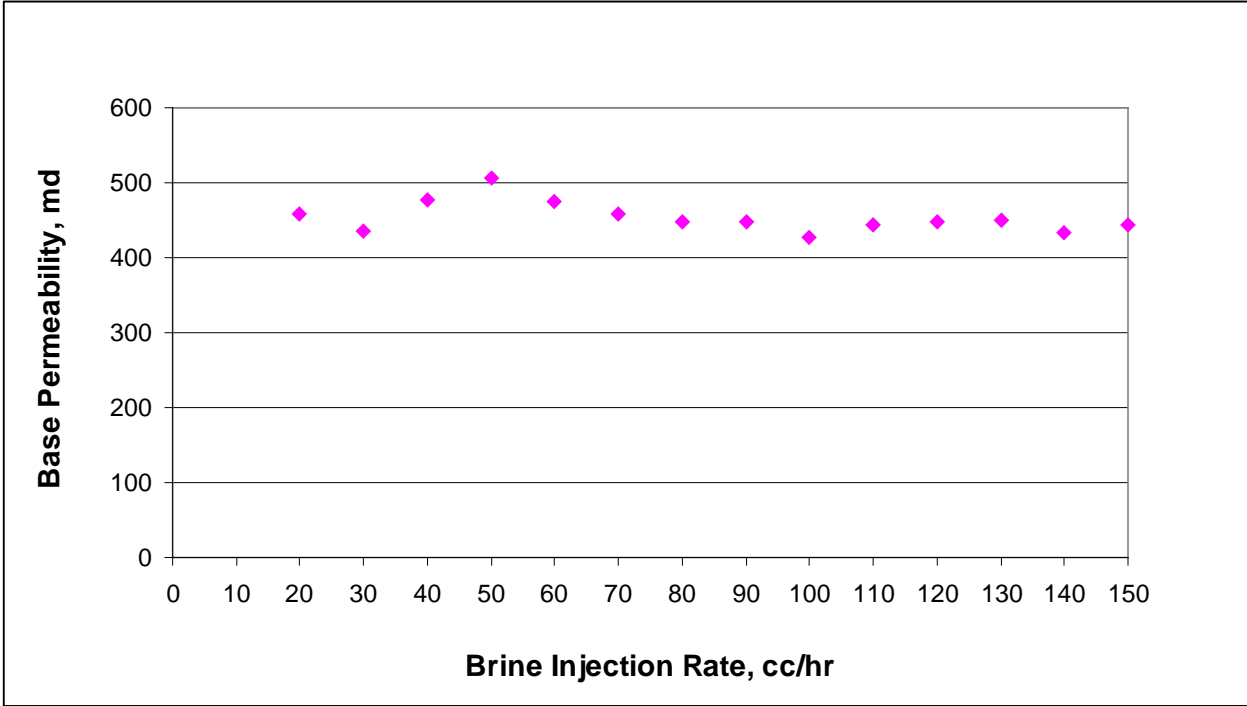


Fig. 36. Core SS-2 initial brine permeability.

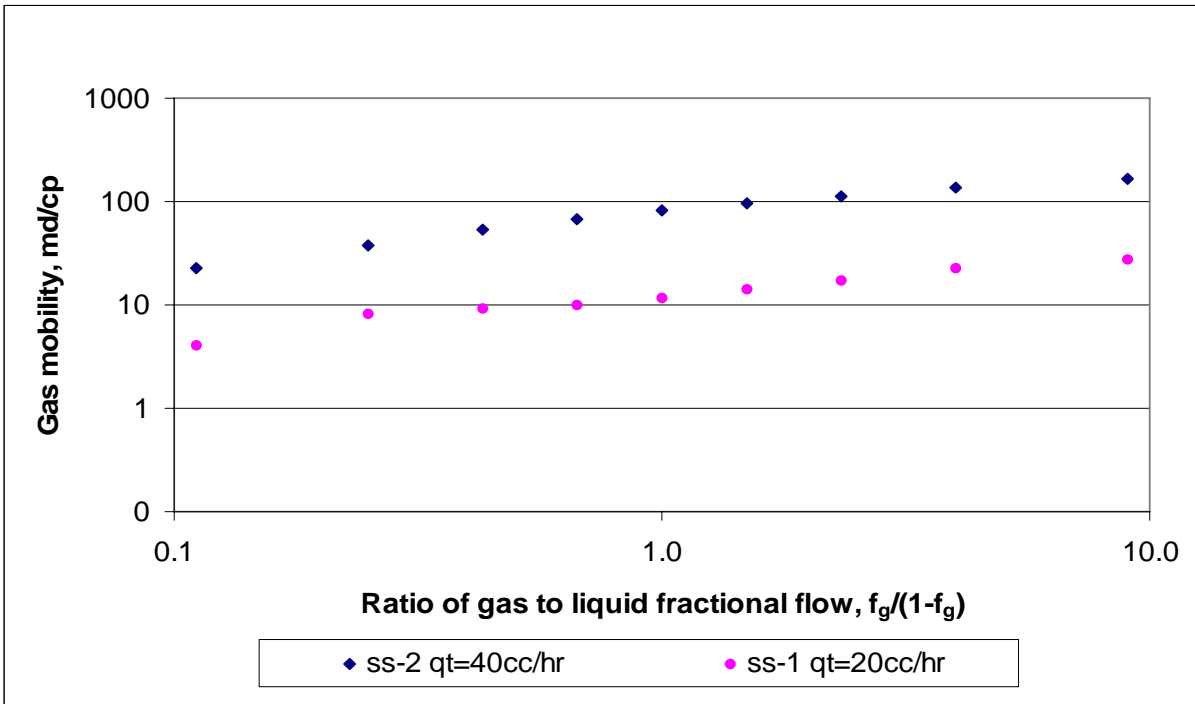


Fig. 37. Gas mobility as a function of  $f_g/(1-f_g)$  at constant total flow rate.

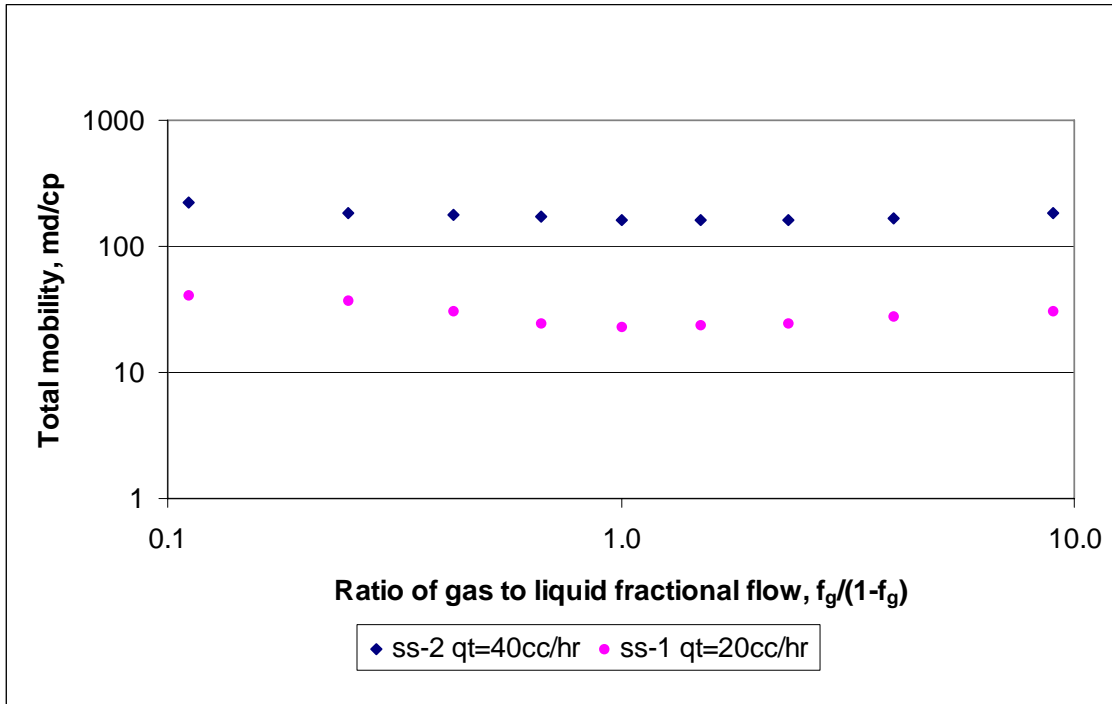


Fig. 38. Total mobility as a function of  $f_g/(1-f_g)$  at constant total flow rate.

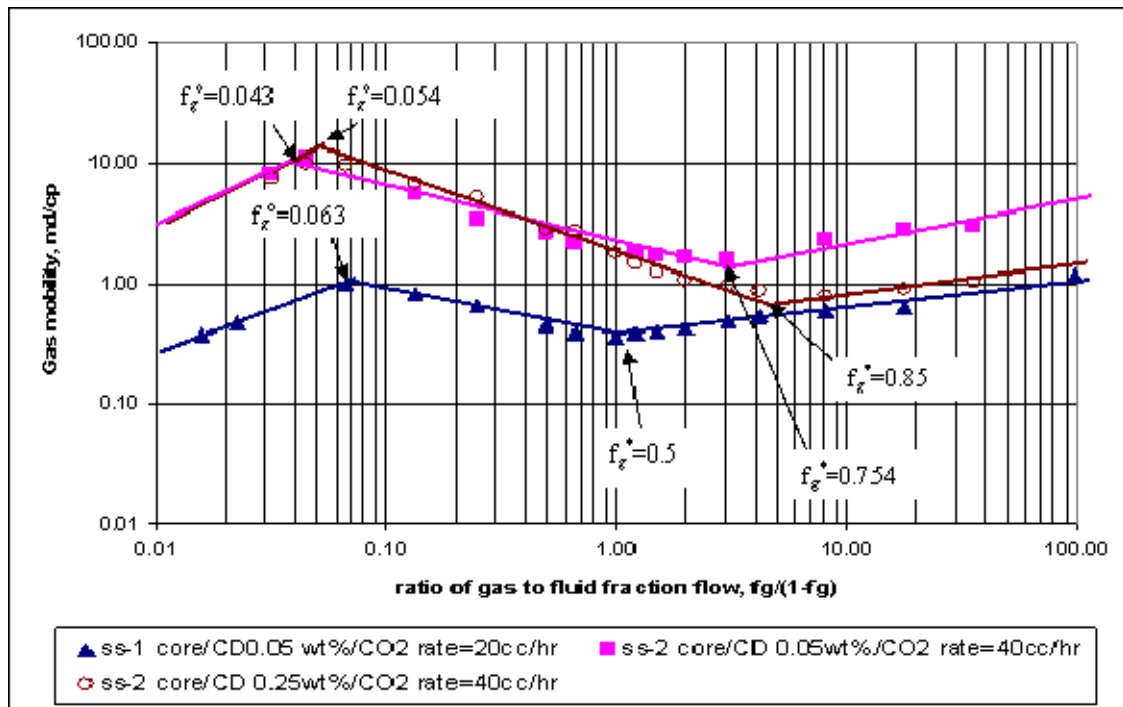


Fig. 39. Determination of  $f_g^*$  at constant gas flow rate with 110°F and 1540 psig in a fired Berea sandstone core.

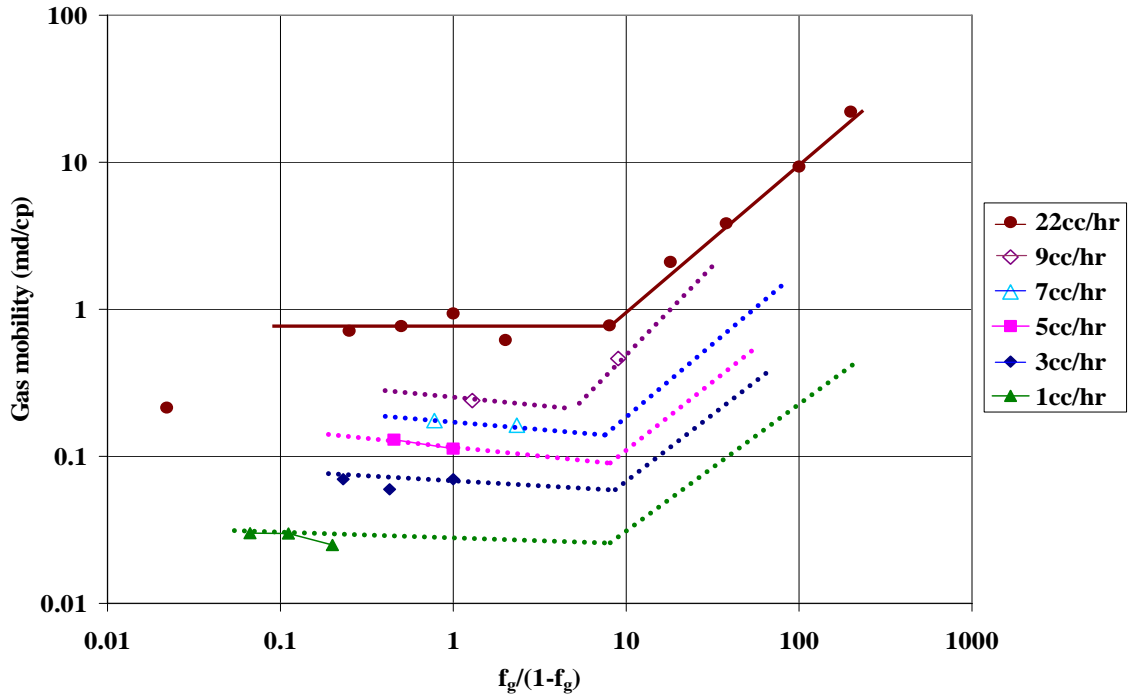


Fig. 40. Determination of  $f_g^*$  for 0.25 wt% CD at constant  $N_2$  gas flow rate at 40°C and 1500 psig in an Indiana limestone.<sup>125</sup>

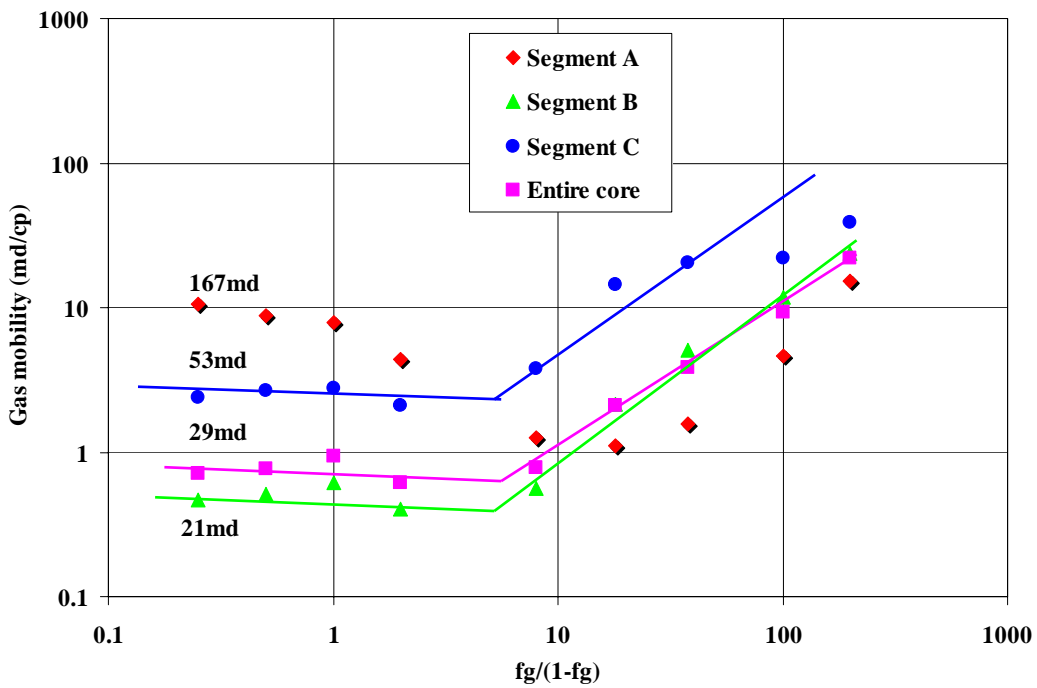


Fig. 41. Permeability effect on  $f_g^*$  for 0.25 wt% CD at 22 cc/hr constant  $N_2$  gas flow rate at 40°C and 1500 psig.<sup>125</sup>

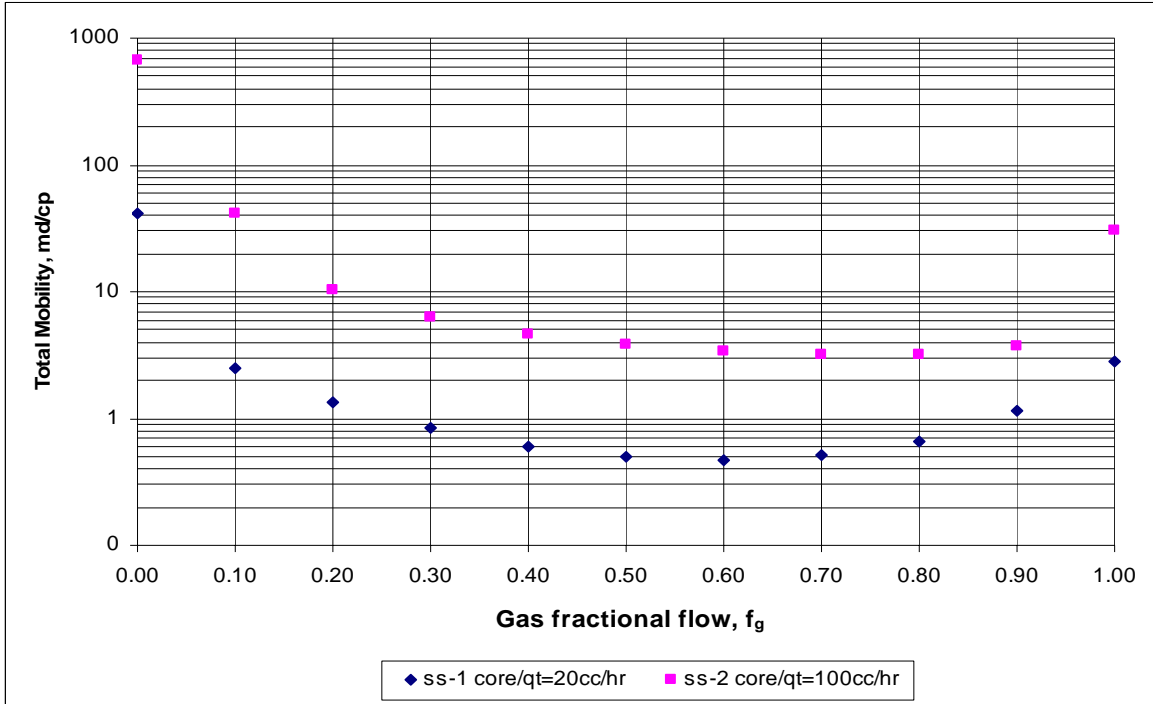


Fig.42. Plot total mobility as a function of  $f_g$  at a constant total flow rate.

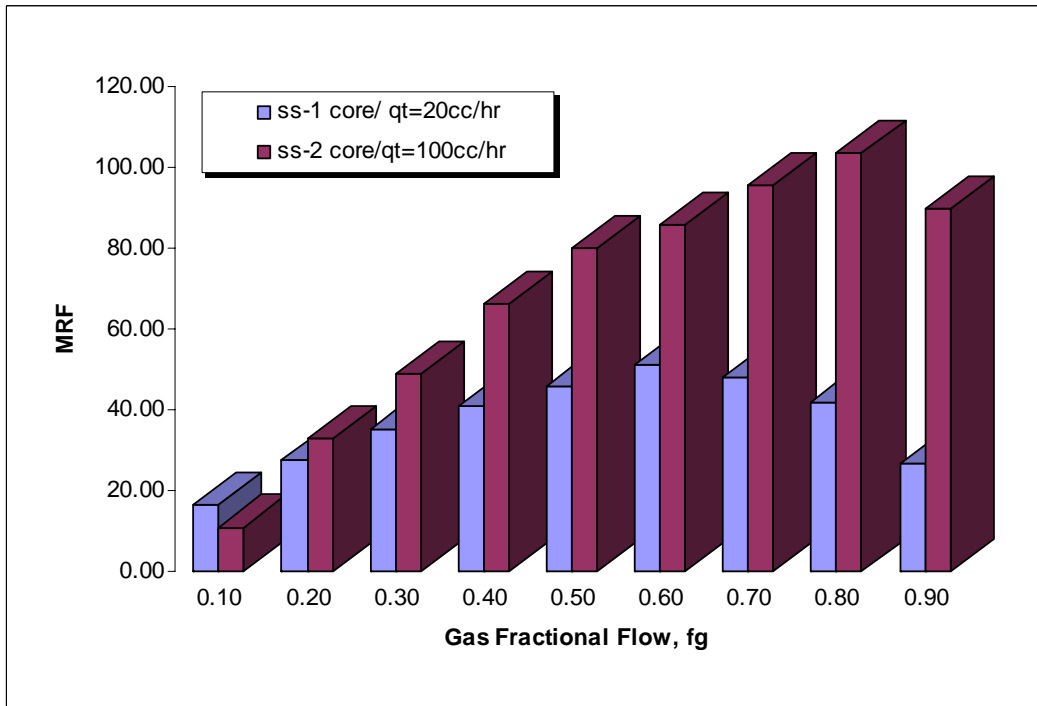


Fig. 43. Schematic graph to determine the optimum  $f_g$  with the maximum MRF.

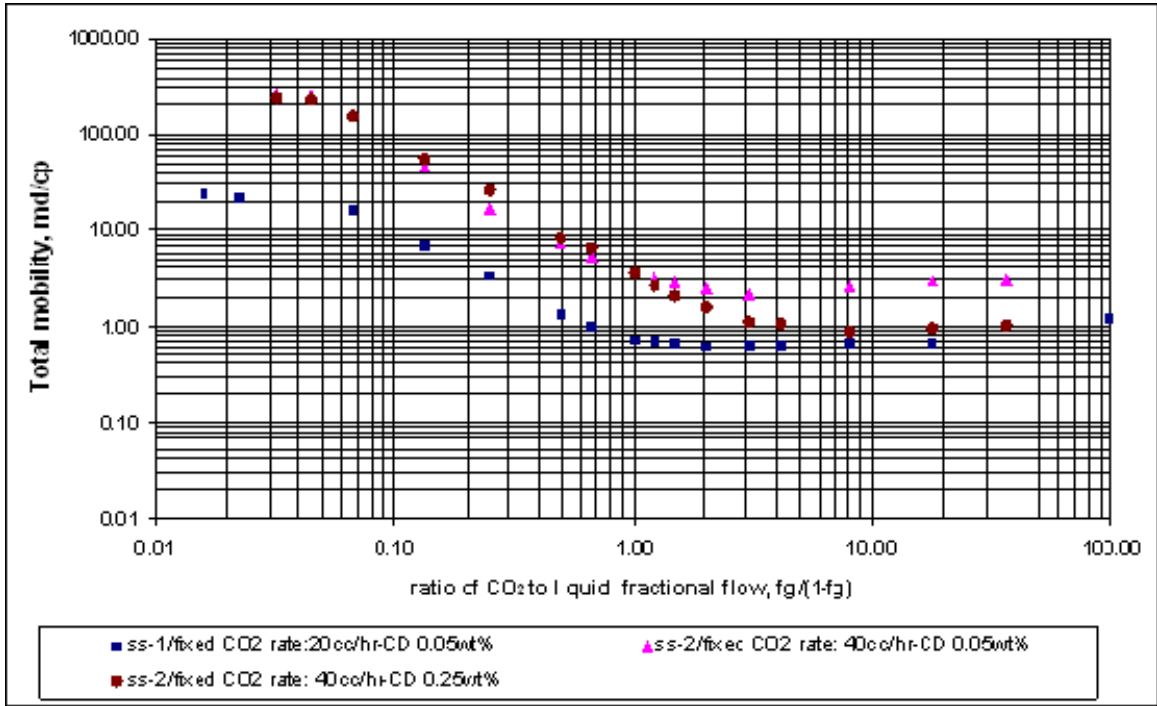


Fig. 44. Plot of total mobility as a function of  $f_g/(1-f_g)$  at a constant CO<sub>2</sub> flow rate.

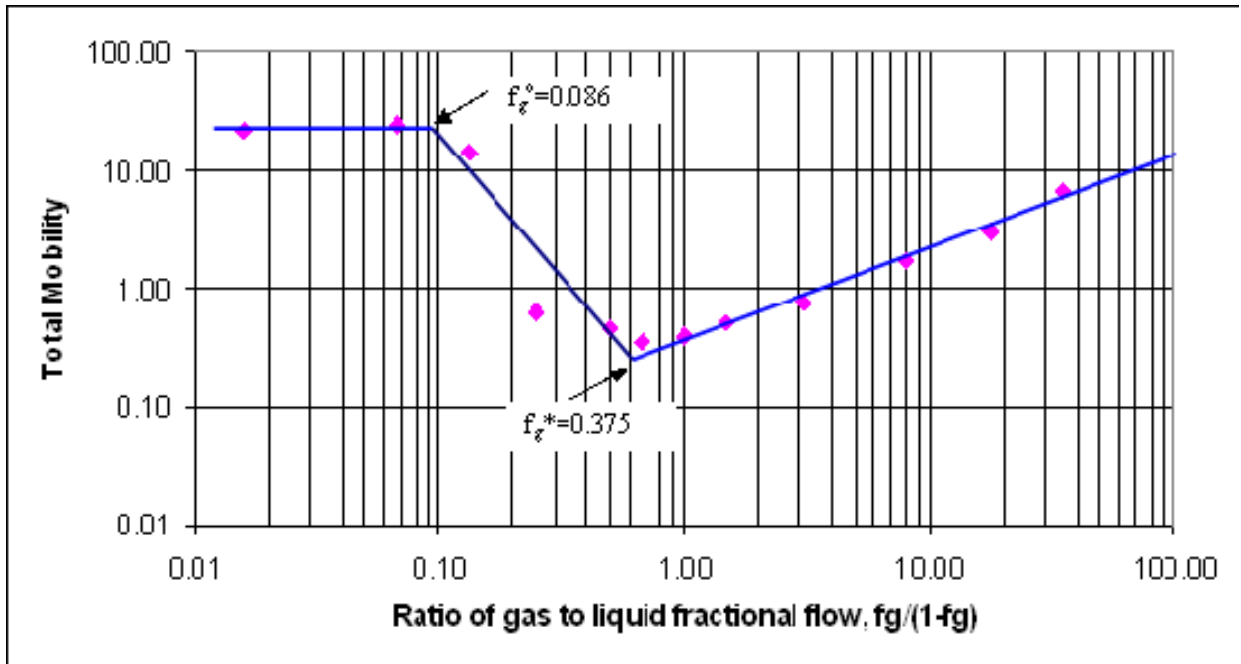


Fig. 45. Plot of relationship between total mobility and ratio of gas to liquid fractional flow  $f_g$ , at a constant CD solution flow rate of 10 cc/hr.

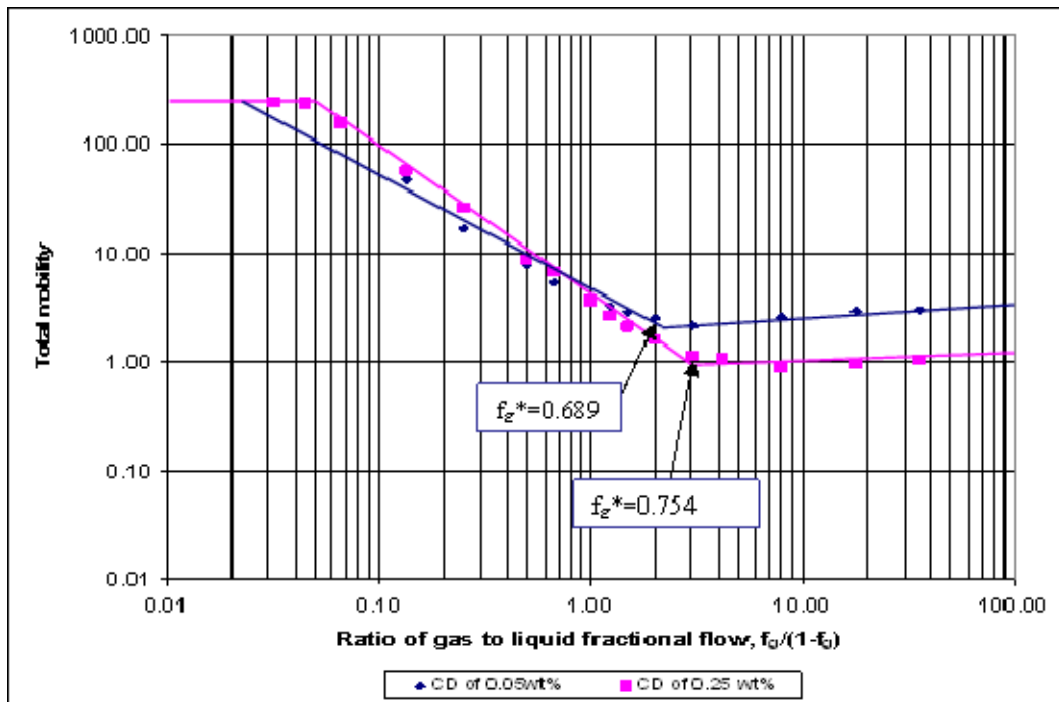


Fig. 46. Schematic representation of  $f_g^*$  reduction owing to a reduction in surfactant concentration at the constant  $CO_2$  flow rate of 40cc/hr for Core SS-2.

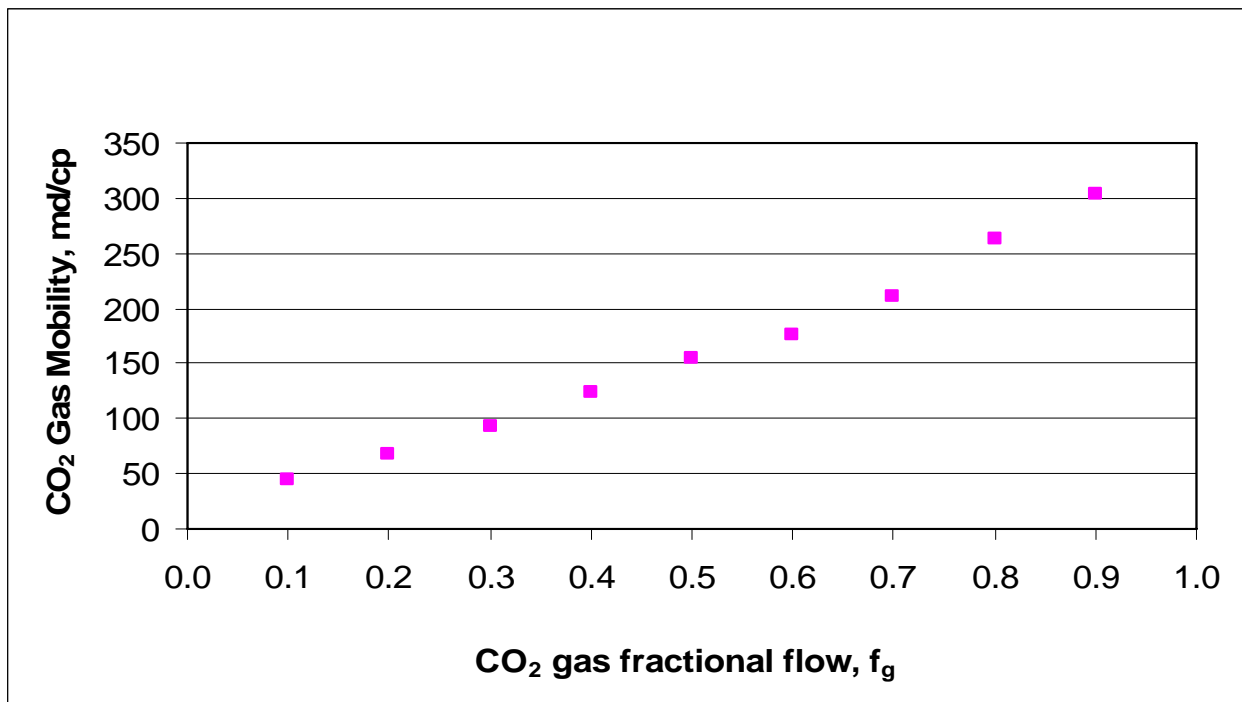


Fig. 47. Plot of  $CO_2$  gas mobility as a function of  $f_g$  in  $CO_2$ /brine co-injection base line test at a total flow rate of 100 cc/hr in Core SS-2 with  $T=110^\circ F$  and  $P=1540$  psig.

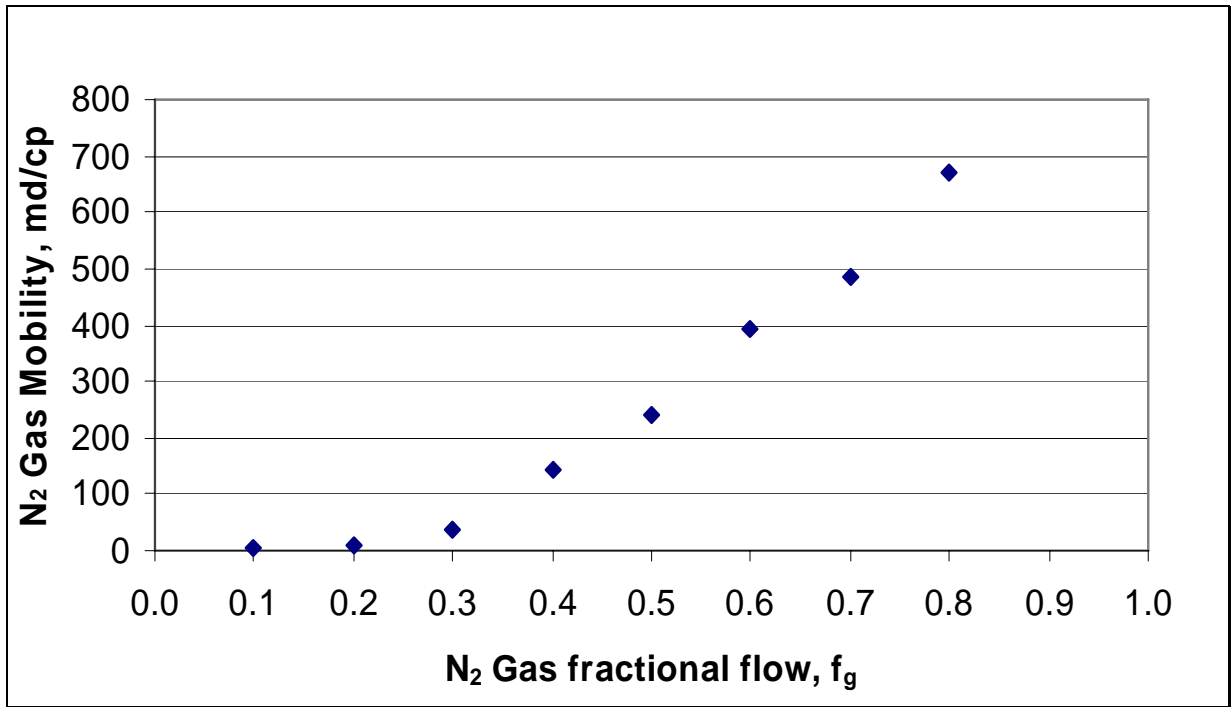


Fig. 48. Plot of N<sub>2</sub> gas mobility as a function of  $f_g$  in N<sub>2</sub>/brine co-injection base line test at a total flow rate of 100 cc/hr in a limestone with T=105° F and P =1500 psig.

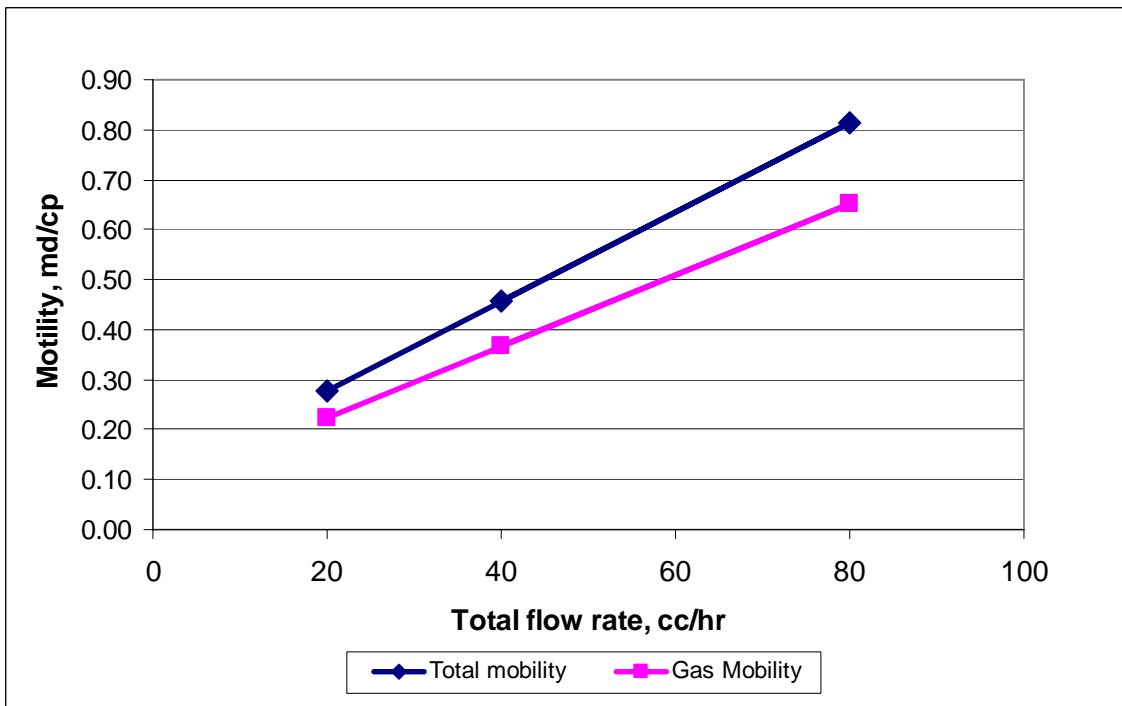


Fig. 49. Plot of gas mobility and total mobility as a function of total flow rate of CD/CO<sub>2</sub> with fixed  $f_g$  for Core SS-2 at T=110° F and P =1540 psig.

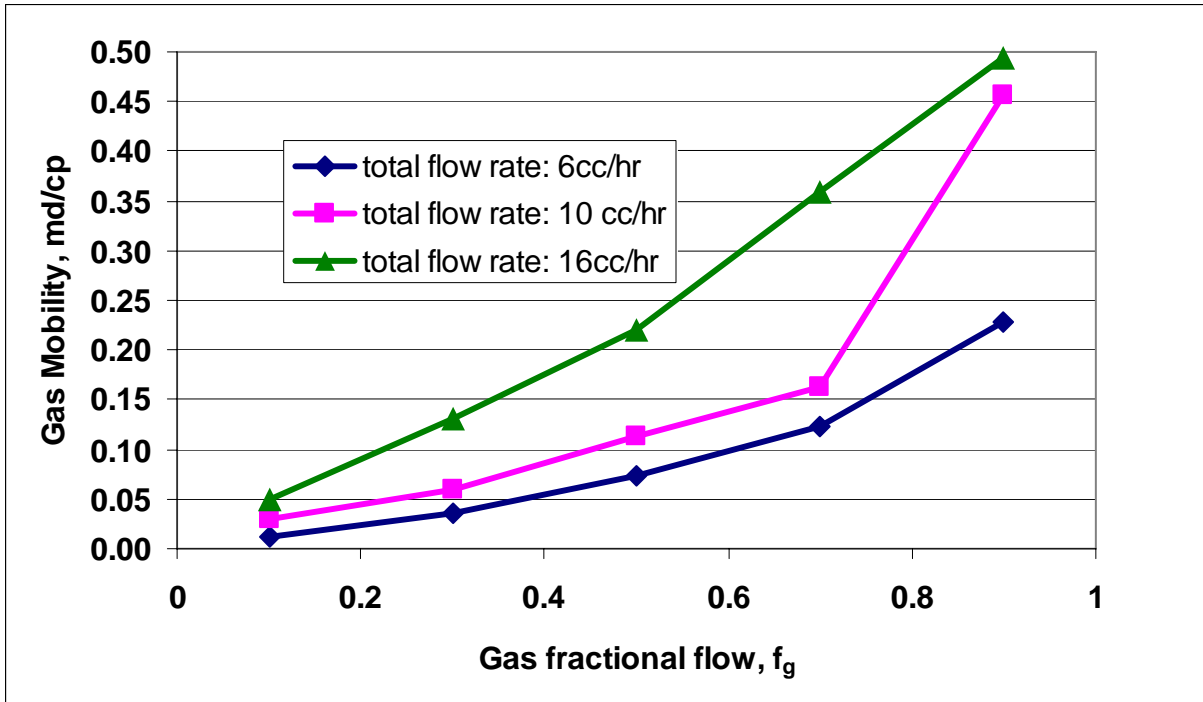


Fig. 50. Gas mobility as a function of gas fraction flow for 0.25 wt% CD at 104°F and 1500 psig in limestone.<sup>126</sup>

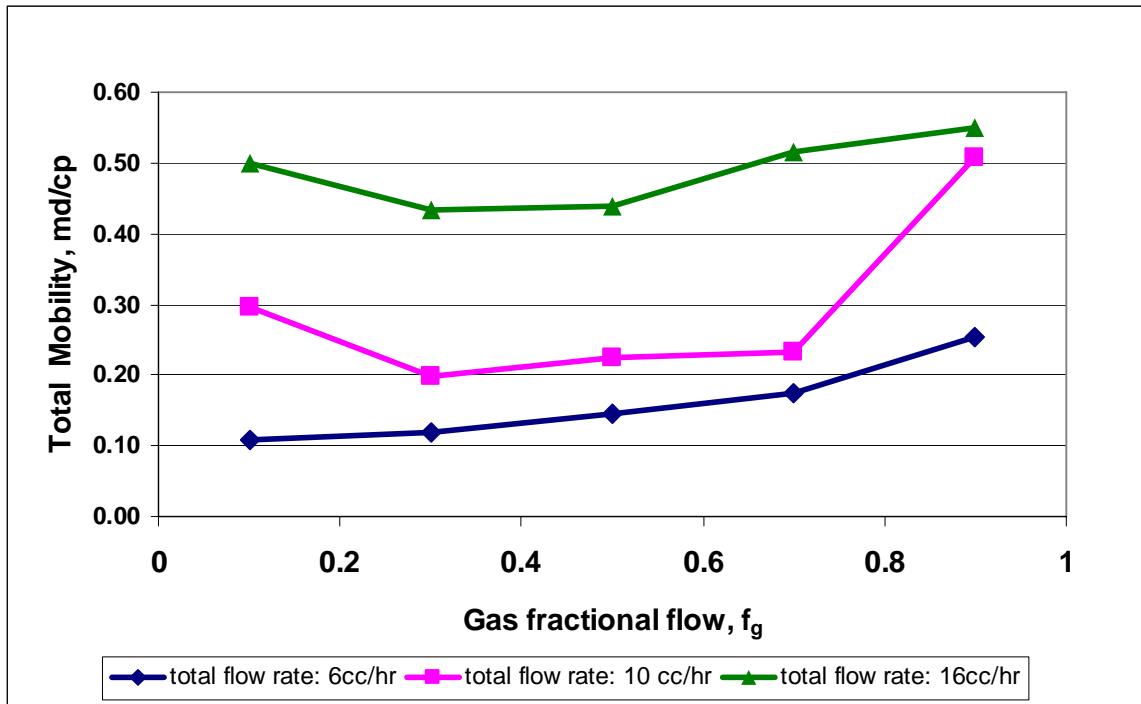


Fig. 51. Total mobility as a function of gas fraction flow for 0.25 wt% CD at 40°C and 1500 psig in Limestone.<sup>126</sup>

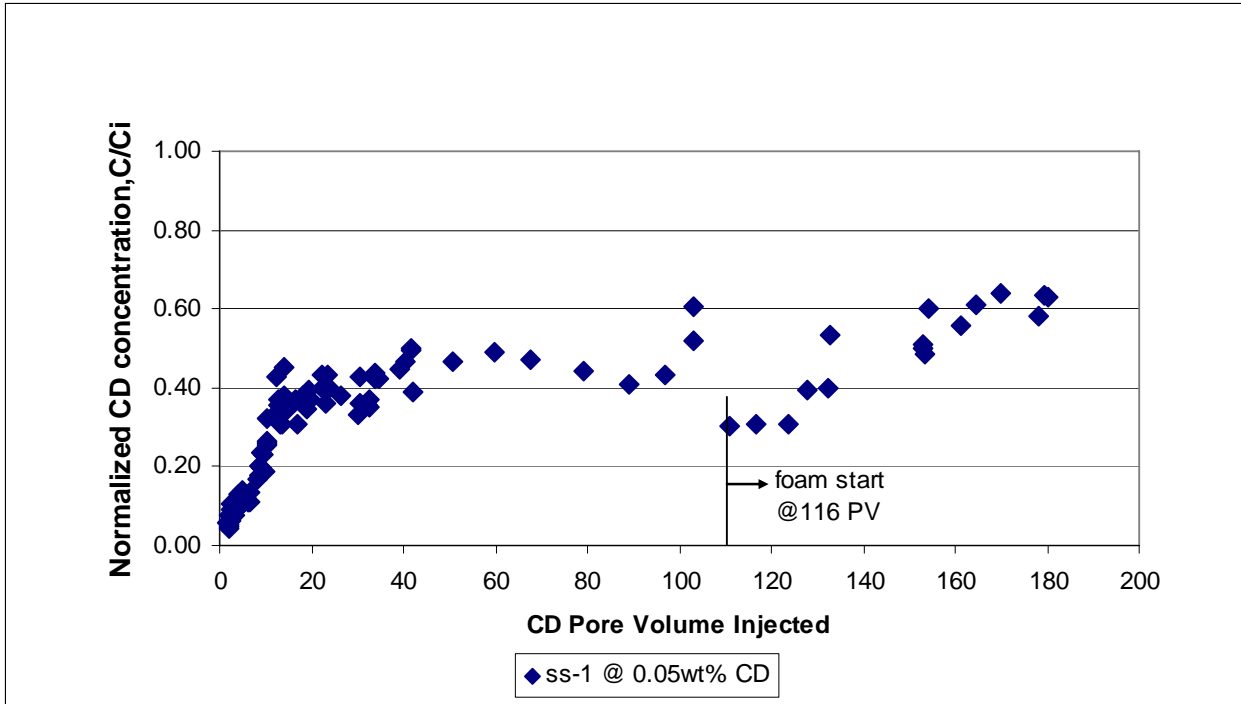


Fig. 52. CD adsorption profile for Core SS-1, concentration of 0.05% at 110°F and 1540 psig.

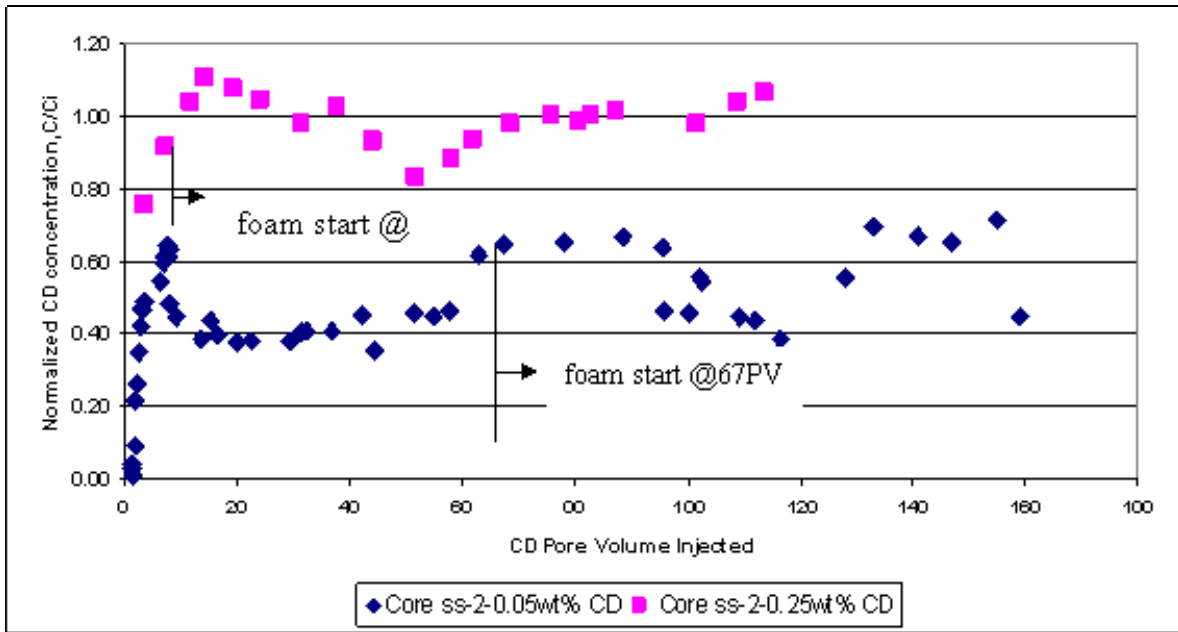


Fig. 53. CD adsorption profile for Core SS-2, concentration of 0.05 wt% & 0.25wt% at 110°F and 1540 psig.

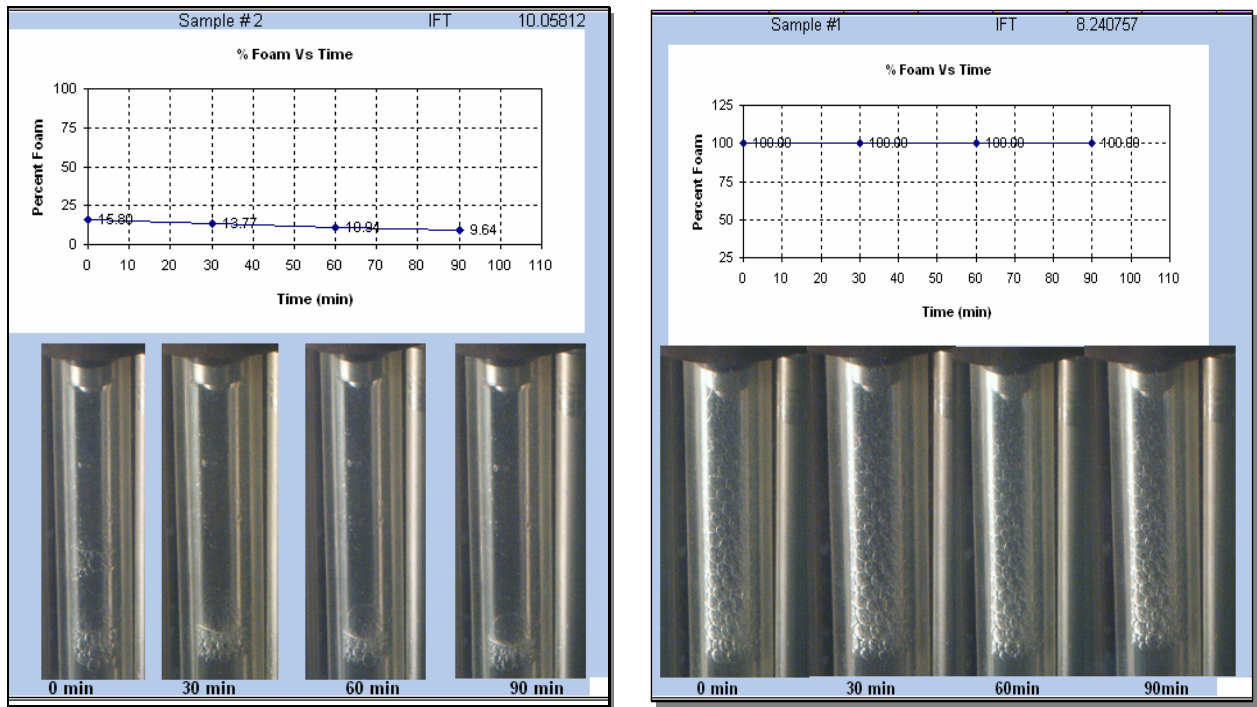


Fig. 54. IFT test results for one foaming sample and one non-foaming sample.

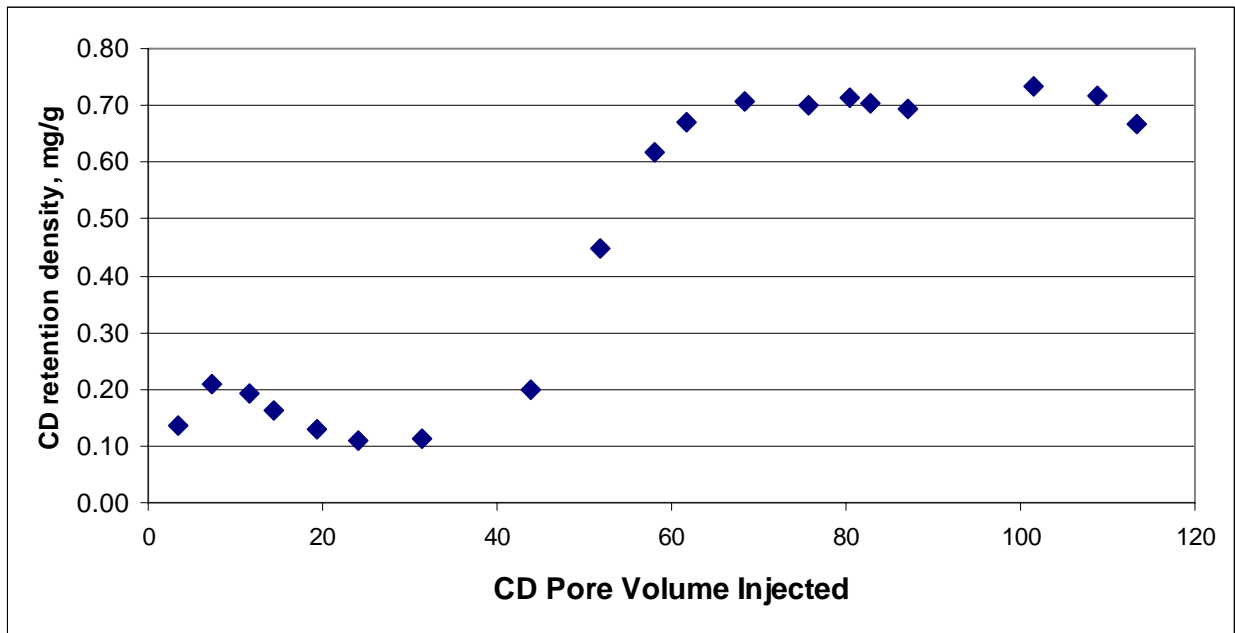


Fig. 55. Core SS-2 retention density of CD surfactant during the co-injection of CO<sub>2</sub> and CD solution of 0.25 wt% concentration at 110°F and 1540 psig.

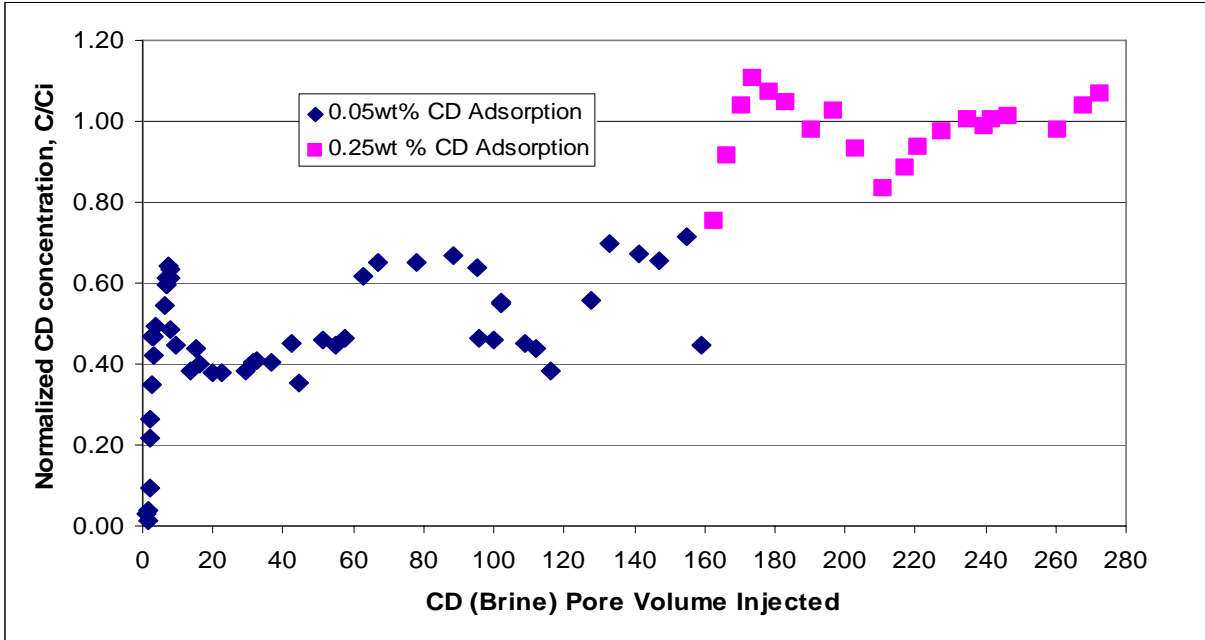


Fig. 56. CD adsorption profiles for Core SS-2.

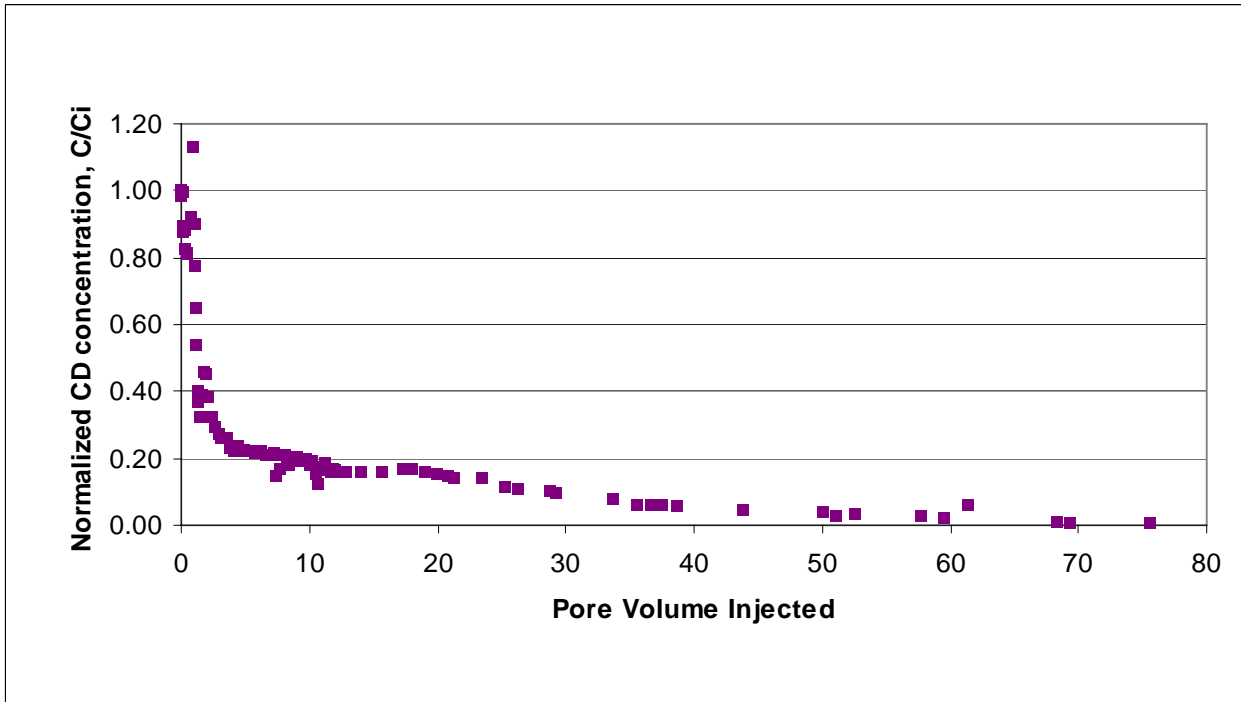


Fig. 57. CD desorption profile for Core SS-2.

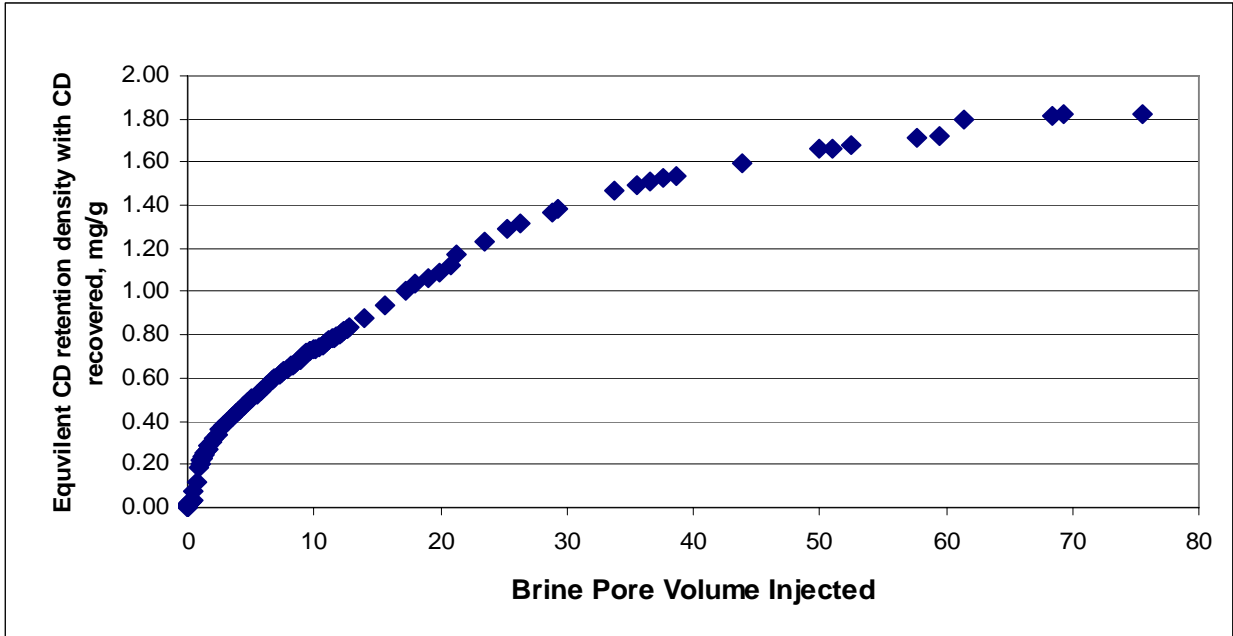


Fig. 58. Equivalent CD retention density decreased from Core SS-2 with CD surfactant recovery during the desorption phase.

## CONCLUSIONS

**Chapter 1.** Cores used for this work were relatively short cores (5.71 to 8.17 cm), about 3.8 cm in diameter, and therefore care must be taken when extrapolating following conclusions to reservoir scale:

1. Of the four core types tested, only in the Queen core was there free CO<sub>2</sub> produced from the core during displacement of CO<sub>2</sub> by brine injection with end-point brine saturation. These findings of end-point saturation are significant parameters in determining flow patterns, retention rates, and injectivity changes and their longevity that will enable improved predictions of CO<sub>2</sub> behavior in reservoirs for EOR and/or sequestration considerations.
2. From 0.2 to 0.3 PV fraction of free-phase CO<sub>2</sub> saturation was required to establish a CO<sub>2</sub> flow path, after which there was little brine production except through evaporation, which is a slow process. The CO<sub>2</sub> saturation can be increased by increasing flow rate, reducing pressure, and water evaporation.
3. At the end of CO<sub>2</sub> injection there is a relatively low CO<sub>2</sub> saturation and high brine saturation in the core, thus no reduction in CO<sub>2</sub> saturation was required to return to brine flow. Only in the Queen sand was free CO<sub>2</sub> produced during brine injection.
4. Brine is equilibrated with CO<sub>2</sub> in a short time frame over a relatively short distance. Only when a channel was formed was brine produced that was not saturated with CO<sub>2</sub> while a significant residual CO<sub>2</sub> remained in the core.
5. The injection of brine into a 100% CO<sub>2</sub> phase required 0.2 to 0.3 PV fraction saturation to establish a brine flow path.
6. The sandstone and carbonate systems initially performed similarly. This was changed when through dissolution of the rock matrix a solution channel was formed in the limestone, creating a dominant flow path that significantly altered the flow behavior of the core.

**Chapter 2.** Conclusions of the effects of three types of flow behavior schemes on adsorption (surfactant solution flow through core samples, diffusion into core samples, and missed with crushed core mixed with surfactant solution) are:

1. Values of CD adsorption density on crushed and non-flow solid limestone cubes were found to be the same and are best described as a function of surfactant availability (mass of surfactant available per mass of solid) in the system.
2. The shape of the adsorption isotherms on crushed sandstone, comparing surfactant availability with adsorption density, suggests the slopes and possibly the density plateau depend on surfactant concentration and availability.
3. Adsorption time dynamic depends on the state of solid and flow conditions. Time to reach equilibrium in nonflow core volumes was an order of magnitude greater compared to the circulation experiment, and 3 orders of magnitude greater compared to the crushed rock. Thus the rate of adsorption is dependent on the availability of surfactant with the kinetics and equilibrium being comparably very rapid.
4. When comparing flow versus nonflow systems in cube or core samples, the adsorption density on limestone underwent a significant decrease due to the flow in porous media while adsorption density on sandstone remained the same. This might be an indication of different adsorption mechanisms and/or energy levels that occur on limestone and sandstone surfaces. Tests such as heats of adsorption that are planned for the future should shed some light on the cause of these differences.
5. The results should be considered when determining reservoir adsorption requirements.

**Chapter 3.** Conclusions from the development of kinetic models of a CO<sub>2</sub>-foaming surfactant onto Berea Sandstone from adsorption and desorption experimental results are:

1. The pseudo-first and second order kinetic models for adsorption and desorption were derived in a mathematically complete format. These models are nonlinear. The adsorption models have two unknown parameters, and the desorption models have three unknown parameters.
2. A simplex nonlinear optimization method was adapted for the determination of the unknown parameters for these kinetics models. This algorithm can be applied to determine not only the parameters of these nonlinear models, but also the absolute error between the model and the measured results.
3. The adsorption and desorption processes of surfactant CD1045 onto and from Berea sandstone were found to obey the pseudo-second order adsorption model and the pseudo-

first order desorption models, respectively. More experimental work under different conditions will be carried out to better understand the influences of different factors on the sorption processes.

**Chapter 4.** Conclusions from corefloods on two Berea sandstone samples to determine gas mobility of CO<sub>2</sub>/brine systems at reservoir conditions are:

1. Gas mobility of CO<sub>2</sub>/brine increases with increasing of  $f_g$ . The total mobility of CO<sub>2</sub>/brine increases with increasing  $f_g$  ranging from 0.6 to 0.9; but decreases with increasing  $f_g$  when  $f_g$  is less than 0.6.
2. Total mobility (and or gas mobility) as a function of  $f_g$  is characterized by three intersecting straight lines with two crossed points  $f_g^o$  and  $f_g^*$ . Three foam flow regions are described in this study: a single-phase region, a low gas fractional flow region and a high gas fractional region. In the single-phase region, with fixed CO<sub>2</sub> gas flow rate, the gas mobility increases with increasing  $f_g$ . But the total mobility is independent of  $f_g$  no matter what the fixed CO<sub>2</sub> gas flow rate or the fixed CD aqueous flow rate. In the low gas fractional flow region, the gas mobility and total mobility decreases with increasing  $f_g$ . In the high gas fractional flow region, the gas mobility and total mobility increases with increasing  $f_g$ .
3. In different cores, the  $f_g^*$  is generally different. Even in the same core, due to different flow rates and different foam flow modes,  $f_g^*$  may also vary. The higher the permeability and flow rate, the higher the  $f_g^*$ .
4. The mobility reduction factor for Cores SS-1 and SS-2 reaches maximum at  $f_g=0.6$  and  $f_g=0.8$ , respectively.
5. Gas mobility and foam mobility increases with increase in total flow rate if the foam flow is shear-thinning.
6. During CO<sub>2</sub> foam flooding, with CD solution of 0.05 wt% concentration, it was difficult to establish adsorption equilibrium. Exploration of the reason for this would be an important task for future work.
7. The adsorption/desorption of the surfactant are characterized as a rapid short period of adsorption/desorption to/from the rock surface followed by a long period of slow

adsorption/desorption. The adsorption of surfactant onto rock increases with the occurrence of foam.

8. A CD surfactant solution with a higher concentration will reach adsorption equilibrium in the core faster than a CD surfactant solution with a lower concentration.

## **ACKNOWLEDGEMENTS**

Appreciation is expressed to the Department of Energy and the State of New Mexico for funding this work. Thanks to members of the New Mexico Petroleum Recovery Research center: Reid B. Grigg, Robert K. Svec, Zhengwen Zeng, Baojun Bai, Yi Liu, Alexander Mikhailin, and Guoqiang Yin who have contributed to this work. Also we would like to acknowledge Ms. Liz Bustamante for her assistance in editing this manuscript. For contributions from outside the PRRC we would like to acknowledge George Hirasaki at Rice University for his very helpful suggestions, and Shinichi Sakurai, an Associate at the Bureau of Economic Geology at the University of Texas at Austin, for the core samples.

## REFERENCES

1. Taber, J.J.: "Environmental Improvements and Better Economics in EOR Operations," *In Situ* (1990) 14(4), 345-404.
2. Stalkup, F. I.: "Miscible Displacement," SPE Monograph No. 8, New York (1983).
3. Grigg, R. B., et al.: "Cost Reduction and Injectivity Improvements for CO<sub>2</sub> Foams for Mobility Control," paper SPE 75178 presented at the 2002 SPE/DOE IOR, Tulsa, April 13-17.
4. Cheng, L., et al.: "Simulating Foam Processes at High and Low Foam Qualities," paper SPE 59287 presented at the 2000 SPE/DOE IOR. Tulsa, April 2-5.
5. Shan, D. and Rossen, W.R.: "Optimal Injection Strategies for Foam IOR," paper SPE 75180 presented at the 2002 SPE/DOE IOR. Tulsa, April 13-17.
6. Grigg, R.B., et al.: "Improving CO<sub>2</sub> Efficiency for Recovering Oil In Heterogeneous Reservoirs," First Annual Technical Report, US DOE Contract No. DE-FG26-01BC15364 (2003).
7. Grigg, R.B., et al.: "Improved CO<sub>2</sub> Efficiency for Recovering Oil in Heterogeneous Reservoirs," Second Annual Technical Report, DOE Contract No. DE-FG26-01BC15364 (2003).
8. Grigg, R.B. and Bai, B.: "Calcium Lignosulfonate Adsorption and Desorption on Berea Sandstone," *Journal of Colloid and Interface Science*, 279 (2004) 36-45.
9. Grigg, R.B. and Bai, B.: "Sorption of Surfactant Used in CO<sub>2</sub> Flooding onto Five Minerals and Three Porous Media," paper 93100 presented at the 2005 SPE International Symposium on Oilfield Chemistry, Houston, Feb. 2-4.
10. Bai, B. and Grigg, R.B.: "Kinetics and Equilibria of Calcium Lignosulfonate Adsorption and Desorption onto Limestone," paper 93098 presented at the 2005 SPE International Symposium on Oilfield Chemistry, Houston, Feb. 2-4.
11. Grigg, R.B., Bai, B., and Liu, Y.: "Competitive Adsorption of Hybrid Surfactant System onto Five Minerals, Berea Sandstone, and Limestone," paper SPE 90612 presented at the 2004 SPE ATCE, Houston, Sep. 26-29.
12. blank
13. Rogers, J.D. and Grigg, R.B.: *SPE Reservoir Eval. & Eng.*, Vol. 5, No. 5.

14. Tsau, J.-S. and Heller, J.P.: "Evaluation of Surfactants for CO<sub>2</sub>-Foam Mobility Control," paper SPE 24013, 1992 PBOGR, Midland, March 18-20.
15. Tsau, J.-S., et al.: "Use of Mixed Surfactants to Improve Mobility Control in CO Flooding," paper SPE 39792 presented at the 1998 PBOGR, Midland, March 23–26.
16. Tsau, J.S. and Heller, J.P.: "Evaluation of Surfactants for CO<sub>2</sub>-Foam Mobility Control," paper SPE 24013 presented at the 1992 Permian Basin Oil and Gas Recovery Conference, Midland, March 18-20.
17. Tsau, J-S., et al.: "Smart Foam to Improve Oil Recovery in Heterogeneous Porous Media," paper SPE 39677 presented at the 1998 SPE/DOE IOR, Tulsa, April 19–22.
18. Martin, F.D., et al.: "CO<sub>2</sub>-Foam Field Verification Pilot Test at EVGSAU Injection Project Phase I: Project Planning and Initial Results," paper SPE 24176 presented at the 1992 SPE/DOE IOR, Tulsa, April 22-24.
19. Tsau, J.S., et al.: "CO<sub>2</sub> Foam Field Verification Pilot Test at EVGSAU: Phase IIIA—Surfactant Performance Characterization and Quality Assurance," paper SPE 27785, presented at the 1994 SPE/DOE IOR, Tulsa, April 17-20.
20. Stevens, J. E., and Martin, F. D.: "CO<sub>2</sub> Foam Field Verification Pilot Test at EVGSAU: Phase IIIB—Project Operations and Performance Review," paper SPE 27786 presented at the 1994 SPE/DOE IOR, Tulsa, April 17-20.
21. Harpole, K.J., et al.: "CO<sub>2</sub> Foam Field Verification Pilot Test at EVGSAU: Phase IIIC—Reservoir Characterization and Response to Foam Injection," paper SPE 27798 presented at the 1994 SPE/DOE IOR, Tulsa, April 17-20.
22. Martin, F.D., et al.: "CO<sub>2</sub>-Foam Field Test at the East Vacuum Grayburg/San Andres Unit," *SPE* (November 1995) 10(4), 266-272.
23. Heller, J.P., et al.: "Field Test of CO<sub>2</sub> Mobility Control at Rock Creek," paper SPE 14395 presented at the 1985 SPE ATCE, Las Vegas, Sept.22-25.
24. Jonas, T. M., et al.: "Evaluation of a CO<sub>2</sub> Foam Field Trial: Rangely Weber Sand Unit," paper SPE 20468 presented at the 1990 SPE ATCE, New Orleans, Sept. 23-26.
25. Chou, S. I., et al.: "CO<sub>2</sub> Foam Field Trial at North Ward-Estes," paper SPE 24643 presented at the 1992 SPE ATCE, Washington, DC, Oct. 4-7.
26. Hoefner, M. L., et al.: "CO<sub>2</sub> Foam: Results From Four Developmental Field Trials," paper SPE/DOE 27787 presented at the 1994 SPE/DOE IOR, Tulsa, April 17-20.

27. Holm, L.W. and Garrison, W.H.: "CO<sub>2</sub> Diversion with Foam in an Immiscible CO<sub>2</sub> Field Project," *SPE* (February 1988), Vol. 3, No. 1, 112-118.
28. Moritis, G.: "EOR/Heavy Oil Survey—Special Report" and "2006 Worldwide EOR Survey," *Oil & Gas Journal*, (April 17, 2006) **104:15**, 37-57.
29. Grigg, R.B. and Svec, R.K.: "CO<sub>2</sub> Retention and Injectivity Changes: Laboratory Tests," Paper 145 presented at the Sixth Annual Conference on Carbon Capture and Sequestration – DOE/NETL, Pittsburgh, 7-19 May 2007.
30. Grigg, R.B. and Mikhalin, A.A.: "Effects of Flow Conditions and Surfactant Availability on Adsorption," paper SPE 106205 presented at the 2007 SPE International Symposium on Oilfield Chemistry, Houston, Feb. 28 – March 2.
31. Grigg, R.B.: "Technologies Hold Key to Improving Recovery Efficiency," *The American Oil & Gas Reporter*, February 2007, 106.
32. Grigg, R.B. and Svec, R.K.: "CO<sub>2</sub> Transport Mechanisms in CO<sub>2</sub>/Brine Coreflooding," paper SPE 103228 presented at the 2006 SPE Annual Technical Conference and Exhibition, San Antonio, Sep. 24-27.
33. Zeng, Z-W., Grigg, R.B., and Bai, B.: "Experimental Development of Adsorption and Desorption Kinetics of CO<sub>2</sub>-Foaming Surfactant onto Berea Sandstone," paper SPE 103117 presented at the 2006 SPE Annual Technical Conference and Exhibition, San Antonio, Sep. 24-27.
34. Pawar, R.J., et al.: "Overview of a CO<sub>2</sub> Sequestration Field Test in the West Pearl Queen Reservoir, New Mexico," *Environmental Geosciences*, **V.13**, No. 3 (September 2006), pp. 163-180.
35. Grigg, R.B. and Svec, R.K.: "CO<sub>2</sub> Saturations and Transport Mechanisms in Frio Sandstone," Paper 157 presented at the Fifth Annual Conference on Carbon Capture and Sequestration – DOE/NETL, Washington, D.C., 8-11 May 2006.
36. Grigg, R.B. and Svec, R.K.: "Laboratory and Model Tests at Reservoir Conditions for CO<sub>2</sub>-Brine-Carbonate Rock Systems Interactions," presented at The Fifth Annual DOE Carbon Sequestration Conference, Washington, D.C., 8-11 May 2006.
37. Zeng, Z-W. and Grigg, R.: "A Criterion for Non-Darcy Flow in Porous Media," *Transport in Porous Media*, (2006) **63**: 57-69.

38. Grigg, R.B.: "Improving Gas Flooding Efficiency," DOE Contract No. DE-FG26-04NT15532, first annual report (May 2006)
39. Liu, Y., Grigg, R.B., and Svec, R.K.: "Foam Mobility and Adsorption in Carbonate Core," paper SPE 99756 presented at the 2006 SPE/DOE Symposium on Improved Oil Recovery, Tulsa, 22–26 April.
40. Bai, B., Grigg, R.B., Liu, Y., and Zeng, Z-W.: "Adsorption and Desorption of a CO<sub>2</sub>-Foam-Forming Surfactant onto Berea Sandstone," paper SPE 95920 presented at the 2005 SPE Annual Technical Conference and Exhibition, Dallas, 9 – 12 October.
41. Grigg, R.B.: "Improved CO<sub>2</sub> Efficiency for Recovering Oil in Heterogeneous Reservoirs," Final Report for DOE contract no. DE-FC26-01BC15364, June 2005
42. Grigg, R.B., Svec, R.K., Peter C. Lichtner, P.C., Carey, W., and Lesher, C.E.: "CO<sub>2</sub>/Brine/Carbonate Rock Interactions: Dissolution and Precipitation," presented at the Fourth Annual Conference on Carbon Capture & Sequestration, Alexandria, 2-5 May 2005.
43. Liu, Y., Grigg, R.B., and Svec, R.K.: "CO<sub>2</sub> Foam Behavior: Influence of Temperature, Pressure, and Concentration of Surfactant," paper 94307 presented at the 2005 SPE Production and Operations Symposium, Oklahoma City, 17-19 April.
44. Benson, S.M.: "Overview of Geologic Storage of CO<sub>2</sub>," *Carbon Dioxide Capture for Storage in Deep Geologic Formations*, Volume 2, Introduction, C.C. Thomas and S.M. Benson (Eds.), 2005 Elsevier Ltd.
45. Wiebe R. and Gaddy, V.L.: "The Solubility for Carbon Dioxide in Water at Various Temperatures from 12 to 40°C and at Pressure to 500 Atmospheres. Critical Phenomena," *J Amer. Chem. Soc.*, Vol. 62, 815-817, (April 1940).
46. Enick, R.M.: "CO<sub>2</sub> Solubility in Water and Brine under Reservoir Conditions," *Chem. Eng. Comm.* (1990), Vol. 90, pp 23-33.
47. Grigg, R.B. and Svec, R.K.: "Co-Injected CO<sub>2</sub>-Brine Interactions with Indiana Limestone," SCA2003-19, presented at the Society of Core Analysts Convention SCA 2003 Pau, France, 21-24 September 2003.
48. Wellman, T.P, Grigg, R.B., McPherson, B.J., Svec, R.K., and Lichtner, P.C.: "Evaluation of CO<sub>2</sub>-Brine-Reservoir Rock Interaction with Laboratory Flow Tests and Reactive Transport Modeling," paper 80228 presented at the 2003 SPE International Symposium on Oilfield Chemistry, Houston, Feb. 5–8.

49. Pawar, R.J., et al.: "Geologic Sequestration of CO<sub>2</sub> in a Depleted Oil Reservoir: An Overview of a Field Demonstration Project," paper SPE 90936 presented at the 2004 SPE Annual Technical Conference and Exhibition, Houston, 26-29 September 2004.
50. Pawar, R., et al.: "Geologic Sequestration of CO<sub>2</sub> in West Pearl Queen Field: Results of a Field Demonstration Project," Third Annual Conference on Carbon Sequestration, Washington, DC, May 2004.
51. Schramm L.L. Ed.: *Surfactants: Fundamentals and Applications in the Petroleum Industry*, Cambridge University Press, 2000.
52. Shih-Hsien, C. and Grigg, R.B.: "Foam Displacement Modeling in CO<sub>2</sub> Flooding Processes," *SPE*, (1996), 575.
53. Tsau, J.S. and Heller, J.P.: "Evaluation for Surfactants for CO<sub>2</sub> Foam Mobility control," paper SPE 24013 presented at the 1992 SPE Permian Basin Oil and Gas Recovery Conference, Midland, 18-20 March.
54. Kuhlman, M.I., Lau, H.C., and Falls, A.H.: "Surfactant Criteria for Successful Carbon Dioxide Foam in Sandstone Reservoirs," *SPE*, (2000), 35.
55. Mannhardt, K., Schramm, L.L., and Novosad, J.J.: "Effect of Rock Type and Brine Composition on Adsorption of Two Foam Forming Surfactants," paper SPE 20463 presented at the 1990 SPE Annual Technical Conference and Exhibition, New Orleans, 23-26 September.
56. Smith, D.H.: *Surfactant-Based Mobility Control*, American Chemistry Society, 1988.
57. Kuhlman, M.I., Falls, H.A. Hara, S.K., and Monger McClure, T.G.: "CO<sub>2</sub> Foam with Surfactant Used Below Their Critical Micelle Concentrations," *SPE*, 1992, 445.
58. Enick, R.M., et al.: "Direct Thickeners for Carbon Dioxide," paper SPE 59325 presented at the 2000 SPE/DOE Improved Oil Recovery Symposium, Tulsa, 3-5 April.
59. Mannhardt, K., Schramm, L.L., and Novosad, J.J.: "Colloids and Surfaces," 1992, 68, 37.
60. Schramm, L.L. Ed.: *Foams: Fundamentals and Applications in the Petroleum Industry*, American Chemistry Society, 1994, 259-316.
61. Ogden, P.H. Ed.: *Chemicals in the Oil Industry: Developments and Applications*, Special Publication 97, Royal Society of Chemistry: Cambridge, 1991, 159-173.

62. Tsau, J.S., and Grigg, R.B.: "Assessment of Foam Properties and Effectiveness in Mobility Reduction for CO<sub>2</sub> Foam floods", paper 37221 presented at the 1997 SPE International Symposium on Oilfield Chemistry, Houston, 18-21 February.
63. Tsau, J.S., at al.: "CO<sub>2</sub> Foam Flood Verification Pilot Test at EVGSAU: Phase IIIA: Surfactant Performance Characterization and Quality Assurance," paper SPE 27785 presented at the 1994 SPE/DOE Ninth Symposium on Improved Oil Recovery, Tulsa, 17-21 April.
64. Kuehne, D.L. at al.: "Evaluation of Surfactants for CO<sub>2</sub> Mobility in Dolomite Reservoirs," paper SPE 24177 presented at the 1992 SPE/DOE Symposium on Enhanced Oil Recovery, Tulsa, 22-24 April.
65. Tsau, J.S., Syahputra, A.E., and Grigg, R.B.: "Economic Evaluation of Surfactants Adsorption in CO<sub>2</sub> Foam Application," paper SPE 59365 presented at the 2000 SPE/DOE Symposium on Improved Oil Recovery, Tulsa, 3-5 April.
66. Grigg, R.B. and Svec, R.K.: "CO<sub>2</sub> Transport Mechanisms in CO<sub>2</sub>/Brine Coreflooding," paper SPE 103228 presented at the 2006 SPE Annual Technical Conference and Exhibition, San Antonio, 24–27 September.
67. Somasundaram, P., Shrotri, S. and Huang, L.: "Thermodynamics of adsorption of surfactants at solid-liquid interface," 1998, **70**, 621.
68. Lake, L.W.: "*Enhanced Oil Recovery*", Prentice-Hall Inc., Upper Saddle River, New Jersey (1989) 1-16.
69. Green, D.W. and Willhite, G.P.: "*Enhanced Oil Recovery*", Society of Petroleum Engineers Inc., Richardson, Texas (1998) 1-300.
70. Klins, M.A.: "*Carbon Dioxide Flooding-Basic Mechanisms and Project Design*", International Human Resources Development Corporation, Boston (1984) 1-140.
71. Jarrell, P., Fox, C., Stein, M. and Webb, S.: "*Practical Aspects of CO<sub>2</sub> Flooding*", Society of Petroleum Engineers Inc., Richardson, Texas (2002) 1-38.
72. Heller, J.P.: "CO<sub>2</sub> foams in Enhanced Oil Recovery," In *Foams: Fundamentals and Applications in the Petroleum Industry*, Schramm (ed.) ACS Advances Series, No.242, American Chemical Soc., Washington, DC (1994) 201-234.
73. Martin, F.D., Stevens, J.E. and Harpole, K.J.: "CO<sub>2</sub>-Foam Field Test at the East Vacuum Grayburg/San Andres Unit," *SPE Reservoir Engineering*, Vol.10 (Nov. 1995) 266-272.

74. Chang, S.-H. and Grigg, R.B.: "Laboratory Flow Tests Used To Determine Reservoir Simulator Foam Parameters for EVGSAU CO<sub>2</sub> Foam Pilot," paper SPE 27675 presented at the 1994 Permian Basin Oil and Gas Recovery Conference, Midland, Texas, 16-18 March.
75. Do, D.D.: "*Adsorption Analysis: Equilibria and Kinetics*", Imperial College Press, London (1998) 337-700.
76. Rosen, M.J.: "*Surfactants and Interfacial Phenomena*", third edition, John Wiley and Sons, Hoboken, New Jersey (2004) 208-302.
77. Schramm, L.L.: "*Foams: Fundamentals and Applications in the Petroleum Industry*", American Chemical Society, Washington, DC (1994) 1-200.
78. Azizian, S.: "Kinetics Models of Sorption: A Theoretical Analysis," *Journal of Colloid and Interface Science*, Vol. 276(August 2004) 47-52.
79. Dantzig, G. B.: "*Linear Programming and Extensions*", Prentice-Hall, Englewood Cliffs, New Jersey (1961).
80. Nelder, J.A. and Mead, R.: "A simplex method for function minimization," *Computer Journal*, Vol. 7(1965) 308-313.
81. Jacoby, S.L.S., Kowalik, J.S., and Pizzo, J.T.: "*Iterative Method for Nonlinear Optimization Problems*", Prentice-Hall Inc., Englewood Cliffs, New Jersey (1972).
82. Khatib, Z.I., Hirasaki, G.J., and Falls, A.H.: "Effects of Capillary Pressure on Coalescence and Phase Mobilities in Foams Flowing through Porous Media," *SPEJ*, (August 1988) 919-926.
83. De Vries, A.S. and Wit, K.: "Rheology of Gas/Water Foam in the Quality Range Relevant to Steam Foam," *SPEJ*, (1990), 5 (2), 185-192.
84. Patton, J.T., Holbrook, S.T. and Hsu, W.: "Rheology of Mobility Control Foams," *SPEJ* (June 1983) 456.
85. Hirasaki, G.J. and Lawson, J.B.: "Mechanisms of Foam Flow Through Porous Media- Apparent Viscosity in Smooth Capillaries," *SPEJ* (April 1985) 176-190.
86. Marsden, S.S and Khan, S.A.: "The Flow of Foam Through Short Porous Media and Apparent Viscosity Measurements," *SPEJ* (March 1966) 17; Trans., AIME 237.
87. Chang, S.H. and Grigg, R.B.: " Effects of Foam Quality and Flow Rate on CO<sub>2</sub>-Foam Behavior at Reservoir Temperature and Pressure," paper SPE 56856 presented at the 1998 SPE/DOE Improved Oil Recovery Symposium, Tulsa, OK, 19-22 April.

88. Lee, H.O. and Heller, J.P.; "Laboratory Measurements of CO<sub>2</sub>-Foam Mobility," *SPE* (May 1990) 193-197.
89. Yaghoobi, H. and Heller, J. P.: "Laboratory Investigation of Parameters Affecting CO<sub>2</sub>-Foam Mobility in Sandstone at Reservoir Conditions," paper SPE 29168 presented at the 1994 Eastern Regional Conference and Exhibition, Charleston, Nov. 8-10.
90. Persoff, P. et al.: "A Laboratory Investigation of Foam Flow in Sandstone at Elevated Pressure," *SPE* (Aug. 1991) 365.
91. Hu, P.C. Tuvell, M.E., and Bonner, G.A.: "Evaluation of Alpha-Olefin Sulfonates in Steam Diversion," paper SPE 12660 presented at the 1984 SPE/DOE Symposium on Enhanced Oil Recovery, Tulsa, 15-18 April.
92. Lee, H.O., Heller, J.P., and Hoefler, A.M.W.: "Change in Apparent Viscosity of CO<sub>2</sub> Foam with Rock Permeability," *SPE* (November 1991) 421-428.
93. Chang, S.H. and Grigg, R.B.: "Foam Displacement Modeling in CO<sub>2</sub> flooding Processes," paper SPE/DOE 35401 presented at the 1996 SPE/DOE Symposium on Improved Oil Recovery, Tulsa, 21-24 April.
94. Bernard, G.G., Holm, L.W., and Jacobs, W.A.: "Effect of Foam on Trapped Gas Situation and on Permeability of Porous Media to Water," *SPEJ* (Dec. 1965) 295-300; *Trans.*, AIME, 234.
95. Jensen, J.A. and Friedmann, F.: "Physical and Chemical Effect of an Oil Phase on the Propagation of foam in Porous Media," paper 16375, presented at the SPE California Regional Meeting held in Ventura, California, April 8-10, 1987.
96. Raterman, K.T.: "An Investigation of Oil Destabilization of Nitrogen Foams in Porous Media," paper SPE 19692, presented at 1989 SPE Annual Technical Conference and Exhibition, San Antonio, TX, October 8-11, 1989.
97. Yang S.H. and Reed R.L.: "Mobility Control using CO<sub>2</sub> foams," paper SPE19689 presented at the 64<sup>th</sup> Annual Technical Conference and Exhibition of the SPE held in San Antonio, TX, October 8-11, 1989
98. Manlowe, D.J. and Radke, C. J.: "A Pore-Level Investigation of Foam/Oil Interactions in Porous Media," *SPE*, (Nov. 1990), 5, 4, 495-502.
99. Bernard, G.G., Holm, L.W., and Harvey, C.P.: "Use of Surfactant to Reduce CO<sub>2</sub> Mobility in Oil Displacement," *SPEJ* (August 1980) 281-292; *Trans.*, AIME, 269.

100. Wang, G. C.: "A Laboratory study of CO<sub>2</sub> Foam Properties and Displacement Mechanism," paper SPE/DOE 12645 presented at the 1984 SPE/DOE Symposium on Enhanced Oil Recovery, Tulsa, Oklahoma, April 15–18.
101. Moradi-Araghi, A., Johnston, E.L., Zornes, D.R., and Harpole, K.J.: "Laboratory Evaluation of Surfactants in CO<sub>2</sub>-Foam Application at the South Cowden," paper SPE 37218 presented at the 1997 SPE International Symposium on Oilfield Chemistry, Houston, Feb.18-21.
102. Tsau, J.S., Yaghoobi, H. and Grigg, R.B.: "Smart Foam to Improve Oil Recovery in Heterogeneous Porous Media," PAPER spe39677 presented at the 1998 SPE/DOE Improved Oil Recovery Symposium, Tulsa, April 19-22.
103. Syahputra, A.E., Tsau, J.-S., and Grigg, R.B.: "Laboratory Evaluation of Using Lignosulfonate and Surfactant Mixture in CO<sub>2</sub> Flooding," paper SPE 59368 presented at the SPE/DOE Improved Oil Recovery Symposium, Tulsa, Oklahoma, April 3-5, 2000.
104. Bond, D.C and Holbrook, O.C.: "Gas Drive Oil Recovery Process," U.S. Patent No. 2,866,507 (Dec. 1958).
105. Fried, A.N: "The Foam Drive Process for Increasing the Recovery of Oil," Report RI-5866, U.S. Bureau of Mines, Washington, DC (1961).
106. Heller, J.P. and Taber, J.J.: "Mobility Control for CO<sub>2</sub> Floods—A Literature survey," topical report, Contract No: DE-AC21-79b4C1C689 U.S. DOE, Washington, DC (Oct. 1980).
107. Heller, J.P., Lien, C.L, and Kuntamukkula, M.S.: "Foam like Dispersions for Mobility Control in CO<sub>2</sub> Floods," *SPEJ* (August 1985) 603-613; *Trans.*, AIME, 279.
108. Mamden, S.S.: "Foams in Porous Media," topical report, Contract No. AC03-81SF11564 (SUPRI TR49) U.S. DOE, Washington, DC (July 1986).
109. Hirasaki, G.J.: "The Steam-Foam Process," *JPT* (May 1989a) 449.
110. Hirasaki, G.J.: "Supplement to SPE 19505, The Steam-Foam Process-Review of Steam-Foam Process Mechanisms," paper SPE 19518, SPE, online elibrary, Richardson, TX (1989b).
111. Holm, L.W.: "The Mechanism of Gas and Liquid Flow through Porous Media in the Presence of Foam," *SPEJ*. (1968) 8(4), 359-369.

112. Friedmann, F.: "Some Parameters Influencing the Formation and Propagation of Foams in Porous Media," paper SPE 15087 presented at the SPE 1986 California Regional Meeting, Oakland, April 2–4.
113. Sanchez, J.M., Schechter, R. S.; and Monsalve, A.: "The Effect of Trace Quantities of Surfactant on Nitrogen/Water Relative Permeabilities," paper SPE 15446 presented at the 1986 SPE Annual Technical Conference and Exhibition, New Orleans, Oct. 5–8.
114. Huh, D.G. and Handy, L. L.: "Comparison of Steady- and Unsteady-State Flow of Gas and Foaming Solution in Porous Media," *SPEJ*, (1989) 4, (1), 77-84.
115. Derjaguin B.V, and Landau L.: "Theory of the Stability of Strongly Charged Lyophobic Sols and the Adhesion of Strongly Charged Particles in Solutions of Electrolytes," *Acta Physico-Chimica* (URSS) 14,633–662 (1941).
116. Overbeek, J.T.G.: "Black Soap Films," *J. Phys. Chem.* (1960) 64, 1178-83.
117. Khristov, K., Krugljakov, P.M., and Exerowa, D.R.: "Influence of the Pressure in the Plateau-Gibbs Borders on the Drainage and the Foam Stability," *J. Colloid and Polymer Sci.* (1979) 257, 506-511.
118. Khristov K., Exerowa, D.R., and Krugljakov, P.M. : "Determination of Foam Stability at Constant Pressure in the Plateau-Gibbs Borders of the Foam," *J. Colloid Interface Sci.* (1981) 79, 584-586.
119. Khatib, Z.I., Ekserova, D.R., and Kruglyakov, P.M.: "Influence of Film Type on Foam Stability," *Colloid J. USSR* (1981), 43, 80-84.
120. Ettinger, R.A. and Radke, C.J.: "Influence of Texture on Steady Foam Flow in Beria Sandstone," *SPERE*, Vol 7, No 1 (Feb. 1992), 83-90.
121. Alvarez, J.M., Rivas, H.J. and Rossen, W.R.: "Unified Model for Steady-State Foam Behavior at High and Low Foam Qualities," *SPEJ* (September 2001) 325-333.
122. Osterloh, W.T. and Jante, M. J.: "Effects of Gas and Liquid Velocity on Steady-State Foam Flow at High Temperature," paper SPE 24179 presented at the 1992 SPE/DOE Enhanced Oil Recovery Symposium, Tulsa, April 22–24.
123. Prieditis, J. and Paulett, G. S.: "CO<sub>2</sub>-Foam Mobility Tests at Reservoir Conditions, in San Andres Cores," paper SPE24178 presented at the 1992 SPE/DOE Symposium on Enhanced Oil Recovery, Tulsa, Oklahoma, April 22–24.

124. Ely, J.F. and Huber, M.L.: "Equation of State Software **STRAPP**," version 1.0, 1990, National Institute of Standards and Technology, Gaithersburg, MD.
125. Liu, Y., Grigg, R.B., and Svec, R.K.: "Foam Mobility and Adsorption in Carbonate Core," paper SPE 99756 presented at the 2006 SPE/DOE Symposium on Improved Oil Recovery in Tulsa, U.S.A., 22-26 April, 2006.
126. Liu, Y.: "Characteristics Of Static Bulk Foam And Behavior Of Foam Flow In A Porous Medium", dissertation for the degree of Doctor of Philosophy in Petroleum Engineering of New Mexico Tech, Socorro, NM, April 2006.
127. Schramm L.L.: Foams: Fundamentals and Applications in the Petroleum Industry. American Chemical Society, Washington DC, 1994.
128. Rosen, W.R. and Wang, M.W.: "Modeling Foams for Acid Diversion," paper SPE 38200 presented at the 1997 SPE European Formation Damage Conference, The Hague, 2-3 June.
129. Grigg, R.B. and Bai, B.J.: "Sorption of Surfactant Used in CO<sub>2</sub> Flooding onto Five Minerals and Three Porous Media," SPE 93100 presented at the 2005 SPE International Symposium on Oilfield Chemistry, Feb. 2-4.
130. Novosad J.: "Surfactant Retention in Berea Sandstone-Effects of Phase Behavior and Temperature" *SPE Journal*, December 1982.